Renormalization and Knot Theory[*]

Dirk Kreimer[†]
Dept. of Physics
Mainz Univ. and Tasmania Univ.
Staudingerweg   GPO Box 252C
55099 Mainz   Hobart TAS 7001
Germany   Australia

February 6, 2008

Abstract

We investigate to what extent renormalization can be understood as an algebraic manipulation on concatenated one-loop integrals. We find that the resulting algebra indicates a useful connection to knot theory as well as number theory and report on recent results in support of this connection.

Contents

1 Introduction

Renormalization theory is one of the fundamental topics of perturbative Quantum Field Theory (pQFT). Renormalizability was one of the guiding principles in the construction of the Standard Model (SM), our current understanding of particle physics phenomenology. From first insights into the problem of ultraviolet (UV) divergences in a QFT [1] to the understanding of renormalization of gauge theories [2], including spontaneous symmetry breaking and the beautiful interplay with BRST identities [3], our understanding has vastly improved.

The first complete account to renormalization as such has been given by Dyson, Salam and Weinberg [4, 5, 6]. One can derive all properties of a renormalizable QFT from the knowledge of the Dyson Schwinger equations, an understanding of the problem of overlapping divergences [5] and Weinberg's theorem [6]. Later, the subject was reinvestigated thoroughly by the authors of [7]. Their approach was helpful especially in understanding parametric representations, but often the structure of Green functions is less transparent there. Nevertheless, the BPHZ method has become the standard text book approach to renormalization. Few would argue with the view that the structure of a renormalizable pQFT is most successfully encoded in structures like the forest formula [8], the BPHZ formalism and the R-operation [7].

Yet, as we will show, there seems to be still a more fundamental layer behind these structures. This paper is concerned with the exploration of an algebraic structure inherent in all renormalizable quantum field theories, which reveals a connection to knot theory and similar algebraic structures usually assigned to the investigation of braids. We will focus on this connection. We hope to show that these structures are not only of interest in their own right but also allow for a useful simplification of actual computations of renormalized quantities.

This paper is based on the material in [9]. We added an introduction into the subject, refined and extended the arguments at various places and added a section reviewing the results obtained recently.

The paper is organized as follows. In section two we will introduce ideas and notions of perturbative quantum field theory and renormalization theory. This section is by no means a complete account, but should provide for the reader unfamiliar with renormalization the necessary background. We refer to [1, 10, 11] for a more detailed discussion of the subject. This section can be skipped by a reader who is familiar with the topics of Feynman diagrams and renormalization theory.

In section three, we will restrict ourselves to vertex corrections of ladder-type diagrams. This simple topology mainly serves to fix our notations and to exhibit the basic idea. We will introduce a notation which allows us to express results for the simplest topology, the ladder topology, in terms of one-loop functions. The results obtained are not new as such, but allow to prove a remarkable fact: these simple topologies add under renormalization to Z-factors free of transcendental numbers. Sections three to six are mainly concerned with establishing this one-loop algebra in all relevant situations. Section three considers the ladder topology with nested divergences, section four establishes the same for two-point functions, section five considers the case of iterated nested and disjoint topologies. Finally, section six addresses the study of overlapping ladder topologies, remarkably establishing the same one-loop algebra in this case as well. In section three and six we shortly digress to link diagrams, exploiting the fact that the one-loop algebra obtained so far fits into a pattern motivated by skein relations [12] and braid algebras. The core of this paper is section seven, where we present an argument that any ladder topology, realized by what renormalizable theory and Feynman graph whatsoever, is free of transcendental numbers for the Z factors: its UV-divergences have purely rational coefficients.

In fact, we will show that knot theory knows about the renormalization program in the sense that it generates all contributing forests with the help of the

skein relation, revealing the proposed structure behind the recursion which governs renormalization theory.

This opens the arena for a link between the topology of Feynman graphs, expressed in terms of knots associated with the graph, and transcendental coefficients appearing in its Z-factor contributions. So, in section eight, we are concerned with collecting empirical evidence for the appearance of transcendentals in accordance with knots identified in the graphs. We review the results [13, 14, 15, 16, 17, 18] which have been achieved so far. These results point towards an interesting conjecture. Positive knots obtained from Feynman graphs correspond to Euler sums. Indeed, it seems that we can identify as many distinct prime knots in a Feynman graph as we find independent transcendentals in it. These transcendentals appear as generalized ζ-functions - Euler sums, and we collect the evidence for this unsuspected connection between knot theory, number theory and field theory in section eight.

Conclusions and an outlook finish the paper.

We will restrict ourselves to MS schemes in the following and we will use dimensional regularization throughout the paper.

2 Perturbative Quantum Field Theory

In this section we introduce perturbative Quantum Field Theory (pQFT), the idea of renormalization and discuss the necessary technical notions. None of the results derived in following sections is a new result in renormalization theory or uses more than the most basic facts of it. But looking at the structure of renormalization from an new angle we will argue that one can establish a useful connection to knot theory. We are not yet able to provide a field-theoretic derivation of this connection but rather collect empirical evidence by investigating and exploring well known results of perturbation theory. This is not the place to give a full account of renormalization theory, or to investigate the origin of UV divergences from the viewpoint of axiomatic field theory. Rather, we will sketch how pQFT appears as the art of calculating Feynman diagrams, explain the idea of renormalization and introduce the vocabulary.

2.1 pQFT

We now want to introduce pQFT and Feynman diagrams. Our presentation follows [10]. Our aim is to motivate the derivation of the Feynman rules. These rules give a pictorial approach to pQFT. Free propagating particles are specified by lines (propagators) and do interact at vertices, points in space-time where three or more lines merge together. These points describe the coupling of particles, and are specified by a coupling constant determing the strength of the interaction. In this way, each graph built out of propagators and vertices describes a process in pQFT. Specifying a set of initial and final particles, in pQFT one considers all possible graphs which allow for these initial and final states. If there are no closed loops in the graph, we speak of a tree-level graph. It delivers the lowest order contribution to the specified process. These contributions are of no further interest to us. Higher order contribu-

tions in the coupling constant demand more interaction vertices. The specified set of external particles is kept fixed and thus the expansion in the coupling constant becomes a loop expansion. In the presence of closed loops in the graph one has to take into account all possible momenta for these internal particles. This demands to integrate internal loop momenta. For the most interesting theories, these integrations are ill-defined. They diverge for large internal momenta. Quite often one can handle these divergences in an iterative procedure called renormalization. There, we claim, a connection to knot theory appears: the singular contributions to a pQFT are determined by knots derived from the topologies of its Feynman graphs.

So let us now motivate these Feynman rules. Let our starting point be the consideration of a scalar field theory; there is only one self-interacting scalar particle present. More realistic examples involve particles sitting in more complicated representations of the Lorentz group (spin), but we omit these complication in this elementary exposition.

We have a free Lagrangian given by

$$L = \frac{1}{2}(\partial_\mu \phi)^2 - \frac{1}{2}m^2\phi^2. \tag{1}$$

Later we will add interaction terms of the form $g\phi^n, n \geq 3$, to this Lagrangian. But first we consider quantization of the free theory. The classical calculus of variation gives as the equation of motion

$$\partial_\mu \frac{\delta L}{\delta \partial_\mu \phi} - \frac{\delta L}{\delta \phi} = 0 \Rightarrow (\Box + m^2)\phi = 0. \tag{2}$$

With the field $\phi(x)$ acting as the coordinate, parametrized by the space-time point $x = (\mathbf{x}, t)$, we find as its canonical conjugate momentum

$$\pi(\mathbf{x}, t) \equiv \frac{\delta L}{\delta \dot{\phi}} = \dot{\phi}(\mathbf{x}, t), \tag{3}$$

and, accordingly, a Hamiltonian density

$$H = \frac{1}{2}[\pi^2 + (\nabla \phi)^2 + m^2\phi^2]. \tag{4}$$

We recall that the transition to quantum theory emerges when we impose non-vanishing commutators between coordinates and momenta. We consider the commutator at equal time. We demand that commutators between expressions separated by space-like distances vanish.[1] At equal time, this becomes

$$[\phi(\mathbf{x}, t), \pi(\mathbf{x}, t)] = i\delta^3(\mathbf{x} - \mathbf{y}). \tag{5}$$

Note that this separation is Lorentz invariant. Lorentz transformations map space-like distances to spacelike distances.

---

[1] This incorporates a notion of causality. Fields with spacelike separation do not influence each other.

We are now looking for fields $\phi(x)$ fulfilling the Klein Gordon equation and the commutation relations. One readily verifies that the *Ansatz*

$$\phi(x) = \frac{1}{(2\pi)^{3/2}} \int d^4k \delta(k^2 - m^2)\Theta(k_0)[A(k)e^{-ikx} + A^\dagger(k)e^{ikx}], \tag{6}$$

has the required properties. We use

$$\omega_k : = \sqrt{\mathbf{k}^2 + m^2}, \; e^{ikx} = \exp(i\omega_k t - \mathbf{k} \cdot \mathbf{x}),$$

$$\int d^4k \delta(k^2 - m^2)\Theta(k_0) = \int \frac{d^3k}{2\omega_k},$$

$$a(k) := \frac{A(k)}{\sqrt{2\omega_k}}. \tag{7}$$

Upon Fourier transformation, we obtain expressions for ϕ, π where the operator valued Fourier coefficients $a, a^\dagger$ have to obey commutation relations as well:

$$[a(k), a^\dagger(k')] = \delta^3(\mathbf{k} - \mathbf{k}'). \tag{8}$$

Then we obtain the Hamiltonian as

$$H = \int d^3k \; \omega_k \left[a^\dagger(k)a(k) + \frac{1}{2}\right] = \frac{1}{2} \int d^3k \; \omega_k \left[a^\dagger(k)a(k) + a(k)a^\dagger(k)\right]. \tag{9}$$

The Hamiltonian is the generator of the time evolution,[2] and accordingly we find the generator of spacelike translations by replacing ω_k by the spacelike components of the four vector $k_\mu = (\omega_k, \mathbf{k})$

$$P_i = \int d^3k \; k_i \left[a^\dagger(k)a(k) + a(k)a^\dagger(k)\right]. \tag{10}$$

By comparison with quantum mechanics we recognize the Hamiltonian as a sum (integral) over harmonic oscillators, one for each mode k. Accordingly, we assume the existence of a ground state $|0>$ annihilated by $a(k)$ for all k:

$$a(k)|0>= 0. \tag{11}$$

We also want to define normalized states

$$a^\dagger(k)|0>= |k>. \tag{12}$$

But the energy of this ground state is ill defined

$$\int^\infty dk \; \omega_k = \infty. \tag{13}$$

We discard the unobservable ground state energy by introducing a normal ordering of creation operators $a^\dagger(k)$ and annihilators $a(k)$. We write all creation operators to the left, and all annihilators to the right:

$$:a(k)a^\dagger(k'): \; = 0, \; :a^\dagger(k)a(k'): \; = a^\dagger(k)a(k'), \tag{14}$$

$$\Rightarrow H = \int d^3k \; \omega_k \; :a^\dagger(k)a(k): \; .$$

---

[2] $\phi(x)$ transforms as $U\phi(x)U^{-1} = \phi(x')$ which defines it to be a scalar field.

Next we introduce states $|k_1, \ldots, k_n>$ as

$$|k_1, \ldots, k_n> = a^\dagger(k_1), \ldots, a^\dagger(k_n)|0>, \quad <k_1, \ldots, k_n| = <0|a(k_1), \ldots, a(k_n), \quad (15)$$

with normalization

$$<k'|k> = <0|a(k')a^\dagger(k)|0> = <0|[a(k')a^\dagger(k) - a^\dagger(k')a(k)]|0> = \delta(\mathbf{k} - \mathbf{k'}). \quad (16)$$

We interpret the states above as multiparticle states for particles with momenta k_i. There are no interactions present, cf. Fig.(1). By now we have achieved the
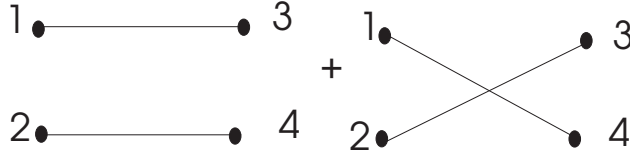

Figure 1: It is easy to see that states like $<k_1, k_2|k_3, k_4>$ can be graphically represented as above. Their normalization demands either $k_1 = k_3$, $k_2 = k_4$ or $k_1 = k_4$, $k_2 = k_3$. In general, multiparticle states $<k_1, \ldots, k_n|q_1, \ldots, q_m>$ do vanish for $n \neq m$, and for $n = m$ their normalization delivers all pairings of the k_i with the q_j. There is no interaction between the straight lines corresponding to these pairings, which is indicated by straight lines in the figure. The straight line represents an incoming particle with momentum k_i propagating undisturbed to become an outgoing particle with momentum $q_j = k_i$.

quantization of the free Klein Gordon field.

To proceed, we introduce a source term in the Klein Gordon equation:

$$(\Box + m^2)\phi = J(x). \quad (17)$$

We look for a Green-function (the propagator) $\Delta_F(x - y)$ solution of

$$(\Box + m^2)\Delta_F(x - y) = -\delta^4(x - y). \quad (18)$$

One easily sees that

$$\begin{aligned}
\Delta_F(x - y) &= \int \frac{d^4k}{(2\pi)^4} e^{-ik(x-y)} \Delta_F(k), \\
\Delta_F(k) &= \frac{1}{k^2 - m^2 + i\eta},
\end{aligned} \quad (19)$$

is a solution, where the presence of the small imaginary part $i\eta$ specifies boundary conditions.[3] Using our Ansatz for the fields ϕ one finds that the propagator can be written with the help of a time-ordered product T:

$$\begin{aligned}
\Delta_F(x - y) &= <0|T[\phi(x)\phi(y)]|0>, \\
T[\phi(x)\phi(y)] &:= \phi(x)\phi(y) \Leftrightarrow x_0 > y_0, \\
T[\phi(x)\phi(y)] &:= \phi(y)\phi(x) \Leftrightarrow y_0 > x_0.
\end{aligned} \quad (20)$$

---

[3] One can show that these boundary conditions are in accord with causality: positive energy solutions propagate forwards in time. Nevertheless, in a relativistic covariant theory we also have negative energy solutions propagating backwards in time, corresponding to antiparticles propagating forwards in time.

Having solved for the Green function of the Klein Gordon field we are ready to introduce perturbation theory. To get acquainted with it, we consider an example borrowed from non-relativistic quantum mechanics. We assume the existence of a Hamiltonian $H = H_0 + H_I$, with a free part H_0 and an interaction term H_I. The Schrödinger equation is

$$(i\partial_t - H)\psi = 0 \;\Rightarrow\; (i\partial_t - H)G(\mathbf{x}, t; \mathbf{x}', t') = \delta^3(\mathbf{x} - \mathbf{x}')\delta(t - t'), \qquad (21)$$

and we can use the Green function $G(\mathbf{x}, t; \mathbf{x}', t')$ to express the wave function using Huygens principle:

$$\psi(\mathbf{x}, t) = \int d^3x' G(\mathbf{x}, t; \mathbf{x}', t')\psi(\mathbf{x}', t'), \;\; t > t'. \qquad (22)$$

Pondering the trivial identity

$$\frac{1}{A + B} = A^{-1} - A^{-1}BA^{-1} + A^{-1}BA^{-1}BA^{-1} + \ldots, \qquad (23)$$

and setting

$$A = -H_0 + i\partial_t \;\;,\;\; B = -H_I,$$
$$G = \frac{1}{A + B} \;\;,\;\; G_0 = \frac{1}{A}, \qquad (24)$$

we get a solution for the Green function in terms of iterated interactions, graphically described in Fig.(2):

$$
\begin{aligned}
G(\mathbf{x}, t; \mathbf{y}, s) \;\; &= \;\; G_0(\mathbf{x}, t; \mathbf{y}, s) \\
&\;\;\;\; + \int d^4x' G_0(\mathbf{x}, t; \mathbf{x}', t')H(\mathbf{x}', t')G_0(\mathbf{x}', t'; \mathbf{y}, s) + \ldots, \\
G \;\; &= \;\; G_0 + G_0 H G_0 + \ldots \text{higher order in } H. \qquad (25)
\end{aligned}
$$

Figure 2: The full Green function G is a series starting with the bare Green function G_0, denoted by a straight line in the above. Interaction (for example with a classical background field $\cong$ dotted lines) takes place at various points, which we describe by vertices. We have to integrate over these points. Asymptotically, we assume that we have incoming and outgoing plane waves.

We can define the matrix element between an initial plane wave and a final plane wave:

$$S_{fi} := \delta_{fi} + \int d^4x' \phi^*(x')H_I(x')\phi(x') + \ldots, \qquad (26)$$

where we used that we can express the free Green function G_0 itself in terms of plane waves.

We now want to come back to relativistic quantum field theory. We change from non-relativistic single-particle quantum mechanics to relativistic multi-particle quantum field theory. Instead of considering the interaction with a classical source we will have to consider the full selfinteraction of a quantized field. Nevertheless, we will see that perturbation theory still allows for a pictorial representation, and will now sketch the remaining steps leading us to the celebrated Feynman rules.

We are interested in the S-matrix. It describes transitions between incoming particles and final particles. This is the sitution which we confront in particle physics: one has a set of well defined incoming particles $|i>_{in}$ (prepared in some beam, say) assumed to be non-interacting, one further has an interaction regime (a collision, say, of two beams or a beam and a target) and detects a set of outgoing particles $|f>_{out}$, again assumed to be non-interacting.

We define the S matrix, which describes the probability of a transition from an initial state $|i>_{in}$ to a final state $|f>_{out}$.

$$S_{f,i} := {}_{out}<f|i>_{in} . \tag{27}$$

We assume that the asymptotic states ${}_{out}|f>$ and $|i>_{in}$ are related by a basis transformation:

$$|f>_{in} = R|f>_{out}, => S_{f,i} = {}_{in}<f|R|i>_{in} = {}_{out}<f|R|i>_{out} . \tag{28}$$

Asymptotic states are assumed to fulfil the free Klein Gordon equation, and thus allow for a spectral decomposition similar to a free field:

$$|q>_{in} = a^\dagger(q)|0>, \tag{29}$$

where $a^\dagger(q)$ is the usual generator of a free one-particle state with momentum q. Our goal is to replace the fully interacting field ϕ everywhere by asymptotic fields,[4] as we did before in the quantum mechanics example. This is the so-called LSZ formalism [19]. After a bit of algebra using the explicit representation of $a^\dagger$ in terms of free fields one finally obtains

$$
\begin{aligned}
{}_{out}<p_1, \ldots, p_n|q_1, \ldots, q_m>_{in} = \\
(iZ^{-\frac{1}{2}})^{n+m} \int d^4 y_1 \ldots d^4 x_m \prod_{i=1}^{n} \prod_{j=1}^{m} e_{p_i}^*(y_i) e_{q_j}(x_j) \\
\times (\Box + m^2)_{y_1} \ldots (\Box + m^2)_{x_m} \\
<0|T[\phi(y_1) \ldots \phi(x_m)]|0>,
\end{aligned}
\tag{30}
$$

where $e_q(x) := e^{iqx}/\sqrt{2\omega_q(2\pi)^3}$. We have expressed the abstract S-matrix element as a vacuum expectation value of fully interacting fields. To find such expectation values we again refer to perturbation theory. As an example, we consider an

---

[4]Asymptotically, we assume that the free fields and the full interacting fields are connected in the weak sense: $\lim_{t \to \infty} <r|\phi|s> = Z^{\frac{1}{2}} <r|\phi_{in}|s>$. At asymptotic times before any interaction takes place the matrix elements of the full field approach the matrix elements of the free field.

interaction Hamiltonian

$$H_I = \int d^3x \, \mathcal{H}_I = \int d^3x \, \frac{g}{4!}\phi^4. \tag{31}$$

Assuming the existence of an unitary operator $U(t)$ such that

$$\phi(\mathbf{x},t) = U(t)\phi_{in}(\mathbf{x},t)U^{-1}(t), \tag{32}$$

one can show that $U(t)$ fulfils the requirements of a time evolution operator

$$U(t) := U(t,-\infty), \ U(t_1,t_1) = 1,$$
$$U^{-1}(t_1,t_2) = U(t_2,t_1), \ U(t_1,t_2)U(t_2,t_3) = U(t_1,t_3), \tag{33}$$

with boundary condition $\lim_{\to\infty} U(-t)|0> = |0>.$[5] $U(t)$ being a time evolution operator, it fulfils a differential equation:

$$\partial_t U(t) = -iH_I(t)U(t). \tag{34}$$

Solving this equation as an exponential one finally obtains a perturbative expansion for $U(t)$:

$$U(t) = 1 + \sum_{n=1}^{\infty} \frac{(-i)^n}{n!} \int_{-\infty}^{t} d^4x_1 \int_{-\infty}^{t} d^4x_2 \ldots \int_{-\infty}^{t} d^4x_n T[H_I(x_1)\ldots H_I(x_n)], \tag{35}$$

which eventually serves to give the perturbation expansion for the Green function

$$G(x_1,\ldots,x_n) := <0|T[\phi(x_1)\ldots\phi(x_n)]|0> \tag{36}$$

as

$$G(x_1,x_2,\ldots,x_n) =$$
$$\sum_{m=1}^{\infty} \frac{(-i)^m}{m!} \int_{-\infty}^{\infty} d^4y_1 \ldots d^4y_m <0|T[\phi_{in}(x_1)\ldots\phi_{in}(x_n)H_I(y_1)\ldots H_I(y_m)]|0> \tag{37}$$

From these vacuum correlators one can obtain all S-matrix elements.

We see that we obtain the Green function as a time ordered product of free fields, with interactions H_i inserted at various points. We proceed by using the Wick theorem. This theorem allows us to express the time-ordered product of fields as a normal-ordered product (which has vanishing vacuum expectation value by definition Eq.[14]) and products of free propagators. Using the spectral properties of free fields one easily establishes

$$T[\phi_{in}(x_1)\phi_{in}(x_2)] =: \phi_{in}(x_1)\phi_{in}(x_2) : + <0|T[\phi_{in}(x_1)\phi_{in}(x_2)]|0>, \tag{38}$$

---

[5]The assumption that such an unitary operator connecting the full field ϕ and the asymptotic field ϕ_{in} exists cannot be maintained in a strict approach to QFT and has to be relaxed somewhat. A good account of the problem can be found in [20]. Nevertheless, it allows a quick derivation of perturbation theory. It is not understood why, then, perturbation theory works so well.

and derives the vacuum expectation of free fields as

$$< 0|T[\phi_{in}(x_1)\phi_{in}(x_2)\ldots\phi_{in}(x_n)]|0> = \sum_{\text{perm}} < 0|T[\phi_{in}(x_1)\phi_{in}(x_2)]|0 > \ldots$$
$$< 0|T[\phi_{in}(x_{n-1})\phi_{in}(x_n)]|0 > . \quad (39)$$

Upon using Eq.(18) one can discard the Klein-Gordon factors in Eq.(30) as they become delta functions.

Finally we obtain to first order in H_I for our example of $H_I \sim \phi^4$

$$G(x_1, x_2, x_3, x_4) = -\frac{ig}{4!}\int d^4y < 0|T[\phi_{in}(x_1)\ldots\phi_{in}(x_4)\phi_{in}(y)^4]|0> + \ldots =$$
$$(-ig)\int d^4y \prod_{i=1}^{4}(-\Delta_F(x_i - y)) + \ldots, \quad (40)$$

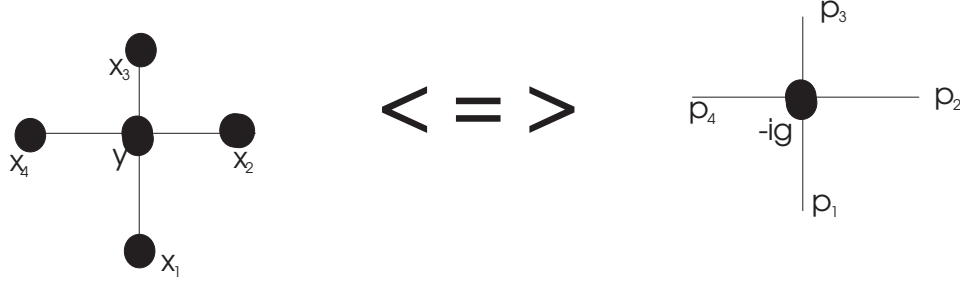which is described in Fig.(3). We are now prepared to introduce the Feynman rules

Figure 3: A graphical illustration of Eq.(40). Upon Fourier-transformation we obtain overall momentum conservation $p_1 + p_2 + p_3 + p_4 = 0$, where $\Delta_F(x_i - y) = \int d^4p_i e^{ip_i(x_i-y)}/(p_i^2 - m^2 + i\eta)$.

of the theory. We give them in momentum space. So we Fourier transform all our Green functions and use the Fourier transformed propagators $\Delta_F(q_i)$. We can now do the y integral in Eq.(40). It delivers a δ-function which guarantees momentum conservation: $\int d^4y \ \exp[i(p_1 + p_2 + p_3 + p_4)y] = \delta^4(p_1 + p_2 + p_3 + p_4)$. Note that we only Fourier transform the arguments of the Green functions. Internal points like y are to be integrated. In momentum space this amounts to an integration over internal loop momenta, which appear when we have closed loops in the graph.

So here come the Feynman rules for ϕ^4 theory:

- For each internal scalar field line, associate a propagator given by:
  $i\Delta_F(p) = \frac{i}{p^2-m^2+i\eta}$,

- at each vertex place a factor of:
  $-ig$,

- for each internal loop, integrate over:
  $\int \frac{d^4q}{(2\pi)^4}$, where q is a loop momentum.

11

- Divide by the symmetry factor of the graph G, which is assumed to contain r vertices, say. It is given by the number of possibilities to connect r vertices to give G, divided by $(4!)^r$.

The reader can easily check that the free propagator is a solution of the free Klein-Gordon equation, and that the vertex is mainly the coefficient of the interaction term in the Lagrangian.

We can now use these Feynman rules to construct the perturbative expansion of the Green functions. Fig.(4) gives examples, this time for a theory with a cubic selfinteraction.
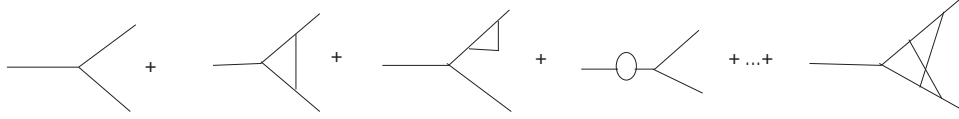

Figure 4: Increasing the number of interaction terms amounts to a loop expansion of the theory. This time we consider an interaction of the form $g\phi^3$, so that three free propagators merge at a vertex. Each extra propagator provides a factor g^2, so that a n-loop graph provides a correction of order g^{2n}. These loop graphs have to be integrated over internal loop momenta. This corresponds to a sum over all possibilities for the momenta of the internal particles. Momentum conservation at each vertex, and the resulting overall momentum conservation for external particles, are not able to fix these internal loop momenta. They have to be integrated over the full four dimensional d^4q space.

At this stage we pause. We can use the Feynman rules to build an expansion in graphs with increasing loop number, for a given Green function. This amounts to a perturbative expansion in the coupling constant. Such an approach has proven extremely successful in particle physics. Nevertheless, there is a major obstacle: the presence of divergences in these integrals with respect to the internal loop momenta. So, having established the Feynman rules, we immediately run into a problem. To see the obstacle consider a one-loop graph like Fig.(5) for ϕ^3 theory in six dimensions. According to our Feynman rules we have to integrate the internal
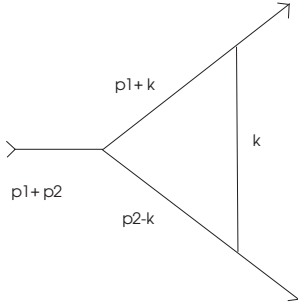

Figure 5: Such a one-loop graph demands an integration of internal momenta. It turns out to be ill-defined. This is a well-known obstacle in pQFT.

momentum. The analytic expression is of the form

$$\int d^6 k \frac{1}{[k^2 - m^2 + i\eta][(k+p_1)^2 - m^2 + i\eta][(k-p_2)^2 - m^2 + i\eta]}$$
$$\sim \int d^6 k \frac{1}{k^6} \sim \int^\infty \frac{dx}{x}. \qquad (41)$$

It is apparent that the integration is ill-defined. In fact, these so-called UV-divergences are the focus of this paper. They appear in all pQFT which are of interest in particle physics. The name stems from the fact that they appear at large internal momentum, corresponding to large internal (ultraviolet) energies. We want to understand how a theory plagued by such infinities can still be well-defined and able to deliver sensible predictions, how it can be *renormalized*.

2.2 The idea of renormalization

The theory we want to explore to understand renormalization is ϕ^3 theory in six dimensions (ϕ^3_6). We will see soon that precisely in six dimensions the theory provides all typical properties of a renormalizable theory. Other theories which we will refer to are given in the appendix. We recall the Lagrangian of ϕ^3_6:

$$L = \frac{1}{2}(\partial_\mu \phi)^2 - \frac{1}{2}m^2 \phi^2 + \frac{g}{3!}\phi^3. \qquad (42)$$

Before we start to introduce renormalization which gives a meaning to our momentarily ill-defined field theory we have to introduce regularization. This serves the more modest demand to give a meaning to the ill-defined loop integrals themselves. In fact, the whole purpose is to have a calculational tool which maps these loop integrals to some Laurent series. This series is with respect to some regularization parameter, and the pole terms in the series should reflect the divergences of the integrals. The most common regulator is dimensional regularization. For our purposes, it is sufficient to define it by the following formulas [11]

$$\int d^D k \frac{[k^2]^a}{[k^2 - m^2]^b} = \pi^{D/2}[-m^2]^{D/2+a-b}\frac{\Gamma(a + \frac{D}{2})\Gamma(b - a - \frac{D}{2})}{\Gamma(\frac{D}{2})\Gamma(b)}, \qquad (43)$$

$$\int d^D k \frac{1}{[k^2]^a\,[(k+q)^2]^b} = \pi^{D/2}[q^2]^{\frac{D}{2}-a-b}\frac{\Gamma(a+b-\frac{D}{2})\Gamma(\frac{D}{2}-a)\Gamma(\frac{D}{2}-b)}{\Gamma(a)\Gamma(b)\Gamma(D-a-b)} \qquad (44)$$

$$\int d^D k (k^2)^\alpha = 0, \ \forall \alpha. \qquad (45)$$

Whenever the parameter D equals the space-time dimension N of the field theory under consideration we recover the original integrals. For small deviations from this integer, we obtain a Laurent series in $2\epsilon := N - D$, which serves as our regularization parameter. For example, the above graph in ϕ^3 theory delivers[6]

$$G(p_1, p_2, m^2) = g^3 \frac{1}{2^D \pi^{D/2} 2\epsilon} + g^3 F(p_1, p_2, m^2) + \mathcal{O}(\epsilon), \qquad (46)$$

---

[6]conventions as in [11]. In our conventions, we would drop the $\frac{1}{2^D \pi^{D/2}}$-term. See the appendix for our conventions.

where $F(p_1, p_2, m^2)$ is independent of ϵ. Note that the pole term is independent of masses and momenta p_1, p_2. In general, one obtains a proper Laurent series in $D-N$ of degree n in a n-loop calculation. The pole terms reflect the UV-divergences of the Feynman graphs. Renormalization theory dictates how to handle these divergences. For the moment we want to have a first look at renormalization theory in action by handling the divergences present up to order g^2 in the coupling which is the one-loop case. Let us rewrite the Lagrangian

$$L = Z_2 \frac{1}{2}(\partial_\mu \phi)^2 - Z_m \frac{1}{2}m^2\phi^2 + Z_1 \frac{g}{3!}\phi^3. \tag{47}$$

We want to derive conditions for these Z-factors so that they could render the theory finite. First we note that they correspond to a change in the Feynman rules:

- vertex: $ig \to iZ_1 g$,

- propagator: $\frac{1}{k^2 - m^2 + i\eta} \to \frac{Z_2}{k^2 - Z_m m^2 + i\eta}$.

Now, for simplification, we assume to live in a world where only this vertex correction is divergent. Accordingly we set $Z_m = Z_2 = 1$ and check if we can determine Z_1 as to render the theory finite. The new Feynman rules change the result for the one-loop graph

$$G^{(1)}(p_1, p_2, m^2) = Z_1^3 \left[g^3 \frac{1}{2^D \pi^{D/2} 2\epsilon} + g^3 F(p_1, p_2, m^2) + \mathcal{O}(\epsilon) \right]. \tag{48}$$

We know already that the pole term of the one-loop expression is independent of masses and momenta.

Our one-loop vertex function $G^{(1)}(p_1, p_2, m^2)$ is of order g^3, while the tree level vertex ($\sim \Gamma^{(0)}$) is g.[7] We want to render the theory finite at the one-loop level which means that we want to have a finite result to order g^3 for the vertex function. With our modified Feynman rules, to order g^3 we have

$$\Gamma(p_1, p_2, m^2) = Z_1 g + Z_1^3 (g^3 \frac{1}{2^D \pi^{D/2} 2\epsilon}) + \dots, \tag{49}$$

where now $\Gamma(p_1, p_2, m^2)$ refers to the amputated Green function where the external propagators have been removed. We see that Z_1 must have the following form

$$Z_1 = 1 - \frac{g^2}{2^6 \pi^3 2\epsilon}. \tag{50}$$

To make the one-loop renormalization complete, we would have to include also the other Z-factors, all of them of the form

$$Z_i = 1 - \sum_{j=1}^{\infty} \sum_{k=0}^{j} (g^2)^j \frac{c_{jk}^{[i]}}{\epsilon^k}. \tag{51}$$

---

[7]To infer the coupling constant from the vertex function we have to strip off the propagators for the external particles. The resulting Green function is called the amputated vertex function $\Gamma(p_1, p_2, m^2)$. It is obtained most easily by multiplication with the inverted propagators in momentum space.

Each monomial in the Lagrangian density obtains such a Z-factor.[8] Theories which can be rendered finite by introducing one Z-factor for each monomial in the original Lagrangian are called renormalizable. We more or less focus on these theories for our purposes.[9] Higher order corrections -loop corrections- are obtained by considering the Green-functions for each of these monomials, with $< 0|T[\phi_{in}(x_1)\phi_{in}(x_2)]|0 >$ generating divergences to be absorbed by Z_2 and Z_m, while the divergences in $< 0|T[\phi_{in}(x_1)\phi_{in}(x_2)\phi_{in}(x_3)|0 >$ demand Z_1 as well.

Let us come back to our example. Assume that we also have determined Z_m, Z_2 so that the two- and three-point Green functions are finite at the one-loop level. But these finite values are not determined yet. They depend on our choice for the Z factors, according to Eq.(51). Assume further that we now calculate some n-point Green function, $n \geq 4$, at the one-loop level. Fig.(6) gives examples for the four-point function. Finally assume that we determine the Z factors so that the
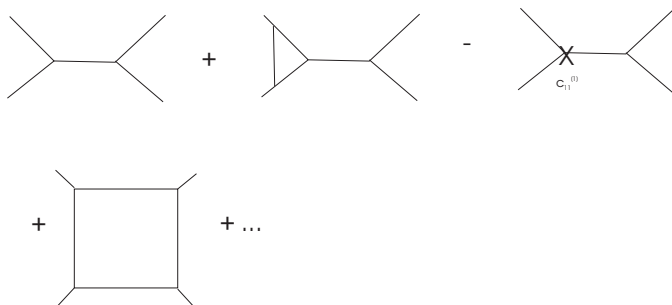

Figure 6: All divergences of the four-point Green function $G(x_1, x_2, x_3, x_4)$ in ϕ_6^3 stem from divergences of two- and three-point functions. Our Z-factors remove these divergences, but the result for the four-point function depends on the finite values of our *counterterms*. We only indicated divergences resulting from the vertex function Eq.(49) and indicate the contribution from the Z_1 factor by a cross. Each divergent vertex function has a compensating counterterm at the same order in the coupling.

values for masses and coupling constants inferred from Green functions $G(x_1, x_2)$ and $G(x_1, x_2, x_3)$ coincide with the experimental values for masses and coupling constants. Specifying such a set of *renormalization conditons* determines the finite part in the Z-factors. Renormalization conditions as just described are known as on-shell conditions. We do not use them here. We are solely interested in the divergences of the theory. In this paper we use MS conditions, for which all $c_{j0}^{[i]} = 0$. With these conditions one only removes the pure UV divergences, so that $\overline{\text{MS}}$ Z-factors provide a book-keeping of the UV singular structure of the theory - with this choice we subtract only the pure pole part of the Green functions.

---

[8] In our notation $c_{11}^{[1]} = \frac{1}{2(2^6\pi^3)}$.

[9] One can relax this restriction somewhat. Calculable theories may have an increasing number of terms in the Lagrangian. At each loop order the need to compensate divergences introduces new monomials in it. As long as the number of these monomials remains finite at each loop order, one still can give these theories some sense. It is an open research problem to what extent the results obtained in this paper generalize to such theories.

We make this choice only for the Green functions which suffer from divergences. Their finite values cannot be predicted by a renormalizable theory. They have to be taken from experiment, if one wants to test the theory. But then all other Green functions can be calculated in a unique manner. So the result for the four-point function in Fig.(6) is all fixed. Success or failure of pQFT then depends on the answer to the following question: Do the S-matrix elements for processes involving Green functions like the above four-point function (involved in $2->2$ particle scattering for example) correctly describe experimentally observed cross sections for these processes? Will our pQFT be predictive for general S-matrix elements, once a finite set of parameters is taken from experiment? The answer is affirmative; any observed particle scattering process is successfully described by a renormalizable pQFT. This is the motivation for pQFT, and the motivation for the enormous effort put into loop calculations these days.

Let us now understand renormalization in more detail. We have to clarify the following points:

- We need a notion how to decide if a given Green function is plagued by infinities - we have to introduce power-counting.

- We have to understand how subdivergences are entangled - we have to introduce nested and overlapping subdivergences.

- We have to understand how to iterate the process of cancellation of divergences with the help of Z-factors - we have to understand the iterative structure of renormalization.

We will introduce these notions by simply considering a two-loop example. Consider Fig.(7). It is a two-loop graph. This is obvious by inspection. We can also
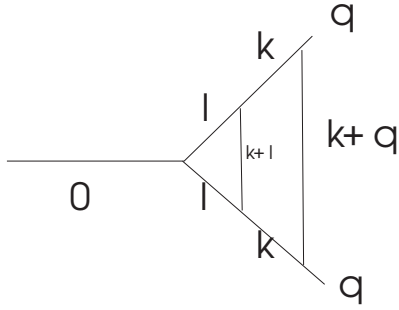

Figure 7: Momentum flow in the two-loop graph. We recognize the one-loop vertex as a subgraph.

infer this from counting the number of propagators. The one-loop vertex correction has three internal propagators. In the next loop order we have to specify two points somewhere in the one-loop graph, which become internal vertices and are to be connected by a propagator. Altogether this generates three more propagators. In general for a theory with a cubic interaction each loop order produces three more propagators. So the number of propagators determines the loop order. In our example we have realized a very special two-loop graph. We see that the one loop

graph is nested in the whole graph as a subgraph. So what are our expectations for the divergent structure of the graph? We have two internal loop momenta. We route them as indicated in the figure. The loop momentum l runs solely through the one-loop subgraph. We do expect to see a divergence when $l \to \infty$ simply because the one-loop subgraph is the divergent one-loop vertex function of Fig.(5), only this time with momenta $0,k,k$ at its vertices. So for any finite value of k we expect a divergence from large l. Now assume we keep l fixed, with $k \to \infty$. We observe that k runs through a four-point function, and thus through four propagators. It converges: $\int d^6k/k^8$ is finite for large k. So we expect no divergence from the sector (l fixed, $k \to \infty$).

Let us next consider the sector where ($l \to \infty, k \to \infty$) jointly, $k \sim l$. Altogether our two-loop graph has six internal propagators. Each propagator behaves as $1/l^2$ or $1/k^2$. In the region $l \sim k$ the whole integrand behaves as $1/l^{12}$, and the whole graph as $\int d^6k d^6l \frac{1}{(l^4(l+k)^2k^6)} \sim \int dr/r$. So we expect a divergence for large l and k. We call it a logarithmic degree of divergence for obvious reasons.

That this somewhat naive analysis is correct and the determination of divergent sectors reduces to a counting of propagators ("edge counting") is due to Weinbergs theorem [6]. The resulting method we now describe is known as power counting.

Any graph consists of a product of propagators. Let us assume that our Feynman rules are such that all vertices are dimensionless.[10] Each propagator P_i has a weight c_i. We determine this weight as the degree of the inverse propagator, for example for a scalar propagator $1/(p^2 - m^2)$ the degree is two, because the inverse propagator behaves as p^2 for large p. We consider a n-loop Feynman graph. Each loop contributes an N-dimensional integration measure, with $N = 6$ in our ϕ_6^3 example. Assume we have n_i propagators of weight c_i in the graph, and r different sorts of propagators altogether. Then we call a graph overall divergent if

$$\omega := nN - \sum_{j:=1}^{r} c_j n_j \geq 0. \tag{52}$$

For Fig.(5) and Fig.(7) we have $\omega = 0$. Such graphs we call logarithmic divergent, while $\omega = 1$ or 2 refers to linear or quadratic divergent graphs.

A few remarks are in order. Note that an addition of extra loops will not change the degree of divergence in our ϕ_6^3 theory. Any new loop generates three more propagators, while on the other hand we have one more integration to do. So the net change vanishes: $6 - 2 \times 3 = 0$. So in six dimension any three point vertex function in ϕ^3 theory is overall logarithmic divergent, while any two-point function is overall quadratic divergent and any Green function with four or more external particles remains overall convergent. This depends on the dimension. In $d < 6$ dimensions for example even the vertex function in ϕ^3 is overall convergent, and addition of further loops reduces the degree of divergence by $d - 6$. On the other hand, in $d > 6$ dimension any r-point Green function becomes divergent for a sufficiently high loop-number, as $d - 6$ now worsens the degree of divergence with each loop number.

---

[10]Otherwise we have to count weighted vertices as well in our powercounting. The weight of the vertices here is zero.

We call $d = 6$ the critical dimension of ϕ^3 theory. It is renormalizable in this dimension. Precisely in this critical dimension the coupling constant is dimensionless. Only the Green functions corresponding to fundamental monomials in the Lagrangian evolve divergences in loop integrals. In $d > 6$ dimensions the theory becomes non-renormalizable. Any Green function diverges at a sufficiently high loop number. The coupling constant has negative dimension. In $d < 6$ dimension the theory is superrenormalizable. Divergences appear only at a sufficiently low loop number and the coupling constant has positive dimension.

These notions of criticality and renormalizability extent to other pQFT in an obvious manner. All other theories we refer to in this paper are critical in four dimensions. Particle physics seem to favour pQFTs which are critical in four dimensions.

Back to our two-loop example in Fig.(7). Power counting tells us that it has an logarithmic overall degree of divergence. We also expect a divergence from its one-loop subgraph. We can indeed extend the notion of powercounting in an obvious manner. Let us in our mind put a little box around any divergent subgraph g_i which we detect in a Feynman graph G. We do a powercounting for the Feynman graph in this box, and say that the degree of divergence of the subgraph g_i is its overall degree of divergence ω_i. We then say that G has an overall degree of divergence ω and subdivergences contributed by subgraphs g_i of degree of divergence ω_i.

Fig.(8) provides examples for various different ways how subdivergences can appear. They will all be considered in the following sections. They can come in nested form and as disjoint subdivergences, and they can appear to be overlapping. This last form is the most complicated one. Renormalization theory is an iterative
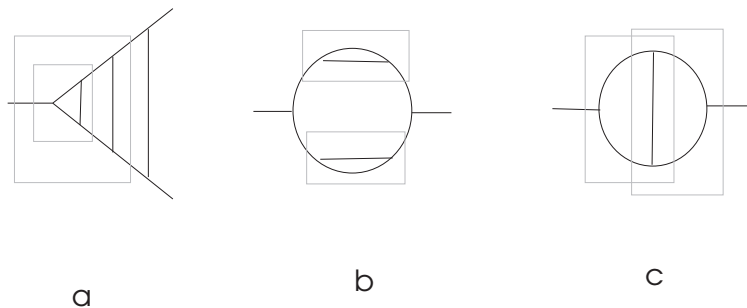

a   b   c

Figure 8: There are various ways subdivergences can appear. They can be nested as in (a), disjoint as in (b) or overlapping as in (c). We put every subdivergence in a dashed box. These boxes are called forests. Forests which are not nested in a larger one are called maximal.

procedure to eliminate the divergences of the theory. One first eliminates the subdivergences, and then hopes to control the remaining overall degree of divergence. This iteration procedure can be summarized in a forest formula [7, 25] but we now rather study our two-loop example to see how the iteration works.

We have already added a one-loop Z_1-factor to our Lagrangian. We are interested now to obtain a finite result at order g^5. At this order we not only have the two-loop graph, but also a one-loop graph with a counterterm insertion from the

renormalization of the one-loop divergence. This term appears due to our replacement $g\phi^3 \rightarrow Z_1 g\phi^3 = g\phi^3 - g^3 \frac{c_{11}^{[1]}}{\epsilon}\phi^3$. We have to add this counterterm graph to the two-loop graph, as it is done in Fig.(9). The counterterm was determined to render
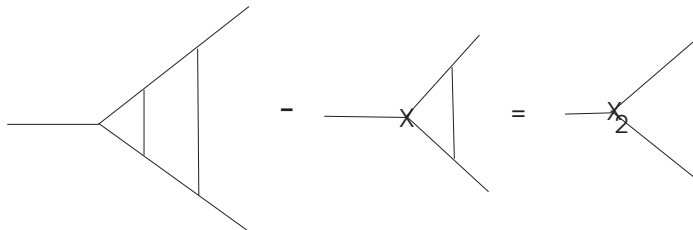

Figure 9: We add a counterterm graph. It absorbs the subdivergence in the subgraph, present for $l \rightarrow \infty$, k fixed. We should also add counterterm contributions at the other two vertices. They would absorb the subdivergences of the two-loop graphs where the one-loop subgraph is located at these other vertices. After subtraction of the one-loop counterterm graph we can determine the two-loop Z-factor, indicated by X_2.

the one-loop vertex function finite. This function appears as a subgraph in the full two-loop graph, and it is indeed so that for any fixed k the difference of the full two-loop contribution and the counterterm contribution is finite. The only remaining divergence appears when both loop momenta tend to infinity jointly. This is the overall divergence. This is true in general. After elimination of all subdivergences by counterterms the remaining divergences appear when all loop momenta tend to infinity jointly.

So now our renormalization program continues as for the one-loop case. The difference of the full two-loop graph and counterterm contribution has the form

$$g^5\left[\frac{c_2}{\epsilon^2} + \frac{c_1}{\epsilon} + \ldots\right] \Rightarrow c_{21}^{[1]} = -c_1, c_{22}^{[1]} = -c_2. \tag{53}$$

and the finite parts $c_{20}^{[1]}$ must again be determined by the renormalization conditions, and do vanish in the MS scheme.[11]

It is only in this combination of the full two-loop graph with the counterterm contribution that the $c_{2i}^{[1]}$, $i \in \{1, 2\}$, come out as pure numbers as they should. The two-loop graph itself will contain divergences of the form $\log q^2/\epsilon$, where the divergence comes from the divergent subgraph, and multiplies a $\log q^2$ which appears in the finite part of the second loop integral. In fact, much more complicated non-polynomial functions of q^2 and masses could be present. Fortunately, after addition of the counterterm contribution, these non-local contributions cancel, and the $c_{2i}^{[1]}$ appear as pure numbers. This is a general property as well: after adding the appropriate counterterms for subdivergences the overall divergences remain local.[12] We will see later explicitly how to handle disjoint or overlapping cases.

The whole renormalization procedure was remarkably successful in QED as well as in the standard model of elementary particle physics and still provides the only systematic mechanism for calculations in elementary particle physics.

---

[11]For ϕ_6^3 one finds explicitely $c_1 = \frac{1}{16(2^{2D}\pi^D)}$ and $c_2 = \frac{-1}{8(2^{2D}\pi^D)}$.

[12]Only polynomials in momenta give local operators after Fourier transformation.

3 Planar Vertex Corrections

In this section we explore algebraic structures of nested divergences as generated by ladder graphs. Ladder topologies are the easiest accessible and serve as a convenient means to introduce our approach. Here we will for the first time draw a connection between renormalization theory and link diagrams. Subsequent sections will show that the connection goes via number theory: the trivial nested topologies considered here provide rational coefficients for the UV divergences, while transcendentals encountered in more complicated examples faithfully describe the knots derived via link diagrams from our Feynman graphs.

3.1 The vertex ladder

We consider theories with renormalizable three-point couplings. As pointed out in the previous remarks on renormalization theory this means for us a theory with vertex corrections of logarithmic degree of divergence, corresponding to a dimensionless coupling constant. Further, for simplification, we again restrict ourselves to vertex corrections. We collect our conventions in an appendix.

Let us simplify for a start even further to topologies of the form given in Fig.(10). We have omitted all dressing of the internal vertices and propagators here. In gen-
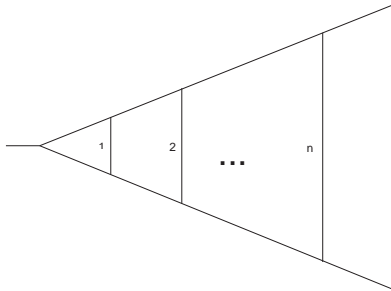

Figure 10: The ladder topology for vertex corrections. We indicate loop momenta $l_1, \ldots, l_n$. The ladder topology might be realized by different Feynman graphs. Our graphical representation of Feynman diagrams usually refers only to the topology of the graph, so that lines may describe various different particles according to the Feynman rules of the theory.

eral, the iteration of loops is controlled by the Schwinger-Dyson equations. We explain these equations in Fig.(11). These equations nicely organize the perturbative expansion. Each Feynman diagram consists of propagators and vertices. These are themselves Green functions which allow for a perturbative expansion. The Schwinger Dyson equations are coupled integral equations which iterate these Green functions in terms of themselves. Knowing their full solution would correspond to knowing the full non-perturbative Green functions. A peculiar role is played by the skeleton diagrams. They furnish four-point functions which serve as a kernel in the Schwinger Dyson equations. These skeleton diagrams are Feynman diagrams which are the basic blocks of iteration in the equations. Any proper skele-

ton contribution is not two-line reducible. When we close two of its lines we get a vertex function free of divergences, as long as the vertices and propagators of the skeleton were undressed, cf. Fig.(12).
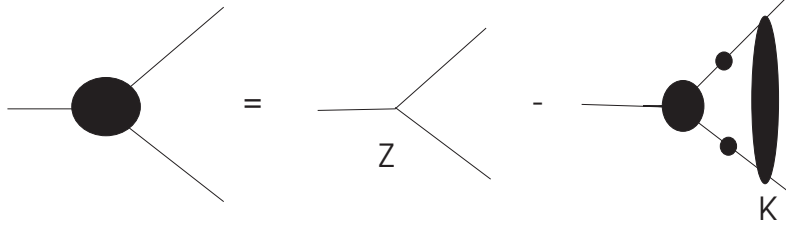

Figure 11: We can generate the full three-point Green function iteratively. An integration over the internal momentum in the loop on the rhs is understood. The kernel K allows a skeleton expansion. Usually, all propagators and internal vertices represent the full Green-functions, and the coupled system of equation for these functions is hard to solve. Full Green functions are indicated by black blobs. In the ladder approximation considered here we restrict ourselves to bare propagators (indicated by straight lines), bare internal vertices (no blobs) and to the lowest order in the skeleton expansion.
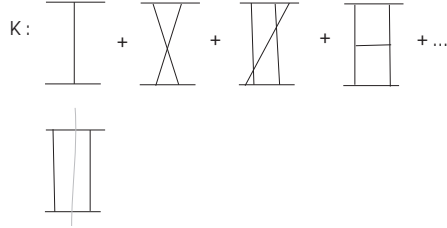

Figure 12: The skeleton expansion given for bare internal propagators and vertices. In its dressed form (reinserting blobs for very internal vertex or propagator) it generates the kernel K of the Schwinger Dyson equations. Note that the lowest order skeleton is the one-particle exchange graph of order g^2. We also indicate a graph which is not a skeleton. It is an iteration of the lowest order skeleton. It separates in two pieces when we cut it a two propagators, and thus it is two-line reducible.

In our limit, the Schwinger Dyson equation generates the ladder graphs by iteration of the lowest order in the skeleton:

$$\begin{aligned}
\Gamma(p_1, p_2) &= Z_g \Gamma^0 \\
&\quad - \int d^D k \ \Gamma^0 D(k) \ \Gamma^0 \ D(k+p_1) \ \Gamma(k+p_1, k-p_2) \ D(k-p_2), \quad (54)
\end{aligned}$$

here Γ^0 is the tree-level vertex, and D the bare propagator, which is the inverse of the free Klein-Gordon equation.[13] The equations thus iterate the full vertex Γ in terms of itself and the propagator function D.

For a start let us simplify even more and consider the two-loop case as in Fig.(13).

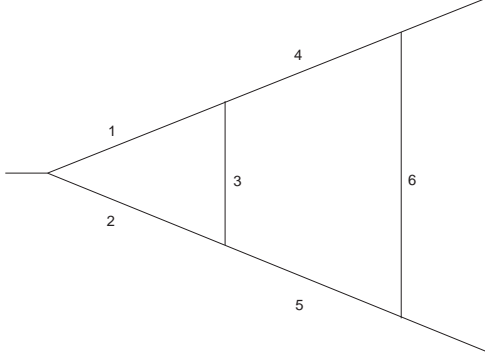[13]Or the inverse of any other appropriate equation of motion.

Figure 13: The two-loop function of the previous section. Our considerations are now valid for any Green function in a pQFT realizing this topology. We denote propagators by numbers for later reference.

Normally, one would calculate this graph, then calculate its counterterm graphs (thereby incorporating the one-loop Z-factor), and finally add all contributions. This is what we did in the previous section. In the sum one would observe all the expected cancellations necessary to give a local two-loop Z-factor. One might do better by subtracting out the subdivergences from the very beginning. Thus, subtract from this vertex correction $\Gamma^{(2)}$ another vertex function, forming a new function $\Gamma_\Delta^{(2)}$:

$$\Gamma_\Delta^{(2)} := \Gamma^{(2)} - \tilde{\Gamma}^{(2)}, \tag{55}$$

where we define

$$\tilde{\Gamma}^{(2)} := \Gamma^{(2)} \mid_{m_1=m_2=m_3=p=0}; \tag{56}$$

in $\tilde{\Gamma}^{(2)}$ we have set all masses in the subdivergence to zero and evaluate the vertex at zero momentum transfer. Due to the fact that the subdivergence itself is independent of the masses and exterior momenta, $\Gamma_\Delta^{(2)}$ is a finite Green function:

$$\Gamma_\Delta^{(2)} = \int (\Gamma^{(1)} - \tilde{\Gamma}^{(1)})K, \tag{57}$$

is finite. This is also clear as the iteration of the integral kernel K, -which is a finite four-point function-, with the finite $(\Gamma^{(2)} - \tilde{\Gamma}^{(2)})$ has a subtracted form.
Three examples:[14]
for ϕ^3 in six dimensions we have

$$\tilde{\Gamma}^{(2)} = \int d^D l d^D k \, \frac{1}{l^4(l+k)^2(k^2-m^2)^2((k+q)^2-m^2)}, \tag{58}$$

---

[14]For all these examples one can consider the difference in Eq.(57). For power counting purposes one considers the equation on a common denominator and easily verifies its finiteness.

with a tree-level vertex $\Gamma^0 = 1$, while for massive QED in four dimensions, in the Feynman gauge

$$\tilde{\Gamma}_\sigma^{(2)} = \int d^D l \, d^D k \; \gamma_\mu \frac{1}{\not{k} - m} \gamma_\rho \frac{1}{\not{l}} \gamma_\sigma \frac{1}{\not{l}} \gamma^\rho \frac{1}{\not{k} - m} \gamma^\mu \frac{1}{(l+k)^2} \frac{1}{(k+q)^2}, \tag{59}$$

corresponding to the Feynman graph in Fig.(14). Here, the tree level vertex is γ_σ. A convenient example is also provided by Yukawa theory, the coupling of a fermion
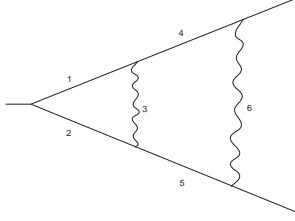

Figure 14: The QED graph corresponding to the example Eq.(59).

to a scalar particle. For a massive fermion, we obtain

$$\tilde{\Gamma}^{(2)} = \int d^D l \, d^D k \; \frac{1}{\not{k} - m} \frac{1}{\not{l}} \frac{1}{\not{l}} \frac{1}{\not{k} - m} \frac{1}{(l+k)^2} \frac{1}{(k+q)^2}, \tag{60}$$

again with a tree-level vertex $\Gamma^0 = 1$. Note that in the above examples the propagators of the innermost loop are massless, according to our definition of $\tilde{\Gamma}$. We see that in all examples the l-integration over the subdivergence becomes particularly simple. It depends solely on the other loop momentum.

Apart from the UV divergences at large internal momentum there are no other divergences present. In particular, we do not encounter IR singularities (which appear for small internal momenta) in any of our considerations.

Now consider $\Gamma_\Delta^{(2)}$. It is UV convergent, both in its subdivergent and overall divergent behaviour, which can as well be concluded from power-counting. Our subtraction at the subdivergence improves the power-counting for the inner loop momentum by one degree, but it improves also the overall degree of divergence by the same amount, as the subtracted term was only modified in exterior parameters like masses and momenta, and the overall degree of divergence is independent of these parameters [22].

Accordingly, we have shown that the UV divergences of Γ are located in a simpler Green function $\tilde{\Gamma}$, where we could set some masses to zero and evaluate the whole function at vanishing momentum transfer.

From now on we make use of the following notation:

$$< \Gamma > = < \Gamma_\Delta + \tilde{\Gamma} > = < \Gamma_\Delta > + < \tilde{\Gamma} > = < \tilde{\Gamma} > . \tag{61}$$

Here we introduce a projector $< \ldots >$ onto the UV-divergences (the proper part of a Laurent expansion of Γ in ϵ, where ϵ is the DR regularization parameter) so that, by definition,

$$< \text{UV-finite expression} > = 0. \tag{62}$$

We also use the n-th order complete Z-factor and various Green functions defined as follows:

$$
\begin{aligned}
\mathbf{Z}_1^n &:= 1 - c_1^{(1)} - c_1^{(2)} \ldots - c_1^{(n)}, \\
\mathbf{\Gamma}^n &:= \Gamma^{(0)} + \Gamma^{(1)} \ldots + \Gamma^{(n)}, \\
\tilde{\Gamma}^{(n)} &:= \Gamma^{(n)}|_{m_1=m_2=m_3=p=0}, \\
\bar{\Gamma}^{(n)} &:= \tilde{\Gamma}|_{m_i=0\forall i}.
\end{aligned}
\tag{63}
$$

We redefined our notation for the Z factor somewhat. Compared with Eq.(51) the c_i incorporate all the pole terms to a given loop order. Note that we have two modified Green functions: $\tilde{\Gamma}^{(n)}$, which has only a modification in its innermost loop, and $\bar{\Gamma}^{(n)}$, where all masses are set to zero. We consider the case of zero momentum transfer throughout.

For the ladder diagrams, the index n coincides with the loop order. Now, having absorbed the UV-divergence of $\Gamma^{(2)}$ in $\tilde{\Gamma}^{(2)}$ let us add the counterterm graph

$$
\tilde{\Gamma}^{(2)} \to Z_1^{(2)} := < \tilde{\Gamma}^{(2)} - Z_1^{(1)}\tilde{\Gamma}^{(1)} >,
\tag{64}
$$

$Z_1^{(2)}$ contains $< \Gamma^{(2)} >$ plus its counterterm graph. We will become more acquainted with its use in the following.

With the above definitions we have

$$
< \tilde{\Gamma}^{(2)} - \bar{\Gamma}^{(2)} - Z^{(1)}(\tilde{\Gamma}^{(1)} - \bar{\Gamma}^{(1)}) >= 0,
\tag{65}
$$

since the overall divergent behaviour of

$$
(\tilde{\Gamma}^{(2)} - Z_1^{(1)}\tilde{\Gamma}^{(1)}),
$$

and

$$
(\bar{\Gamma}^{(2)} - Z_1^{(1)}\bar{\Gamma}^{(1)}),
$$

are the same. This is exactly what we expect. Both expressions have the same asymptotic behaviour with regard to their overall degree of divergence. They further have the same subdivergence $Z_1^{(1)}$. After eliminating this subdivergence by an appropriate subtraction in the first step the difference of the two terms is necessarily UV convergent. This is nothing else than the statement that $Z_1^{(2)}$ must be polynomial in exterior masses and momenta. Powercounting confirms that such trivial subtractions render our two-loop examples finite.

By use of Eq.(65) we have absorbed all UV singularities in the expression

$$
Z_1^{(2)} = \bar{\Gamma}^{(2)} - Z_1^{(1)}\bar{\Gamma}^{(1)}.
\tag{66}
$$

It is significant that *only massless three-point functions at zero momentum transfer* appear in the above expression. The significance stems from the fact that now each loop integration depends only on one parameter: the momentum of the next loop integration. Only the last loop integration depends on the exterior momentum q.

The one-loop Z-factor from the vertex correction, $Z_1^{(1)}$, has the form

$$\bar{\Gamma}^{(1)} = \Delta(\epsilon) \, (q^2)^{-\epsilon} \Gamma^{(0)} \Rightarrow Z_1^{(1)} = < \bar{\Gamma}^{(1)} >, \tag{67}$$

where we used the fact that $\bar{\Gamma}^{(1)}$ scales like $(q^2)^{-\epsilon}$ in DR. This equation means the following: $\bar{\Gamma}^{(1)}$ can only depend on one variable: q^2, the square of the external momentum. Its dependence is determined by the scaling properties of the Green function. $\bar{\Gamma}^{(1)}$ also factorizes the tree level vertex $\Gamma^{(0)}$. The q^2 dependence is a trivial scaling $\sim (q^2)^{(D-N)/2}$, so that $\bar{\Gamma}^{(1)}(q^2) = (q^2)^{(D-N)/2}\bar{\Gamma}^{(1)} \, |_{q^2=1}$, where the exponent $(D-N)/2$ follows from dimensional considerations. $\frac{\bar{\Gamma}^{(1)}|_{q^2=1}}{\Gamma^{(0)}}$ is then a sole function of $\epsilon = (D-N)/2$, which is the content of the previous equation.

As we are calculating in a MS scheme we were allowed to project onto the divergent part in the Laurent expansion of $\bar{\Gamma}^{(1)} \, |_{q^2=1}$. The fact that all the dependence on the exterior momenta q is in the scaling behaviour $(q^2)^{-\epsilon}$ is important. It allows to define a function Δ which only depends on the DR parameter D and incorporates all the information to obtain MS Z-factors.

Let $F(k,q)$ be the integrand for the calculation of $\bar{\Gamma}^{(1)}$. We see that (using Eq.(67))

$$\bar{\Gamma}^{(2)} = \Delta \int d^D k (k^2)^{-\epsilon} F(k,q) = \Delta \, {}_1\!\Delta \, (q^2)^{-2\epsilon} \, \Gamma^{(0)}, \tag{68}$$

where we define for later use ${}_j\!\Delta$ by

$$\int d^D k (k^2)^{-\epsilon j} F(k,q) =: \, {}_j\!\Delta \, (q^2)^{-\epsilon(j+1)}. \tag{69}$$

We consider the functions ${}_j\!\Delta$ as modified one-loop functions. For any renormalized theory they can be obtained from the corresponding standard one-loop integral by a change in the measure

$$\int d^D k \rightarrow \int d^D k (k^2)^{-\epsilon j}.$$

Throughout we tacitly assumed that the massless one-loop vertex function at zero momentum transfer only reproduces the tree-level vertex $\Gamma^{(0)}$ as a form factor (Eq.(67)). This is not necessarily so. Even a theory as simple as massless QED delivers a counterexample, by providing two formfactors, generated by the two spin structures $\gamma_\sigma, q_\sigma \not{q}$. But it turns out that the modifications due to this complication do not spoil our general reasoning. We will present the necessary changes in an appendix.

We denote the parameter j above as the 'writhe number' in the following, for reasons which will become clear below.

Finally, for the two-loop case

$$Z_1^{(2)} = < \Delta \, {}_1\!\Delta - < \Delta > \Delta >, \tag{70}$$

by virtue of Eq.(67,68).

Our next step will be to generalize the above approach to the n-loop case. We still pretend that the world consists only of ladder-type vertex corrections, in which case our approach would deliver the full Z-factor for the vertex correction.

Again we define

$$\Gamma_\Delta^{(n)} := \Gamma^{(n)} - \tilde{\Gamma}^{(n)}, \tag{71}$$

We still evaluate at zero momentum transfer. By setting the masses m_1, m_2, m_3 of the inner loop to zero in the second term we remove *all* subdivergences of the graph. It follows that $< \Gamma_\Delta^{(n)} >= 0$. This is obvious as all existing forests include the innermost loop as a nest. All divergent sectors in Fig.(15), which are all logarithmic divergent, thus have an improvement in power counting when we have such an improvement for this inner loop. It follows as well by considering $\Gamma_\Delta = \int \ldots \int (\Gamma^{(1)} - \tilde{\Gamma}^{(1)}) K \ldots K$, and writing out the iteration of the bubble in the Dyson-Schwinger equations explicitly. To calculate $Z_1^{(n)}$ we have to consider
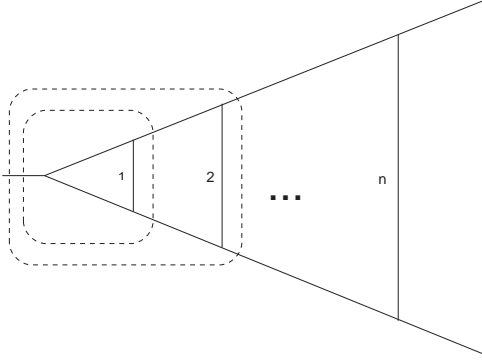

Figure 15: The dashed boxes denote the divergent sectors of the ladder topology. These give rise to the restricted set of counterterms we are interested in. The divergent sectors are, from the left to the right, the domains $\lambda \to \infty$ in $\{\lambda l_1\}, \{\lambda l_1, \lambda l_2\}, \ldots, \{\lambda l_1, \ldots, \lambda l_{n-1}\}$.

$$Z_1^{(n)} = < \bar{\Gamma}^{(n)} - \sum_{i=1}^{n-1} Z_1^{(i)} \bar{\Gamma}^{(n-i)} > . \tag{72}$$

The sum on the rhs adds the appropriate counterterms which compensate all subdivergent sectors of the full Green function. We are allowed to consider only massless quantities here as the overall degree of divergence is mass independent, and the term in angle brackets is free of subdivergences by construction.

We have

$$\bar{\Gamma}^{(n)} = (q^2)^{-\epsilon n} \prod_{i=0}^{n-1} {}_i\Delta, \tag{73}$$

according to our definition Eq.(69). Here sequential expressions like $\Delta_1\Delta \ldots$ denote a concatenation of one-loop functions as shown in Fig.(16). Again, in case that there
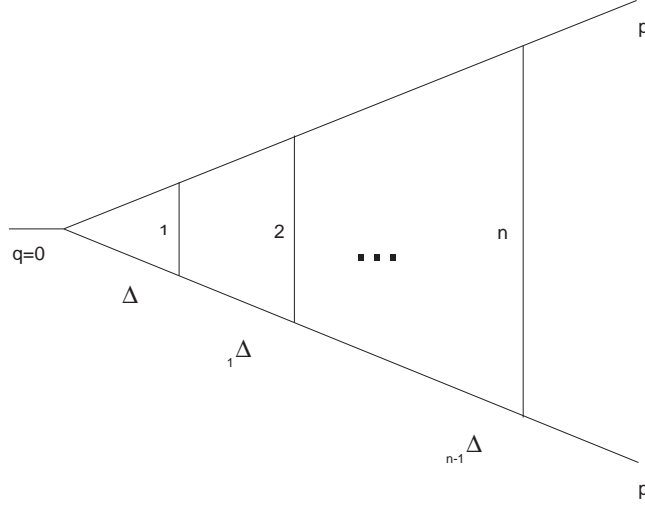
Figure 16: By evaluating at zero momentum transfer the calculation of a massless ladder becomes a concatenation of $_j\Delta$ functions.

is more than one form factor in this concatenation some technical subtleties are involved which are given in the appendix. By investigating counterterm expressions and Green-functions we see that only two type of operations on $_j\Delta$ are needed to give the Z-factor: a concatenation of these functions for the Green functions, and a projection onto their divergent parts to find counterterms. This justifies to define two operators

$$
\begin{aligned}
B^k(\Delta) &:= \prod_{i=0}^{k} {}_i\Delta, \\
A^r(\alpha) &:= \Delta <<< \ldots < \alpha > \Delta > \ldots \Delta >, \\
&\quad\quad \text{r} <> \text{brackets} \\
\Rightarrow A^r(B^k(\Delta)) &= \Delta <<<< \ldots < \prod_{i=0}^{k} {}_i\Delta > \Delta > \ldots \Delta >, \\
B^k(A^r(\Delta)) &= <<< \ldots < \Delta > \Delta > \ldots \Delta > \prod_{i=0}^{k} {}_i\Delta, \\
B^0(\Delta) = A^0(\Delta) &= \Delta.
\end{aligned}
\tag{74}
$$

B acts by concatenating massless one-loop functions with increasing writhe number, A by projecting on the divergent part iteratively.

We can now give the general result for $Z_1^{(n)}$:

$$
Z_1^{(n)} = < [-A + B]^{(n-1)}(\Delta) > .
\tag{75}
$$

27

For $n = 3$ this gives explicitly

$$Z_1^{(3)} = < \Delta \, _1\Delta \, _2\Delta - [< \Delta \, _1\Delta > - << \Delta > \Delta >] \, \Delta$$
$$- < \Delta > \Delta \, _1\Delta > . \tag{76}$$

It should be clear that in the above expressions we have on the rhs the proper three-loop Green-function, next the two-loop Z-factor times the one-loop Green function, and the one-loop Z factor times the two-loop function. We remind ourselves that the functions $_j\Delta$ are simple modifications of the corresponding three-point one-loop function, evaluated in the massless limit at zero momentum transfer. The above concatenation properties are universal for all these functions, as long as they are generated by a renormalizable theory. We note that there might be in fact a whole 'bouquet' of these functions at our disposal. This is so as in more realistic theories our ladder topology might consist of various different Δ^i's, as in the example of Fig.(17).
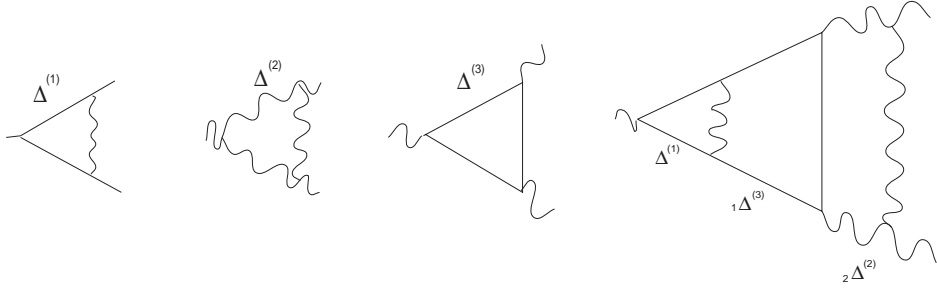

Figure 17: Various different $\Delta^{(i)}$'s. We understand that in our result Eq.(75) we have to consider the appropriate combination of Δ's as arguments for the A and B operators. Examples here are taken from non-abelian gauge theories which provide various kinds of couplings. Here we see cubic selfcouplings of the gauge boson and the usual coupling of a fermion to a gauge boson.

Recalling our definition for the full vertex function

$$\mathbf{\Gamma}^{(n)} \quad := \quad \Gamma^{(0)} + \sum_{i=1}^{n} \Gamma^{(i)},$$
$$\Rightarrow < \mathbf{\Gamma}^{(n)} > \quad = \quad < \bar{\mathbf{\Gamma}}^{(n)} >, \tag{77}$$

we have its MS renormalized form,

$$\mathbf{\Gamma}_R^{(n)} = \mathbf{Z}_1^{(n)} \mathbf{\Gamma}^{(n)}. \tag{78}$$

We can easily check that $\mathbf{Z}_1^{(n)}$ renders $\mathbf{\Gamma}_R^{(n)}$ finite. Indeed, we only have to check that $\bar{\mathbf{\Gamma}}_R^{(n)}$ is finite and easily calculate this expression to be (using Eq.(73,75))

$$\bar{\mathbf{\Gamma}}_R^{(n)} \quad = \quad (1 + \sum_{i=0}^{n} [B]^i(\Delta))(1 - \sum_{i=0}^{n-1} < [-A + B]^i(\Delta) >),$$

28

$$= 1 + \sum_{i=0}^{n-1} ([-A+B]^i(\Delta) - <[-A+B]^i(\Delta)>), \qquad (79)$$

which is evidently finite. In some obvious shorthand notation we can write this result to all orders as

$$\bar{\mathbf{\Gamma}}_R = \frac{1}{1-[-A+B]}(\Delta) - <\frac{1}{1-[-A+B]}(\Delta)> . \qquad (80)$$

In our conventions we never have written the coupling constants explicitly. But each application of A or B increases the loop number by one, and thus the order of our expansion. Thus an expansion in the coupling constant is understood in Eq.(80). ($A^r B^m$ is of order $\mathcal{O}(g^{2(r+m)})$). Before we extend this rather academic example to more realistic situations, including the other topologies, self-energies and the like let us summarize what we have achieved so far: mainly we have calculated the ladder-type vertex corrections of Fig.(16), including the counterterms as depicted in Fig.(18). Our intention is to generalize this to all possible topologies, including
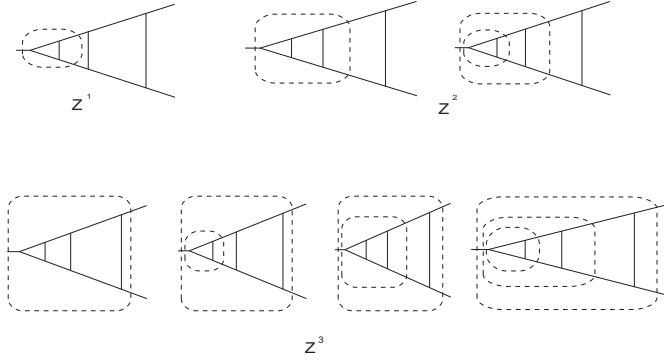

Figure 18: We have calculated $< \Gamma^{(n)} >$ so far, including the counterterms for the dashed divergent sectors, taking into account all possible forests.

dressing of internal lines and vertices, and, crucially, including overlapping divergences. But before we do so in the next sections, let us have another look at our ladder. At this stage we have introduced a sufficient amount of notation so that we can start to consider our example again, this time turning to knot- and link-theory as another approach to obtain our results Eq.(75).

3.2 Links and ladders

In the previous section we reduced the renormalization procedure of ladder graphs to algebraic operations on concatenated one-loop functions. We now want to compare this result with the behaviour of link diagrams in the presence of a skein relation acting on the diagram. It will turn out that we identify a link diagram with the Green-function plus all its counterterms. Individual terms in renormalization theory should correspond to individual terms obtained after skeining the link diagram.

In the course of this skeining, one generates from a n-component link diagram in particular a one-component link diagram, a knot, amongst other terms. Later we see that this knot gives us some information about the numbers we should expect when we calculate the divergences of the corresponding graph. We use some elementary notions of link and knot theory, as provided for example in [12].

According to the rules we give below, the individual components in the link diagrams of interest are all trivial circles (unknots from the viewpoint of knot theory). Only through the entanglement do we generate non-trivial topological structure in the link diagrams. Using a skein relation to disentangle the diagrams we will then generate knots in intermediate steps of this algorithm; in fact applying the skein relation $n - 1$ times to a n component link will generate the one-component knots which we are after. These knots classify our Feynman graph and determine their UV divergences.

For a start, let us introduce the following two rules to map any Feynman diagram into a link diagram, as shown in Fig.(20).

- Every loop in the Feynman diagram corresponds to a link. Correspondingly, a n-loop diagram will map to a link diagram consisting of n components.

- The links are oriented according to the flow of loop momenta, and follow the rule that at every vertex the momentum coming from the right is overcrossing as in Fig.(19).
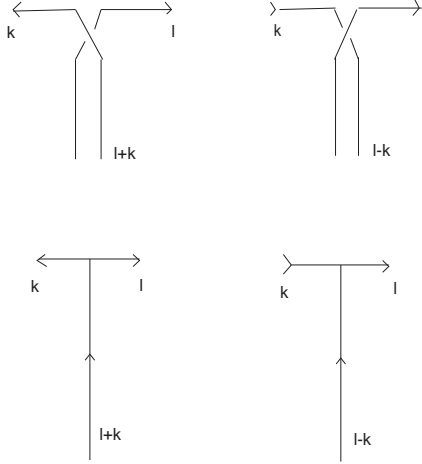

Figure 19: The replacement of a three-point vertex by an overcrossing. When we reverse the orientation of lines at the vertex, we have also to reverse the orientation of lines in the link diagram, and, accordingly, exchange the over- to an undercrossing. All cases follow from strict obedience to a "traffic rule": the momentum from the right is overcrossing.

We ignore exterior momenta in this process. For the ladder topology we also understand that each crossing in our link diagram should correspond to a vertex in the
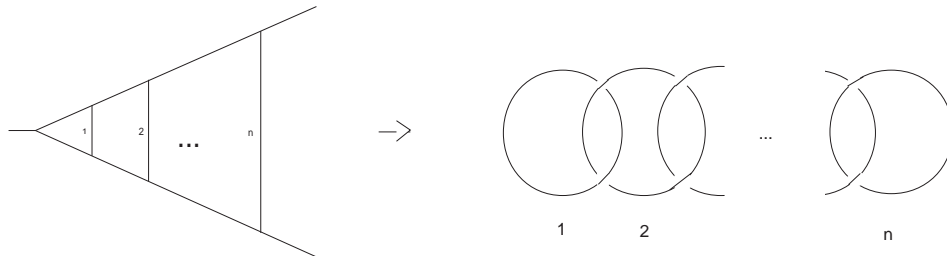
Figure 20: The translation from a Feynman diagram to a link diagram. Each vertex is replaced by an over/undercrossing according to the momentum flow at the vertex. We follow the convention to have the momentum flow in each loop counterclockwise. Here we used a momentum routing so that each propagator $P_i, i = 1, \ldots, n$, appearing as a rung in the Feynman graph above, carries loop momentum $l_i - l_{i+1}$.

Feynman graph. Our nested loop structure results in a sequence of (Hopf-) links as in Fig.(20).

For the momentum routing as envisaged in Fig.(20) we can now start moving these Hopf-links into different positions, using Reidemeister moves. It is not too difficult to see that this corresponds to other momentum flows, still in accordance with our rules given above. We then use the skein relation, and disentangle the link diagram until we end with a collection of disjoint unknots, where the unknots may have non-trivial curl, see below.

The states which are generated in this manner we identify with the terms demanded by renormalization theory. We will survey in a later section results which concern Feynman diagrams of a much more complicated topology.

The empirical results to be discussed there justify the following remarks on the way how to assign link diagrams to Feynman diagrams, and how to incorporate the skein relation.

According to the momentum flow, we assign a link diagram to a Feynman diagram. The demand that every vertex in the Feynman diagram should correspond to a crossing in the link diagram sets a lower boundary for the number of crossings in the link diagram. Further crossings will be generated solely by the topological complexity of the Feynman diagram. Such topological complexity is absent from the simple ladder topologies considered here, but will be present in the examples discussed in the chapter on knots and transcendentals.

These extra crossings in the link diagram shall be of the least number possible in accordance with the two rules above. This is a non-trivial restriction on the allowed Reidemeister moves, which we hope to set in a more axiomatic context in future work. So far, we embodied it in our investigations by regarding the Feynman diagram as built up from a ladder diagram: for every Feynman diagram it is true that when we remove a sufficient number of propagators, we obtain a simple (ladder) topology. Reinserting the other propagators step by step amounts to adding link component after link component. The basic ladder topology is assumed to correspond to the Hopf link as described here. The extra components are then added so as to minimize the number of extra crossings, that is we add the next

propagator which specifies the location of two more crossings in the diagram, and then try to connect these in the way which avoids as many crossings as possible. The reader will find it instructive to study Figs.(50,51,53,56) in the light of these considerations.

Once the set of link diagrams assigned to a Feynman diagram is found, we will apply the skein relation to those crossings which correspond to proper vertices in the diagram. For a n-loop Feynman diagram we apply the skein relation $n-1$ times.

We do so as we are particularly interested in the one-component link diagrams, *knots*, which one obtains from the link diagram during this procedure. They cannot appear before the skein relation is applied $n-1$ times. For the simple examples here, one always finds at this stage unknots, which, as we will see, is reflected in number theoretic properties of the counterterms (absence of knots = absence of transcendentals).

In general, we stop skeining at this stage and find that the knots resulting after skeining $n-1$ times faithfully predict the transcendentals encountered in the calculation. Once we have applied our skein relation and disentangled the link diagram as described here, we do allow for Reidemeister moves in the generated knots.

Recent results [39, 40] point towards a connection of this process with chord diagrams, and indicate that the whole procedure can be understood in the context of a four-term relation.

We now continue to presume that some sort of braid structure underlies the algebraic systematics of renormalization theory. So we assume that we can establish a skein relation of the form as indicated in Fig.(21). This assumption is at the

Figure 21: The skein relation, an exchange identity which allows the disentangling of the link diagram. X and Y have to be regarded as operators to be identified with A and B in an appropriate manner. As usual, we assume that the operations appear locally on a specified crossing in the link diagram.

moment based only on the vague evidence that the ladder topologies renormalize according to Eq.(75), which, as we will see below, fits into the pattern suggested by a skein relation. In the course of the following sections we will look for further evidence to justify this assumption.

Let us consider Fig.(22), a two-link diagram and its disentanglement. It gives us a clue how to interpret the coefficients X and Y in the skein relation. The three-link diagram, corresponding to $\Gamma^{(3)}$,
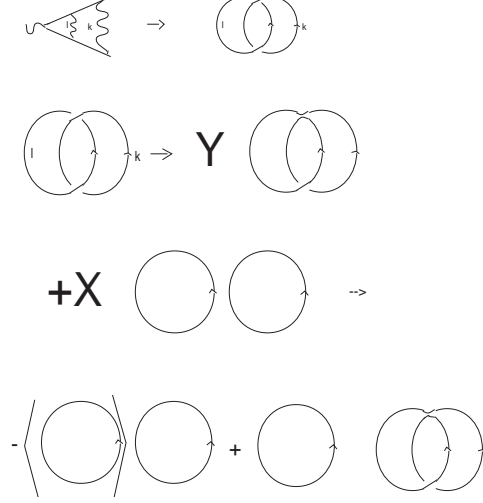
 $\rightarrow$
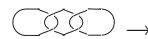
Figure 22: An explicit two-loop example. The first line maps a Feynman diagram to a link diagram. This link diagrams then, under the skein operation, gives two terms. We compare these two terms with the terms which we need to renormalize the diagram. We identify the Y term of the skein relation with the B operator, and the X term with the removal of subdivergences as provided by the operator A.

confirms this in this graphical calculation for the three-loop case. We already identified the operators X, Y and we obtain the correct result. We conclude that the identification

$$
\begin{aligned}
X^{r-1}(\bigcirc \bigcirc \dots \bigcirc) &\Rightarrow [-A]^{r-1}(\Delta), \\
Y^{r-1}(\overline{}\dots\overline{}_{r-1}) &\Rightarrow B^{r-1}(\Delta),
\end{aligned}
$$

delivers our previous results. We identify the unknot with an appropriate one-loop function $_0\Delta$ and links of the form

$$\overline{}\dots\overline{}_j \text{ A link with writhe number } j.$$

with the corresponding function $_j\Delta$. Note that this implies that we have no invariance under Reidemeister type I moves. Accordingly, we work with a regular isotopy. Furthermore, the above result is independent of the routing of momenta in the Feynman graph, as all possible routings will generate only pairwise concatenated rings, so that under the action of the skein relation we would always obtain

33

the same result. In fact, we add to our rules the further demand that each crossing in the link diagram should either correspond to a vertex in the Feynman diagram, or must necessarily be generated by a non-trivial topological structure of the diagram. In this respect ladder diagrams are trivial.

We conclude that the n-link diagram of the form of Fig.(20) delivers, via the skein relation and appropriate identification of the operators A and B, the Z-factor, $Z_1^{(n)}$, as drawn below.

$$
\begin{aligned}
&\hspace{3.5em} \overbrace{\text{◯◯◯◯}\ldots\text{◯}}_{n} = \\
&- < \text{◯} > \; \overbrace{\text{◯◯◯}\ldots\text{◯}}_{n-1} \\
&+ \text{◯} \; \overbrace{\text{◯◯◯}\ldots\text{◯}}_{n-1} = \\
&+ << \text{◯} > \text{◯} > \; \overbrace{\text{◯◯}\ldots\text{◯}}_{n-2} \\
&- < \text{◯} > \; \overbrace{\text{◯◯◯}\ldots\text{◯}}_{n-2} \\
&- < \text{◯} \; \text{◯} > \; \overbrace{\text{◯◯}\ldots\text{◯}}_{n-2} \\
&+ \text{◯} \; \text{◯} \; \overbrace{\text{◯◯◯}\ldots\text{◯}}_{n-2}
\end{aligned}
$$

... The skein tree in general.

Let us briefly discuss how the above approach looks from the point of view of a braid group approach. Every closed link entangled in some other closed link generates a braid diagram with a very peculiar topology:

The braid diagram.

A closure of all strands is always understood.

The braid would be generated in the case $n = 4$.

$$= \sigma_1^2 \sigma_2^2 \sigma_3^2 \qquad (81)$$

We infer such a braid diagram from our standard link diagram by the help of Fig.(23). Every crossing of a braid i with a braid $(i+1)$ in Eq.(81) corresponds to the action of a braid group generator σ_i. We follow the convention to orient our loops consistently so that all braid generators have positive powers. We will see that empirical evidence supports this convention, so that only positive knots determine the UV-divergent structure of a perturbative quantum field theory.

The n-link diagram Fig.(20) we identify with $Z_1^{(n)}$

$$
\begin{aligned}
\sigma_1^2 \ldots \sigma_{n-1}^2 \;&\leftrightarrow\; Z_1^{(n)}, \\
\sigma_i^2 \;&=\; Y\sigma_i + X\mathbf{1}, \qquad (82)
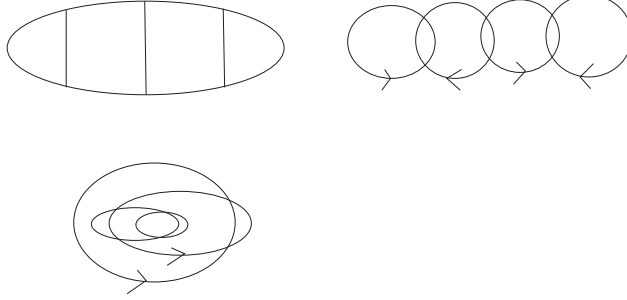\end{aligned}
$$

Figure 23: One way to obtain the braid of Eq.(81) is to route momenta as in this diagram.

which implies the usual identification of the skein relation with the Hecke algebra relation $\sigma = X\sigma^{-1} + Y\mathbf{1}$, so that we would recover our previous expressions, e.g.

$$
\begin{aligned}
Z_1^{(3)} \quad &\leftrightarrow \quad \sigma_1^2\sigma_2^2 \Rightarrow \\
&= \quad X^2 - XY\sigma_1 - YX\sigma_2 + Y^2\sigma_1\sigma_2 \Rightarrow \\
&= \quad [-A+B]^2(\Delta).
\end{aligned}
\tag{83}
$$

Here we used a Hecke algebra representation of the braid group. At this point the algebraic structure is in fact not fully developed. Our n-link corresponds to words containing nothing else than products of the form $\prod_i \sigma_i^2$, so that we can draw the braid diagram in the simple block form of Eq.(81). Other routings of loop momenta map to expressions containing the same braid generators in various orders, but reduce to the same set of terms after skeining. Due to this simple structure we do not, at this level, see anything of the proper braid algebra structure, encoded in relations as

$$
\sigma_i\sigma_{i+1}\sigma_i = \sigma_{i+1}\sigma_i\sigma_{i+1}.
\tag{84}
$$
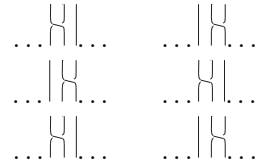
The Reidemeister type III move corresponding to Eq.(84).

We will not dwell on this point here but will have more to say later on. Now we establish similar algebraic structures in more general circumstances.

3.3 A generalization to ladder cables

This generalization shows mainly that also more complicated vertex graphs follow a behaviour which fits into the pattern established so far. We do now allow for

higher terms in the skeleton expansion of the vertex. They correspond to more complicated link diagrams not encountered yet. Non-trivial terms in the skeleton expansion will have a non-trivial link structure, and the question is how these links are entangled. Here we do not investigate the link structure of each term, but only pursue how renormalization theory concatenates them.

We denote different topologies by α_i. A Feynman graph of topology α_i has $n(\alpha_i)$ loops. For the time being we regard any topology α_i as corresponding to a cable (this cable being a $n(\alpha_i)$-component link itself) and ignore the 'fine structure' of these cables. The sole question is how higher terms in the skeleton expansion are concatenated from the viewpoint of renormalization theory. Later we might have a conjecture how the corresponding cables are knotted. So let us now slightly generalize the ladder topology of Fig.(20). We want to include all sorts of vertex corrections which are themselves free of subdivergences. This corresponds to a full skeleton expansion of the vertex as in Fig.(24). We label the different topologies
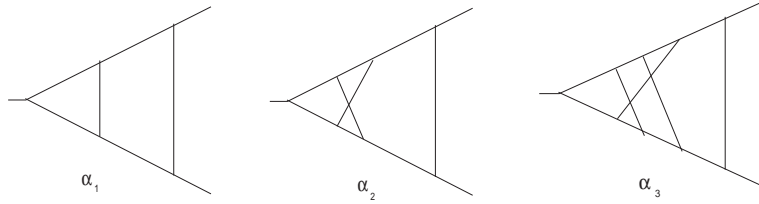

Figure 24: The general ladder topology. Every cable of lines defining a new subdivergence is labelled according to its topology. The examples given here have different topologies α_i for their subdivergences. We replaced the one-loop subdivergence by the first terms in the bare skeleton expansion for the vertex, cf. Fig.(12).

by indices α_i but still omit the dressing of internal vertices and propagators. So the subscript i labels different terms in the skeleton expansion. Note that every topology gives rise to a simple pole in ϵ only

$$\Delta^{\alpha_i} = \frac{c^{\alpha_i}}{\epsilon} + d^{\alpha_i}, \tag{85}$$

due to the fact that it has no subdivergences by the very definition of a skeleton expansion. A Feynman graph as in Fig.(25) will then result in a Z-factor contribution

$$Z = \prod_{i=1}^{3}[-A+B](\Delta^{\alpha_i}), \tag{86}$$

with the obvious definitions

$$\prod_{i=s}^{r} A(\Delta^{\alpha_i}) := \Delta^{\alpha_r} < \ldots << \Delta^{\alpha_s} > \Delta^{\alpha_{s+1}} > \ldots \Delta^{\alpha_{r-1}} >,$$

$$\prod_{i=s}^{r} B(\Delta^{\alpha_i}) := \Delta^{\alpha_s}{}_{n(\alpha_s)}\Delta^{\alpha_{s+1}} \cdots {}_{[n(\alpha_s)+\ldots+n(\alpha_{r-1})]}\Delta^{\alpha_r}. \tag{87}$$
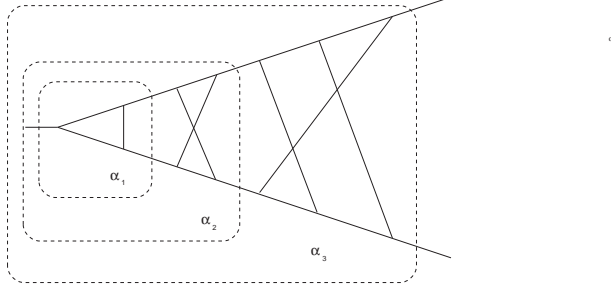
36

Figure 25: The cabling of loops into divergent sectors.

Note that the concatenation in the B operator takes the loop number of each topology into account. That the same algebraic structure appears results from the fact that we still have only nested divergences, with only one maximal forest appearing, as indicated in Fig.(25).

From the viewpoint of braids we would still map this situation to a n-cable link, so that we associate a cable (a collection of links) to each Δ^{α_i}. In braid generator language we would obtain generators σ, each acting on links in a different representation α_i so to speak, where in the 'B' part of the skein relation we have a concatenation of writhe numbers as shown above and taking the various $n(\alpha_i)$'s into account. As an example of this Fig.(25) delivers

$$
\begin{aligned}
Z_1^{(3)}(\alpha_1, \alpha_2, \alpha_3) =& < \Delta^{\alpha_1}{}_{n(\alpha_1)} \Delta^{\alpha_2}{}_{n(\alpha_1)+n(\alpha_2)} \Delta^{\alpha_3} \\
& - (< \Delta^{\alpha_1}{}_{n(\alpha_1)} \Delta^{\alpha_2} > - << \Delta^{\alpha_1} > \Delta^{\alpha_2} >) \Delta^{\alpha_3} \\
& - < \Delta^{\alpha_1} > \Delta^{\alpha_2}{}_{n(\alpha_2)} \Delta^{\alpha_3} > .
\end{aligned}
\tag{88}
$$

The Δ^{α_i} are implicitly defined as the dimensionless function of the regularization parameter ϵ which multiplies the scaling $(r^2)^{-\epsilon n(\alpha_i)}$ of the corresponding $n(\alpha_i)$-loop Green function.

Note that our presentation here was done under the assumption that the Δ^{α_i} are known. This is true for all possible topologies up to the four-loop level, thanks to the major progress in massless two-point functions, obtained by various authors [24]. A summary of the situation in this area can be found in [23]. Later we will see that our knot-theoretic approach suggests a way to obtain these functions to all loop orders for all topologies by associating them with various knots.

To get the final Z-factor we just have to add the results for the various topologies. Define the total loop order n_t by

$$
n_t = \sum_i n(\alpha_i).
\tag{89}
$$

We have for the Z-factor generated from all topologies contributing in a given loop order m

$$
\mathbf{Z}_1^n = 1 - \sum_{m=1}^n \sum_{I_m} Z_1^{(n_t=m)}(I_m),
\tag{90}
$$

37

where $\{I_m\}$ denotes a complete set of topologies such that $n_t = m$, and the sum over I_m runs over all these topologies. Note also that with different topologies the number of different types of graphs per topology proliferates and has to be taken into account by an appropriate choice of basic functions Δ^{α_i}. We stress that at this stage we have not specified the actual link diagrams associated to the different cables, nor the entanglement of the cables with each other. This is already a very difficult problem, as it demands the concatenation of topologically complicated terms in the skeleton, sitting as subdivergences in other such terms. We will learn soon about the complexity of such a problem, but still have to continue our investigations of simple topologies. This finishes our considerations of the vertex ladder topology and we now turn to two-point functions.

4 Corrections at the Propagator: planar, nested

Again we consider only nested divergences. The whole situation is largely a repetition of the situation in the previous section. Nevertheless, we have to comment on some new features. Consider the Feynman graph in Fig.(26). Note that when
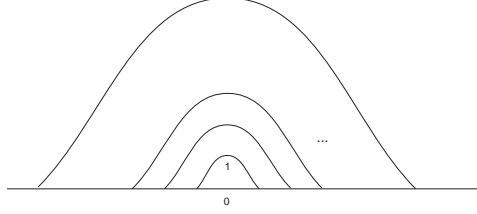

Figure 26: We call this the rainbow topology. For reference, we gave numbers to the various propagators.

we insert a zero-momentum coupling we would recover the situation of the previous section. In the spirit of it we would like to define an expression of the type $[-A + B]^n(\Omega^1)$. We expect Ω^1 to be the one-loop massless two-point function, and would also need to define $_f\Omega^1$, its version with increased writhe number. In fact, this is indeed correct. But this is only so when we restrict ourselves to two-point functions which are at most linearly divergent. Otherwise single subtractions which we have considered so far might not be sufficient to subtract subdivergences. We will briefly comment on this difficulty below and give some more details in an appendix. But let us consider Fig.(26) for linear divergent cases and denote the graph by $\Omega^{(n)}$. Define

$$\tilde{\Omega}^{(n)} := \Omega^{(n)} \downarrow_{m_0=m_1=0} . \tag{91}$$

The notation $\ldots \downarrow_{m_0=m_1=0}$ means the following. Consider the Feynman graph in the form where all propagators have the usual quadratic denominators, and spin structures determine the numerator expression. Then we set $m_0 = m_1 = 0$ in the first two propagators in the denominator. We nullify the masses of the inner loop. One easily shows by powercounting that

$$< \Omega^{(n)} - \tilde{\Omega}^{(n)} >= 0, \tag{92}$$

and it is sufficient to investigate $\tilde{\Omega}^{(n)}$. We add its counterterm graphs. Next we want to set all masses to zero as the remaining overall divergence is mass independent. For a massive theory we typically have to take into account one further subtlety: that there are linear and logarithmic divergent terms to be considered (distributed over two formfactors usually) for the mass and wave-function renormalization. This reflects the fact that the two-point function $< 0|T[\phi_{in}(x_1)\phi_{in}(x_2)]|0 >$ corresponds to two monomials in the Lagrangian usually, the mass term $-m^2\phi^2/2$ and the kinetic term $(\partial_\mu \phi)^2/2$. Note that for a massless theory one directly obtains formulas equivalent to the results in the previous section. For massive particles Ω is a sum of two terms, one providing the mass renormalization, the other one the so-called

wave function renormalization. Together they achieve that the propagator-function and its derivative with respect to the exterior momentum are finite.[15] For example the fermion propagator delivers

$$\Omega = a(q^2, m^2)\slashed{q} + m\, b(q^2, m^2)\mathbf{1}. \tag{93}$$

Therefore this problem resembles the one considered in the appendix, where the case of various form factors is studied. There the reader will find a worked out procedure for the general case.

Here we only describe this general procedure as follows: In the numerator, keep all terms which are overall linearly or logarithmically divergent. That is, consider the numerator as a polynomial in masses and the exterior momentum. Abandon all terms which are of degree two or higher, as they provide only finite contributions. The terms which are now linear in masses are the terms contributing to the mass renormalization, the other terms are necessarily linear in the exterior momentum at the end, so they will give the wave-function renormalization. As an example let us consider massive QED at the two-loop order, Fig.(27). The integration of the
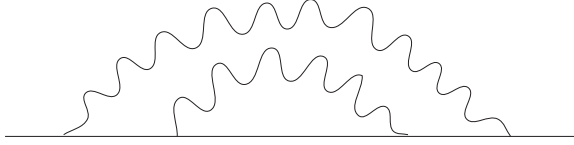

Figure 27: An example for a mass and wave function renormalization.

inner loop gives[16]

$$
\begin{aligned}
\Omega^{(1)} &= (\Omega\slashed{k} + m\Omega_m\mathbf{1})(k^2)^{-\varepsilon}, \\
Z_2^{(1)} &= \; <\Omega\slashed{k} + m\Omega_m\mathbf{1}> = \slashed{k} <\Omega> + m <\Omega_m> \mathbf{1} \\
&=: \; Z_{2,w}^{(1)}\slashed{k} + Z_{2,m}^{(1)}m\mathbf{1}.
\end{aligned} \tag{94}
$$

Adding the two-loop graph and its counterterm $Z_{2,w}^{(1)}\slashed{k} + Z_{2,m}^{(1)}m\mathbf{1}$ gives then

$$
\begin{aligned}
Z_2^{(2)}: \quad & [<\Omega\;_1\Omega> - << \tilde{\Omega}>\Omega>]\slashed{k}, \\
+ \quad & [<2\Omega\;_1\Omega_m + \Omega_m\;_1\Omega_m> \\
& - << 2\tilde{\Omega} + \tilde{\Omega}>\Omega>]m\mathbf{1}.
\end{aligned} \tag{95}
$$

---

[15]Higher order derivatives are finite anyhow. Upon Taylor expanding one verifies that for a Green function of overall degree of divergence ω the first $\omega + 1$ terms in its Taylor expansion in an external momentum are divergent. Accordingly, for a logarithmic divergent vertex function only the first -zeroth- order term is divergent, while a linear divergent propagator function also has a divergent derivative. This can be confirmed by applying the derivative to the integrand and subsequent powercounting.

[16] Depending on the chosen renormalization conditions these Z-factors are not yet the standard mass and wave function renormalization, which can be inferred from a linear combinations of our Z-factors.

The generalization to higher loop orders is obvious and incorporates that the concatenation of terms generated by the B operator will mix the different one-loop functions, as discussed in the appendix.

So far we assumed that the overall degree of divergence was not worse than linear. The case of quadratic divergences can be usually handled by appropriate differentiation with respect to the exterior momentum or by further subtractions. In practical applications one also often uses gauge symmetries, which tend to improve the quadratic degree of divergence for a vector boson propagator to a logarithmic one. Nevertheless we sketch how to treat a two-loop calculation involving a quadratic subdivergence in an appendix. Typically, quadratic divergences involve an integral of the form

$$\int d^D l \frac{(l^2)^{-\varepsilon}}{l^2 - m^2} = \int d^D l \frac{m^2 (l^2)^{-\varepsilon}}{(l^2 - m^2) l^2}, \tag{96}$$

where we used a typical identity (Eq.[45]) in dimensional regularization to transfer a quadratic divergence to a logarithmic one. Note that at no stage do we encounter new infrared singularities as we carefully avoid oversubtractions in this approach [22].

Summarizing we note that we observe in this section similar algebraic structures as in the previous one. All the Feynman graphs considered here can be obtained from the vertex graphs of the previous section by deletion of an external propagator. Consequently the results as far as link diagrams are concerned remain unchanged. For the rainbow topologies considered here the counterterm contributions match the skein algebra for concatenated Hopf links in the same way as before.

5 Simple Entanglements

So far we have considered two cases, ladder and rainbow topologies. In both cases we restricted ourselves to a very simple situation as far as renormalization is concerned: we only had one maximal forest, with subdivergences strictly nested into each other, and all divergences localized at the same vertex (or propagator, for the case of the previous section). Both cases give link diagrams of a simple topology, chains of pairwise concatenated links. The corresponding braid expressions were of second degree in each braid group generator. Correspondingly, after applying skein relations, so far we never met a knot. The most complicated figure generated was the unknot with writhe number $n-1$, for a n-loop graph.

In this section we like to study more general Feynman graphs. We still restrict ourselves to Feynman graphs which are iterated from only the first term in the skeleton expansion. We will have ladder and rainbow topologies. But this time we allow them to be localized at arbitrary different points in the graph.

These graphs are still calculable from our elementary generalized one-loop functions. But we will see that when we localize subdivergences at different points, we will be able to generate more complicated link diagrams.

In a later section we obtain the following result: As long as we have simple iterated ladder (or rainbow) topologies localized at not more than two different points, the pole terms in our Laurent series have purely rational coefficients. We will learn to associate the appearance of transcendentals with the appearance of knots in the link diagrams. Here we will address the question if such transcendentals appear when we localize simple subdivergences at various different points, and if the link diagrams can contain non-trivial structures.

Let us combine the results of the previous two sections. We still consider vertex corrections to provide the basic skeleton graph and begin to dress internal propagators with rainbow diagrams, Fig.(28). Let us start with the simplest possible
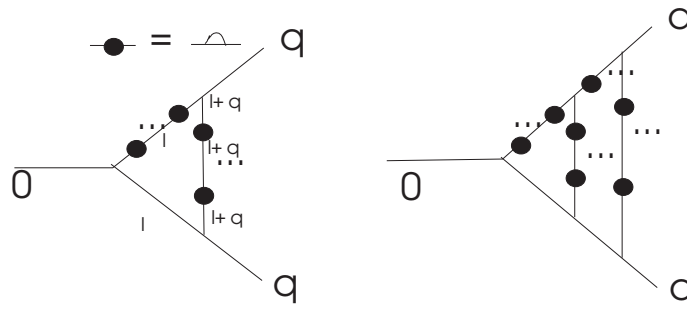

Figure 28: The simplest possibility for divergences located at different points appears with dressings of a one-loop skeleton graph. The dressings, indicated by the black blobs, are assumed to be with one-loop rainbow diagrams. Generalizations as on the rhs are still calculable in a finite set of generalized one-loop functions. Now that we have disjoint subdivergences new phenomena may occur.

example, a one-loop graph dressed with one-loop bubbles at various points, as in Fig.(28) on the lhs. This time we have disjoint subdivergences. We can easily cal-
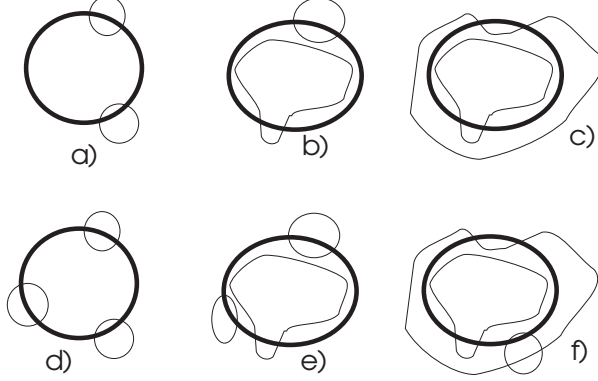
Figure 29: Link diagrams for disjoint subdivergences for a three and four loop example. We follow the guiding principle that all components which correspond to subdivergences shall be concatenated with the appropriate skeleton, indicated by a thick line. We indicate different possible routings of momenta. For the three loop example all routings are equivalent. In the four-loop case we obtain non-trivial entanglements for the first time.

(i_1, i_2)	$\mathbf{G(i_1, i_2)}$	$\overline{\mathbf{G}}(\mathbf{i_1, i_2})$
$(2,0)$	$(-\frac{1}{2}\zeta(2) + \frac{3}{2}\gamma_E^2 - 8\gamma_E + \frac{44}{3})\frac{1}{\epsilon} + (-\gamma_E + \frac{8}{3})\frac{1}{\epsilon^2} + \frac{1}{3\epsilon^3}$	$\frac{1}{3\epsilon^3} - \frac{1}{3\epsilon^2} - \frac{1}{3\epsilon}$
$(1,1)$	$(-\frac{1}{2}\zeta(2) + \frac{3}{2}\gamma_E^2 - 8\gamma_E + \frac{44}{3})\frac{1}{\epsilon} + (-\gamma_E + \frac{8}{3})\frac{1}{\epsilon^2} + \frac{1}{3\epsilon^3}$	$\frac{1}{3\epsilon^3} - \frac{1}{3\epsilon^2} - \frac{1}{3\epsilon}$
$(3,0)$	$(-\frac{83}{6}\zeta(3)+2\zeta(2)\gamma_E-\frac{1}{2}\zeta(2)-\frac{8}{3}\gamma_E^3+22\gamma_E^2-79\gamma_E+\frac{475}{4})\frac{1}{\epsilon}$ $+(-\frac{1}{2}\zeta(2)+2\gamma_E^2-11\gamma_E+\frac{79}{4})\frac{1}{\epsilon^2}+(-\gamma_E+\frac{11}{4})\frac{1}{\epsilon^3}+\frac{1}{4\epsilon^4}$	$-\frac{1}{4\epsilon^4} + \frac{1}{4\epsilon^3} + \frac{1}{4\epsilon^2} + (\frac{1}{4} - \frac{1}{2}\zeta(3))\frac{1}{\epsilon}$
$(2,1)$	$(-\frac{59}{6}\zeta(3)+2\zeta(2)\gamma_E-\frac{11}{2}\zeta(2)-\frac{8}{3}\gamma_E^3+22\gamma_E^2-79\gamma_E+\frac{475}{4})\frac{1}{\epsilon}$ $+(-\frac{1}{2}\zeta(2)+2\gamma_E^2-11\gamma_E+\frac{79}{4})\frac{1}{\epsilon^2}+(-\gamma_E+\frac{11}{4})\frac{1}{\epsilon^3}+\frac{1}{4\epsilon^4}$	$-\frac{1}{4\epsilon^4} + \frac{1}{4\epsilon^3} + \frac{1}{4\epsilon^2} + (\frac{1}{4} - \frac{1}{2}\zeta(3))\frac{1}{\epsilon}$

Table 1: Results for one-loop bubble insertions. We note that $G(3,0) \neq G(2,1)$, while $\bar{G}(3,0) = \bar{G}(2,1)$. We also note that $\bar{G}(3,0) = \bar{G}(2,1)$ contains the transcendental $\zeta(3)$.

culate the graph and its counterterm expressions. At zero momentum transfer, the graph has two different propagators. One of them carries loop momentum l while the other one carries momentum $l + q$. Let us denote the graph with i_1 insertions at the lines carrying momentum l, and i_2 at the line carrying momentum $l + q$, by $G(i_1, i_2)$. In Table(1) we give the results of a calculation of these diagrams. We indicate the values for the pure graph $G(i_1, i_2)$ as well as the results after addition of the counterterms, denoted as $\bar{G}(i_1, i_2)$. To obtain these results one only has to consider combinations of Laurent series generated by

$$I(i_1, i_2) := \int d^D k \frac{1}{[k^2]^{1-i_1\epsilon}[(k+q)^2]^{1-i_2\epsilon}}, \tag{97}$$

in the case of Yukawa theory which was used here as an example.[17] A few remarks are in order. First we observe that the graphs themselves depend on the way how the bubbles are distributed over the graph, for example $G(3,0) \neq G(2,1)$. This

---
[17]Similar results can be obtained for all renormalizable theories, and are discussed in general in [18].

dependence vanishes when one considers the graph together with its counterterm contributions, $\bar{G}(3,0) = \bar{G}(2,1)$. This is a general property. In [18] the reader will find a proof for this result to all orders. These findings are in agreement with the association of link diagrams to the graphs. The link diagram should correspond to the graph including the counterterm expressions, according to our experience in the previous sections. But the link diagram cannot distinguish between bubble insertion at various different points, as demonstrated in Fig.(30). As a consequence,
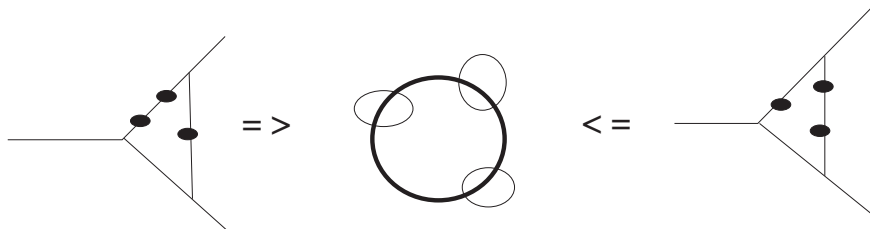

Figure 30: Link diagrams demand certain identities between diagrams. We only give some very basic examples, while such identities can be verified in a much more general context.

we should have identities for the function $\bar{G}(i_1, i_2)$, which is the function $G(i_1, i_2)$ with subtracted subdivergences:

$$\bar{G}(i_1, i_2) = \bar{G}(i_1', i_2'), \quad \text{for } i_1 + i_2 = i_1' + i_2'. \tag{98}$$

We stress that these identities are not fulfilled for $G(i_1, i_2)$ while $\bar{G}(i_1, i_2)$ abides by them, as it should. In [18] it is shown that such identities are in fact fulfilled for a much larger class of diagrams. It occurs that any Feynman diagram is in accordance with the demands of link theory. This very much supports our ideas of mapping Feynman diagrams to link diagrams. In particular, field theory itself does not restrict diagrams to obey such identities, so that this reflects a profound connection between renormalization theory and link theory indeed.

Another fascinating observation is contained in Table(1). At the four loop level we have link diagrams which have a simple structure like the link diagrams in previous sections, but also we have a contribution where a more entangled diagram occurs, see Fig.(29f). On the other hand, in Table(1) we see at the four loop level the transcendental $\zeta(3)$ appearing. These two observations are not unrelated. In anticipation of results we will report on in a later section we assign the transcendental $\zeta(3)$ to the trefoil knot, while purely rational counterterms indicate unknottedness of the corresponding link diagrams. We find this trefoil knot in the link diagram of Fig.(29f). This is demonstrated in Fig.(31). But then in Fig.(29) we see that at the four loop level also simpler link diagrams appear, Figs.(29d,e), and thus we expect the total contribution to obtain a term involving $\zeta(3)$ as well as a term which is a pure rational number. Table(1) demonstrates this indeed. All these results are confirmed to much higher loop numbers in [18]. Let us also list some explicit results for two-loop bubble insertions in Table(2). In Fig.(32) we give some link diagrams for the examples considered in Table(2). We find a consistent description, if we demand that all subdivergences connect to their skeleton. For the two-loop bubble

Figure 31: Explaining the appearance of the trefoil knot.

(i_1, i_2)	$\overline{\mathbf{G}}_2(\mathbf{i_1}, \mathbf{i_2})$
$(3,0)$	$(-\frac{47}{336}\zeta(6)+\frac{11}{56}\zeta(5)+\frac{3}{140}\zeta(4)+\frac{13}{70}\zeta(3)^2+\frac{9}{70}\zeta(3)+\frac{2}{7})\frac{1}{\epsilon}+(-\frac{11}{280}\zeta(5)-\frac{3}{28}\zeta(4)+\frac{1}{70}\zeta(3)+\frac{1}{35})\frac{1}{\epsilon^2}$ $+(\frac{3}{140}\zeta(4)-\frac{1}{14}\zeta(3)+\frac{1}{14})\frac{1}{\epsilon^3}+(\frac{1}{70}\zeta(3)-\frac{39}{280})\frac{1}{\epsilon^4}+(\frac{47}{280})\frac{1}{\epsilon^5}-(\frac{5}{56})\frac{1}{\epsilon^6}+\frac{1}{56\epsilon^7}$
$(2,1)$	$(-\frac{47}{336}\zeta(6)+\frac{11}{56}\zeta(5)+\frac{3}{140}\zeta(4)+\frac{13}{70}\zeta(3)^2+\frac{9}{70}\zeta(3)+\frac{2}{7})\frac{1}{\epsilon}+(-\frac{11}{280}\zeta(5)-\frac{3}{28}\zeta(4)+\frac{1}{70}\zeta(3)+\frac{1}{35})\frac{1}{\epsilon^2}$ $+(\frac{3}{140}\zeta(4)-\frac{1}{14}\zeta(3)+\frac{1}{14})\frac{1}{\epsilon^3}+(\frac{1}{70}\zeta(3)-\frac{39}{280})\frac{1}{\epsilon^4}+(\frac{47}{280})\frac{1}{\epsilon^5}-(\frac{5}{56})\frac{1}{\epsilon^6}+\frac{1}{56\epsilon^7}$

Table 2: Two-loop bubble insertions follow the same pattern as described before. Only the onset of knot-numbers is much more dramatic as can be inferred from study of link diagrams, cf. Fig.(32).

insertions we stress that the inner bubble sees the outer one as its skeleton. It is then this component which is entangled in the basic one-loop skeleton drawn as a thick line. Such a concatenation of skeletons governs how to concatenate our link diagrams in the presence of subdivergences.

All this is in agreement with our previous sections. In the nested cases considered there the i-th link had the $(i+1)$-th link as its skeleton as indicated in Fig.(33). This singles out the standard assignment of concatenated Hopf links as the most appropriate link diagram. For nested divergences this results in a unique link diagram so that the component i connects to the component $i+1$ while here, for disjoint subdivergences, the demand to connect all subdivergences to the same component can result in very different link diagrams, compare Figs.(29,32).

We now consider some examples to show how the differences between nested and disjoint divergences look in terms of our generalized one-loop functions. We start with two disjoint subdivergences, Fig.(34). Note that the dressing does not influence our argument used to reduce the considerations to massless functions at vanishing momentum transfer. This is so because we consider not only the graph but the graph with all its counterterms. They compensate for the divergences generated by the dressing, so that the arguments used in sections three and four remain unchanged. Thus, our basic functions Δ, Ω encountered so far still serve as the appropriate set to express all results.

Back to our example above, renormalization theory tells us that the correct answer is

$$
\begin{aligned}
\text{Fig.(34)} \quad \rightarrow \quad & \Omega\Omega\,_2\Delta\,_3\Delta - 2 < \Omega > \Omega\,_1\Delta\,_2\Delta \\
& + < \Omega >< \Omega > \Delta\,_1\Delta - < \Omega\Omega\,_2\Delta \\
& -2 < \Omega > \Omega\,_1\Delta + < \Omega >< \Omega > \Delta > \Delta, \quad (99)
\end{aligned}
$$

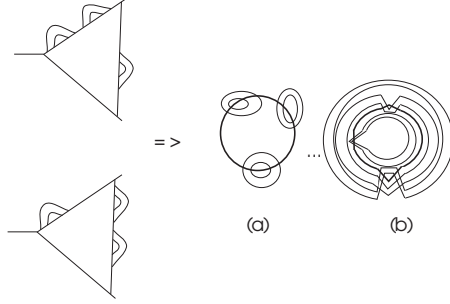in our notation. We see that the presence of disjoint subdivergences is reflected by

Figure 32: The Feynman graph provide two-loop rainbow dressings of the basic one-loop skeleton. They both generate the same set of link diagrams. From the analysis of these link diagrams we expect rational numbers, provided by the knot free link diagram (a), as well as transcendentals, provided by the much more knotted link diagram (b).
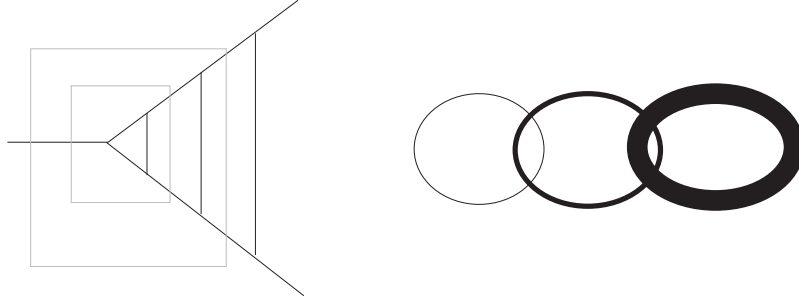

Figure 33: The cases of the previous section were an iterated set of skeletons, determing the entanglement of links. Thicker lines serve as the skeleton for thinner ones.

the presence of expressions like $< \Omega >< \Omega >$. They do not come in concatenated forms like $<< \Omega > \Omega >$ or $\Omega \,_1\Omega$ generated by the A and B operators. These concatenations were due to the total nested structure of the subdivergences considered previously. Let us compare the above example with Fig.(35). Combining our results on ladders and rainbows it delivers

$$
\begin{aligned}
\text{Fig.(35)} \quad \rightarrow \quad & \Omega \,_1\Omega \,_2\Delta \,_3\Delta - < \Omega > \Omega \,_1\Delta \,_2\Delta \\
& - < \Omega \,_1\Omega > \Delta \,_1\Delta + < \Omega < \Omega >> \Delta \,_1\Delta \\
& - < \Omega \,_1\Omega \,_2\Delta - < \Omega > \Omega \,_1\Delta \\
& - < \Omega \,_1\Omega > \Delta + < \Omega >< \Omega > \Delta > \Delta, \quad\quad (100)
\end{aligned}
$$

which is obvious from sections three and four. Both cases are free of transcendentals. All associated link diagrams are free of knots.

In general we follow the rule that the A and B actions in the skein relation concatenate the satellite links towards the skeleton link, and we assume that opearators A, B located at different points act independently. We get correct results, as in Fig.(36).

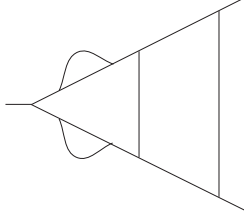We see the underlying principle: A and B treat disjunct subgraphs as disjunct,

46

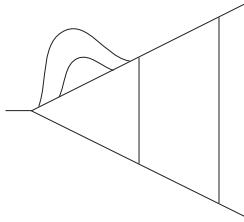Figure 34: A dressing generating disjunct divergences.

Figure 35: Compare this nested case with the previous example.

that is they factorize instead of concatenate the corresponding one-loop functions: $\Omega\Omega$ instead of $\Omega_1\Omega$ and $< \Omega >< \Omega >$ instead of $<< \Omega > \Omega >$. In [18] examples up to ten loop were considered, involving multiloop insertions at various places. The results always match the expectations of link theory, fulfilling a large class of identities where, it seems, no other explanation than an underlying connection to link theory is available.

This finishes our considerations of nested and disjunct divergences and we now turn to overlapping divergences. Our hope is to find a similar structure for topological simple graphs there. This is crucial for our final attempt to identify the topological nature of a Feynman graph with certain properties of its divergent part.

Figure 36: An example calculation using our graphical notation to demonstrate the behaviour of A and B on disjunct subdivergences. We indicated only one possible link diagram, as the others produce equivalent results.

6 Corrections at the Propagator: planar, overlapping

In this section we will address ourselves to overlapping divergences. By now, we have some experience with nested and disjoint subdivergences. In the next section we will see that ladder topologies like the one considered in sections three and four deliver Laurent series with rational coefficients in the proper pole part. This results from the special properties of the A, B operators of Eq.(74) in conjunction with the structure of the generalize one-loop functions. For this result to hold in general, we have to show that also overlapping subdivergences allow for similar algebraic structures.

6.1 The overlapping ladder

We will study graphs of the form as given in Fig.(37). Further we briefly comment on
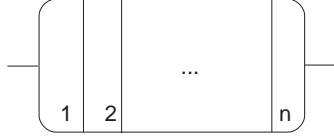

Figure 37: The overlapping ladder. These link topologies are still simple.

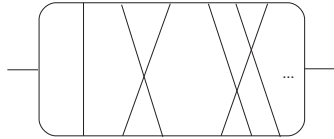their "cable generalizations" as in Fig.(38). So it is the main objective of this section

Figure 38: The generalized case including various topologies for the rungs.

to show that also the overlapping divergences factorize in a manner similar to the cases studied so far. This then allows to classify them by their corresponding link algebra too. The main result of this section is that the overlapping ladder topology gives indeed the same concatenations as before, with the only modification that we have to sum over all possibilities to identify subdivergences in the graph. Once more, this allows us in the next section to establish rationality also for simple topologies in the case of overlapping divergences. This in turn defines transcendentality of Z-factors as a sensible test for knots, that is non-trivial topologies.

Let us start with a simple two-loop example. The graph has two overlapping subdivergences, so we have to calculate the expressions indicated in Fig.(39). We have five propagators. Let N_i the product of all propagators involving the loop momentum l_i. It is implicitly understood that there is some numerator taking particle content and spin structures into account. We operate in the following only
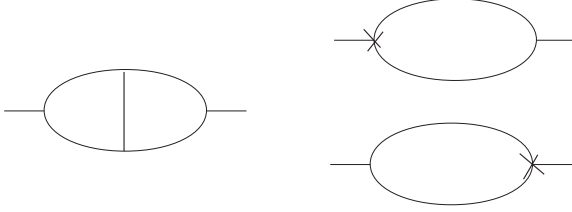
Figure 39: The two-loop example. We have two subdivergences.

on the (scalar) denominator part of the propagators under consideration, without further mentioning the numerator structure. The equations given are literally true for ϕ^3 in six dimensions as an example, but have obvious generalization to other renormalizable theories. Nevertheless we remind the reader that the numerator structure affects the power counting, so that in the following one cannot use the exlicitly given denominator expressions for power counting purposes.

In the above example we have $N_l = P_1 P_2 P_3$, $N_k = P_3 P_4 P_5$. We define

$$\tilde{N}_i := N_i|_{q=0, m_j=0 \,\forall j},$$

$$\mathbf{N_i} := \frac{\tilde{N}_i - N_i}{\tilde{N}_i}. \tag{101}$$

Then we have

$$\frac{1}{P_1 P_2 P_3 P_4 P_5} = \frac{1}{P_1 P_2 P_3 P_4 P_5}\mathbf{N_l}\mathbf{N_k} - \frac{1}{\tilde{N}_l P_4 P_5} - \frac{1}{P_1 P_2 \tilde{N}_k} + \frac{P_3}{\tilde{N}_l \tilde{N}_k},$$

implying

$$\Omega^{(2)} \equiv \Omega_f^{(2)} - \Omega^{(2)}|_l - \Omega^{(2)}|_k + \Omega^{(2)}|_{l,k}, \tag{102}$$

by construction. Note that the last term on the rhs vanishes in DR, according to Eq.(45).

Let us now investigate Eq.(102). The first term on the rhs is UV-convergent, as long as our overall degree of divergence was not worse than linear; this is assumed to be the case. In an appendix we comment on the general case. In practice one has to be cautious about the quadratic divergences of vector-boson propagators. But they are safe by gauge invariance, which reduces the overall degree of divergence to a logarithmic degree.

Back to our considerations of Eq.(102) we notice that the first term on the rhs will not contribute to our MS Z-factor, due to its UV convergence:

$$< \frac{1}{P_1 P_2 P_3 P_4 P_5}\mathbf{N_l}\mathbf{N_k} >= 0. \tag{103}$$

The remaining terms to be considered are the second and third term on the rhs of Eq.(102). The counterterms contribute

$$- Z_1^{(1)} \int d^D l \frac{1}{P_4 P_5} - Z_1^{(1)} \int d^D l \frac{1}{P_1 P_2}. \tag{104}$$

50

Adding these contributions to the remaining two terms on the rhs of Eq.(102) gives us a result free of subdivergences. As usual, the remaining overall degree of divergence is independent of masses in the process. We can set all remaining masses to zero in this sum. In the zero mass case we have $P_1 = P_5, P_2 = P_4$. Our UV-divergences are thus contained in

$$
\begin{aligned}
Z_2^{(2)} = & \ 2 < \Delta \int d^D l \frac{(l^2)^{-\epsilon}}{P_1|_{m_1=0} P_2|_{m_2=0}} \\
& - < \Delta > \int d^D l \frac{1}{P_1|_{m_1=0} P_2|_{m_2=0}} > .
\end{aligned}
\tag{105}
$$

Defining

$$
\begin{aligned}
{}_j\Omega & := \int d^D l \frac{(l^2)^{-\epsilon j}}{P_1|_{m_1=0} P_2|_{m_2=0}}, \\
\Omega & := {}_0\Omega,
\end{aligned}
\tag{106}
$$

we have

$$
Z_2^{(2)} = 2 < \Delta \ {}_1\Omega - < \Delta > \Omega >,
\tag{107}
$$

which has a striking similarity to our result Eq.(70). The main difference is the factor of two which reflects the overlapping structure in this simple example. The apparent structure is typical for overlapping divergences. We have two overlapping subdivergences. But we neither have a concatenation like $< \Delta < \Delta >>$, as we had for nested subdivergences, nor do we have a term $< \Delta >^2$, as it would characterize disjoint subdivergences. Instead, we have a subtraction of subdivergences to the left and right. Due to the symmetry of the graph, this only generates the factor of two in Eq.(107). Note that the two terms can be interpreted as arising from two possibilities: each of both loops can either be the skeleton or the subdivergence of the other one. We sum over both possibilities.

In our above result we used a somewhat condensed notation. $Z_2^{(2)}$ stands for all the two-loop divergences of Fig.(39). It is a notation for the Z-factors corresponding to a two-point function. As mentioned already usually there are two: the mass, $Z_{2,m}$, and wave-function renormalization, $Z_{2,w}$. One would extract them by looking for their corresponding form factors, e.g. $\not{q}$ and $m\mathbf{1}$ for the fermion propagator, and by Taylor expanding on the mass-shell. Again the reader interested in technical details will find further comments in the appendix. Graphically, our result is sketched below.

Some notation emphasizing the fact that the result was just a sum over all possibilities to interpret one loop as the skeleton (Ω) and the other one as the subdivergence (Δ).

We want to generalize this approach to the n loop case. We are looking for a general prescription to convert overlapping topologies back to products of one-loop graphs, as we did before for the nested topologies. We then hope to find a similar correspondence to braid structures as we found there. Consider the n-loop ladder graph Fig.(37). We claim that

$$\begin{aligned}
\Omega_f^n &= \Omega^n - \Omega^n|_{l_1}\Omega^n|_{l_n} + \Omega^n|_{l_1,l_n} \\
&= \Omega^n N_{l_1} N_{l_n},
\end{aligned} \tag{108}$$

is finite. The functions $\Omega^n|_{...}$ used above are implicitly defined by the second line in the above equation. Note that $\Omega^n|_{l_1,l_n}$, the last term on the rhs in the first line, does not vanish if $n \neq 2$. The assertion on Ω_f^n is justified by the fact that all possible divergent sectors cancel in the above expression. This can also easily seen by doing a powercounting for Eq.(108) or by investigating the Dyson Schwinger equations of Fig.(40). This is in agreement with the general result that an overlapping divergence
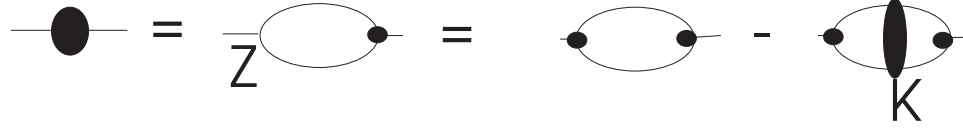

Figure 40: The Dyson Schwinger equations for a propagator. In its second form we reexpressed the Z-factor of the vertex with help of the Dyson Schwinger equation for this vertex. Our subtractions in Eq.(108) on the lhs (l_1) and rhs (l_n) remove the divergences. So the blobs have a subtracted form, cf. section 3.

renormalizes by subtracting out all divergent subgraphs in a manner different from disjunct or nested divergences [25]. Our two loop example above was generic in this respect. While for disjoint cases the product of the operators removing the subdivergences will appear, in the overlapping case this product structure is not maintained. It is replaced by a sum over subtractions at all divergent subgraphs.

What now remains to be calculated are the last three terms on the rhs of Eq.(108).

$$< \Omega_f^n > = 0 \Rightarrow < \Omega^n > = < \Omega^n|_1 + \Omega^n|_n - \Omega^n|_{1,n} > . \tag{109}$$

Let us add our counterterm expressions:

$$\begin{aligned}
-2 &\sum_{i=1...n-1} Z_1^{(i)} \Omega^{(n-i)} \\
+2 &\sum_{\substack{i=1...n-1 \\ j=1...n-1 \\ 1<i+j<n, i\neq j}} Z_1^{(i)} Z_1^{(j)} \Omega^{(n-i-j)} \\
+ &\sum_{i=1...n-1} (Z_1^{(i)})^2 \Omega^{(n-2i)}.
\end{aligned} \tag{110}$$

The whole contribution then is given in the graphical notation of Fig.(41). This
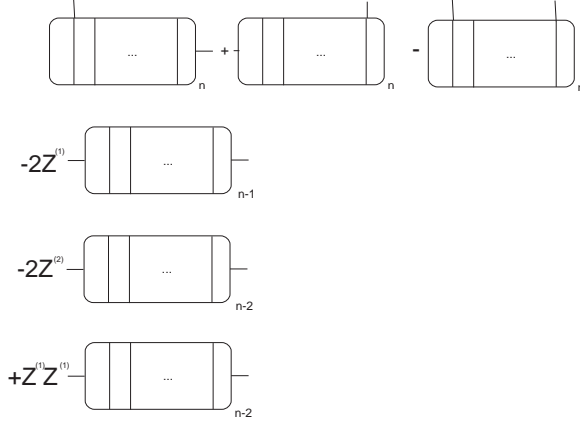

Figure 41: Our ladder with all its counterterms. In the first line wee see the result of Eq.(109). The next line gives a $n-1$ loop graph, multiplied by the one-loop Z-factor. It appears twice, as we identify such a one-loop subdivergence on the rhs as well as on the lhs of the graph. The next lines incorporate the higher contributions in the Z-factors.

expression is free of subdivergences and we can set all remaining masses to zero. It is still not quite what we want as expressions like those of Fig.(42), involve loops
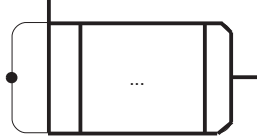

Figure 42: These expressions still involve functions which do not factorize into our basic Δ's and Ω's. Typically, the expressions involve functions to be evaluated at non-vanishing momentum transfer, drawn in thick lines above. The thin line furnishes a further loop momentum flowing through the thick lines, and the exterior momentum is still present.

which are not expressible in terms of our basic functions Δ, Ω. Only expressions such as Fig.(43) where the exterior momentum flows just through one loop are amenable to our procedure.

   The following constructive proof which shows that we can express overlapping divergences in terms of concatenated one-loop functions is somewhat technical. We nevertheless refrain from banning it to an appendix. The fact that all graphs realizing a ladder topology follow the same pattern, even for overlapping divergences, is very important to us. We thus give the construction in some detail.

   To see how to proceed let us recapitulate what we have done in Eq.(108). We wrote the original function $\Omega^{(n)}$ as a difference between a function which was UV-convergent $\Omega_f^{(n)}$ and some simpler functions $\Omega^{(n)}|_i$. The guiding principle was Weinberg's theorem [6]. In the form which is useful for us it states that once an analytic

Figure 43: These '1-state' expressions are easy to calculate. The thick line indicates the sole propagator carrying the external momentum q.

expression is finite by powercounting for its overall degree of divergence *and* all its subdivergences, we are assured that it is convergent. This allows us to conclude that $< \Omega_f^{(n)} >= 0$. But Weinberg's theorem also tells us that an expression is convergent if it has a vanishing overall degree of divergence and either it has no subdivergences (the previous case) or it has all its subdivergences subtracted by appropriate counterterms. This statement is just the underlying principle which determines the counterterms required to make a renormalizable theory finite. Vice versa, we know that for every combination of loop momenta providing a subdivergence, there exist an appropriate counterterm in the sum in Eq.(110). We will show that this gives us an algorithm to continue the process which was started in Eq.(108) to simplify $\Omega^{(n)}$.

But we will give the result first. To this end let us introduce some notation.

- The massless n-loop ladder graph: $^|\Box \ldots \Box^|_n$, where $^|$ indicates the flow of the external momenta. We call this a $(0, n)_n$ state, as the momenta flows through the whole n-loop graph.

- The $(i, j)_n$ state: $\Box \ldots \Box^|_i \Box \ldots \Box^|_j \Box \ldots \Box_n$, we agree to count i from the left and j from the right. There are n-loops altogether. The external momentum flows through $n - i - j$ of them.

- Counterterm graphs: $\Box \ldots \Box_r] \Box \ldots \Box^|_i \Box \ldots \Box^|_j \Box \ldots \Box_{n-r-s}[\Box \ldots \Box_s$ denotes a $(n - r - s)$-loop graph in a $(i, j)_{n-r-s}$ state multiplied by $Z^{(r)} Z^{(s)}$. This is the same as the previous case, only that r loops on the left and s loops on the right are replaced by the corresponding Z factor. Note that this is a condensed notation for a whole Z-factor, e.g.: $\Box \Box] = (< \Box \Box - < \Box > \Box >)]$.

Our final claim is that the following expression, involving 1-states only, gives the correct result for the n-loop Z_2-factor.

$$\sum_{i=0}^{n-1} \Box \ldots \Box^|_i \Box^| \Box \ldots \Box_n$$

$$- \Box] \sum_{i=0}^{n-2} \Box \ldots \Box^|_i \Box^| \Box \ldots \Box_{n-1}$$

$$- \sum_{i=0}^{n-2} \Box \ldots \Box^|_i \Box^| \Box \ldots \Box_{n-1} [\Box$$

$$-\Box\Box]\sum_{i=0}^{n-3}\Box\ldots\Box_i^|\Box^|\Box\ldots\Box_{n-2}$$

$$-\sum_{i=0}^{n-3}\Box\ldots\Box_i^|\Box^|\Box\ldots\Box_{n-2}\,[\Box\Box$$

$$\ldots$$

$$+\Box]\sum_{i=0}^{n-3}\Box\ldots\Box_i^|\Box^|\Box\ldots\Box_{n-2}\,[\Box\ldots$$

$$=\sum_{j=0}^{n-1}\sum_{\substack{i_1+i_2=j\\i_1\geq0,i_2\geq0}}\sum_{i=0}^{n-j}s(i_1,i_2)\underbrace{\Box\ldots\Box}_{i_1}]\Box\ldots\Box_i^|\Box^|\Box\ldots\Box_{n-j}[\underbrace{\Box\ldots\Box}_{j_2},\tag{111}$$

where $s(i_1,i_2)=1$ iff $i_1+i_2=0$ or $i_1i_2\neq0$, and $s(i_1,i_2)=-1$ otherwise.

Now, to prove it as promised, we use the fact that an overall convergent expression, when dressed with internal vertex and self-energy corrections, can be rendered finite by including the appropriate counterterms. So what we have to do is to do the step in Eq.(108) at the same time for a n-loop state and some appropriate chosen counterterm states so that in each step all subdivergences are compensated.

We then want to repeat the step in Eq.(108) $n-1$ times so that we end up with expressions where the exterior momenta flows only through one propagator, -1-states, for which we have:

$$\Box\ldots\Box_i^|\Box^|\Box\ldots\Box_n=B^{i-1}(\Delta)B^{n-i-2}(\Delta)\,_{n-1}\Omega.$$

These 1-states are easy to calculate. All loops which are free of the exterior momentum correspond to functions $_j\Delta$ and the exterior momentum flow is in $_{n-1}\Omega$. So we obtain the usual concatenations with the B operator. In the spirit of Eq.(108) we would like to write

$$\Omega^{(n)}|_1 \quad = \quad \Omega^{(n)}|_1 N_{l_2}N_{l_n}+\Omega^{(n)}|_{1,2}+\Omega^{(n)}|_{1,n}-\Omega^{(n)}|_{1,2,n}.\tag{112}$$

Here $|_1$ denotes the loop which is free of the external momentum already. If we now could push the analogy to Eq.(108) further and conclude

$$<\Omega^{(n)}|_1 N_{l_2}N_{l_n}>=^?0,\tag{113}$$

we would see the beginning of an algorithm leading to the final state in Eq.(111). The problem is that now, in Eq.(112), we have removed the overall degree of divergence but not all subdivergences. We have removed all subdivergences not involving l_1, but the loop corresponding to l_1 produces a problem we have not taken care of yet. We can do so by remembering Weinberg's theorem and picking up the appropriate counterterm expression:

$$<\Omega^{(n)}|_1 N_{l_2}N_{l_n}-Z_1^{(1)}\Omega^{(n-1)}|_1 N_{l_2}N_{l_n}>=0,\tag{114}$$

where $\Omega^{(n-1)}$ was expressed in $n-1$ loop momenta $l_2,\ldots,l_n$. We have in our $\Box$ notation:

$$<\Box_1^|\Box\ldots\Box_n^| \quad - \quad \Box]\,^|\Box\ldots\Box_{n-1}^|>$$

$$=< \square\square_2^|\square\ldots\square_n^| \quad - \quad \square] \,\square_1^|\square\ldots\square_{n-1}^| >$$
$$+ \quad < \square_1^|\square\ldots\square_{n-1}^|\square_n \quad - \quad \square]\,^|\square\ldots\square_{n-2}^|\square_{n-1} >$$
$$- \quad < \square\square_2^|\square\ldots\square_{n-1}^|\square_n \quad + \quad \square]\,\square_1^|\square\ldots\square_{n-2}^|\square_{n-1} >,$$

as a legitimate step.

Applying the above mechanism $n-1$ times for a n-loop graph gives us the sum over 1-states predicted in the final result above. At each step, by the very definition of renormalizability, there is an appropriate set of counterterms available so that the mechanism is justified. It is easy to see that the signs in the relation Eq.(112) conspire in the right way to guarantee that each 1-state appears exactly one time in the final sum.

We give an example for the case $n = 3$:

$$^|\square\square\square^|$$
$$- \;\square]\,^|\square\square^| \;-\; ^|\square\square^|[\square$$
$$- \;\square\square]^|\square^| \;-\; ^|\square^|[\square\square \;+\; \square]^|\square^|[\square$$
$$= \;^|\square\square^|\square \;+\; \square^|\square\square^| \;-\; \square^|\square^|\square$$
$$- \;\square]^|\square\square^| \;-\; ^|\square\square^|[\square$$
$$- \;\square\square]^|\square^| \;-\; ^|\square^|[\square\square \;+\; \square]^|\square^|[\square$$
$$= \;^|\square^|\square\square \;+\; \square^|\square^|\square \;-\; \square^{||}\square\square$$
$$- \;\square^|\square^|[\square \;-\; ^|\square\square[\square \;+\; \square^{||}\square[\square$$
$$+ \;\square\square^|\square^| \;+\; \square^|\square^|\square \;-\; \square\square^{||}\square$$
$$- \;\square]^|\square^|\square \;-\; \square]\square^|\square^| \;+\; \square^{||}\square[\square$$
$$- \;\square\square]^|\square^| \;-\; ^|\square^|[\square\square \;+\; \square]^|\square^|[\square$$
$$= \;^|\square^|\square\square \;+\; \square^|\square^|\square \;+\; \square\square^|\square^|$$
$$- \;\square](^|\square^|\square \;+\; \square^|\square^|) - (^|\square^|\square \;+\; \square^|\square^|)[\square$$
$$-\square\square]^|\square^| \;-\; ^|\square^|[\square\square$$
$$+\square]^|\square^|[\square.$$

Here we used $\square^{||}\square = 0$, as these expressions correspond to graphs where the exterior momentum does not flow at all through the graph. For a massless graph in DR we then have a vanishing tadpole graph, cf. Eq.(45).

6.2 Links and ladders

Now let us derive the same result from knot theory. Let us start again with the two-loop example. According to our rules in the previous section we obtain:

$$\text{⟜ ⟩⟨} \rightarrow {}_\Omega\!\text{⟨⟩}_\Delta + {}_\Delta\!\text{⟨⟩}_\Omega$$
$$= - < \text{○} > \text{Q}_\Omega - \text{Q}_\Omega < \text{○} >$$
$$+ \text{○⟨⟩}_\Omega + \text{⟨⟩}_\Omega \text{○}$$

This time the correspondence between a Feynman graph and a link diagram involves a sum over possibilities opened up by the overlapping topology. We have not changed the rules concerning overcrossings, but now one link will correspond to a vertex correction Δ, the other link to a self-energy Ω. The first question we have to answer is: which link serves as the skeleton and which one as the subdivergence? In case of the nested or disjoint subdivergences considered so far we could always decide this in a unique manner. By the very definition of an overlapping divergence both links above can play the role of the skeleton or subdivergence.

Accordingly, as indicated above, let us sum over both possibilities. Applying now the formalism developed in the previous section, taking into account that the skeleton is necessarily a two point function, the subdivergence necessarily a vertex correction, we obtain

$$
\begin{aligned}
Z_2^{(2)} &= \ - < \Delta > \Omega + \Delta\ _1\Omega - < \Delta > \Omega + \Delta\ _1\Omega \\
&= \ 2(- < \Delta > \Omega + \Delta\ _1\Omega),
\end{aligned}
\tag{115}
$$

which is the desired answer. Extending this result we investigate the three-loop case:

$$
\begin{aligned}
&\Omega\,\text{⬤⬤}+\text{⬤⬤}_\Omega+\text{⬤⬤}_\Omega \ \rightarrow \\
&\quad - < \bigcirc > [_\Omega\text{⬤}+ 2\text{⬤}_\Omega] \\
&\quad +\bigcirc [_\Omega\text{⬤}+ 2\text{⬤}_\Omega\ ] \\
&\qquad\qquad\qquad \rightarrow \ldots
\end{aligned}
$$

A three-loop example for the overlapping ladder topology.

We indicated the skeleton loop by an Ω. Explicitly in our one-loop functions we have

$$
\begin{aligned}
Z_2^{(3)} &= \ 2[- < \Delta > \Delta\ _1\Omega - < \Delta\ _1\Delta > \Omega \\
&\quad + << \Delta > \Delta > \Omega + \Delta\ _1\Delta\ _2\Omega] \\
&\quad -2 < \Delta > \Delta\ _1\Omega + < \Delta >< \Delta > \Omega + \Delta\Delta\ _2\Omega \\
&= \ [2\Delta\ _1\Delta\ _2\Omega + \Delta\Delta\ _2\Omega] \\
&\quad -[4 < \Delta > \Delta\ _1\Omega] \\
&\quad -2[< \Delta\ _1\Delta > \Omega - << \Delta > \Delta > \Omega] \\
&\quad + < \Delta >< \Delta > \Omega.
\end{aligned}
\tag{116}
$$

Note that the case where we read the three-loop overlapping ladder as having a one-loop correction on each side corresponds to two disjunct subdivergences. That was the reason why we discussed disjunct subdivergences in some detail in the previous section.

A comparison with Eq.(111) shows that it is again the correct result. Indeed, the sum over all possible assignments of the skeleton property to one ring equals the sum

over all the possibilities over which ring has to carry the external momentum flow, and we see that the knot theoretic approach gives the correct answer immediately.

6.3   A generalization

In analogy to the previous sections we generalize this result to the case of various topologies. To calculate cases like Fig.(44) one has to introduce a proper notation
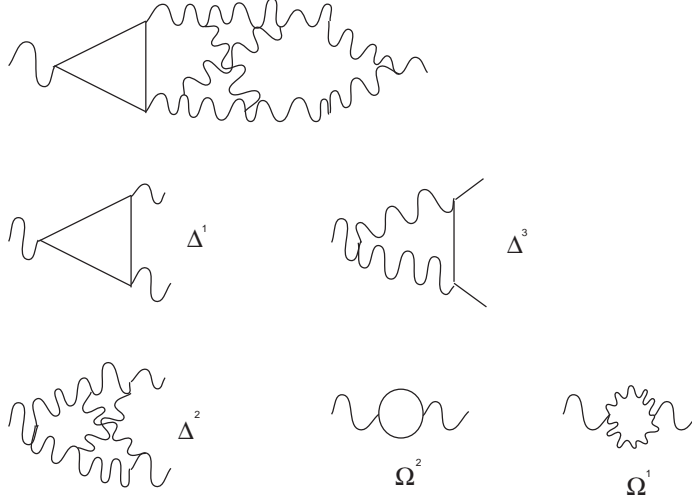

Figure 44: A more general case which demands a proper notation for various types of diagrams and topologies.

for the various one-loop functions. We find as the result in an obvious generalization of the results of Eq.(111):

$$
\begin{aligned}
Z_2(\text{Fig.}(44)) \;=\; & [\Delta^1 \,_1\Delta^2 \,_3\Omega^1 + \Delta^2 \,_2\Delta^3 \,_3\Omega^2 \\
& + \Delta^1\Delta^2 \,_3\Omega^1] \\
& - [< \Delta^1 > \Delta^2 \,_2\Omega^1 - < \Delta^2 > \Delta^3 \,_1\Omega^2 \\
& \quad - < \Delta^1 > \Delta^2 \,_2\Omega^1 - < \Delta^2 > \Delta^1 \,_1\Omega^1] \\
& - [< \Delta^1 \,_1\Delta^2 > \Omega^1 - << \Delta^1 > \Delta^2 > \Omega^1 \\
& \quad + < \Delta^2 \,_2\Delta^3 > \Omega^2 - << \Delta^2 > \Delta^3 > \Omega^2] \\
& + < \Delta^1 >< \Delta^2 > \Omega^1 .
\end{aligned}
\tag{117}
$$

These are the 12 expected terms ($2^{n-1} = 4$, from the skein relation, times 3 possibilities to assign the skeleton property).

In case that the incoming particle and the outgoing particle are different this would blow up the possibilities, e.g. Fig.(45). This completes our treatment of overlapping topologies. We succeeded in representing a sufficient large class of Feynman graphs in terms of concatenated one-loop functions. In general, we arrived at the result that the algebraic structure underlying overlapping divergences is similar to
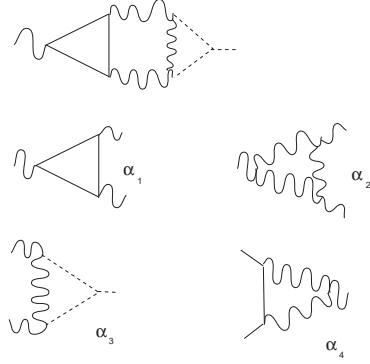
Figure 45: From the left and from the right we get different α's.

the previous cases, as long as we sum over all possibilities how to identify the skeleton graph. Referring to the research problem quoted in section three, we learn that once we have solved how to concatenate higher terms in the skeleton expansion, this knowledge would serve for nested as well as overlapping divergences.

7 No Knots, No Transcendentals

What has been achieved so far? In previous sections we expressed familiar results of renormalization theory in terms of a relative simple one-loop algebra. Occasionally we compared this with the algebraic structure dictated by link diagrams, associated to the Feynman graphs in some prescribed manner. In fact, the results of the previous sections give a complete account on how to treat general ladder-type topologies. But at some stage we want to assign knots to Feynman graphs. More specifically, we want to establish that the transcendentals obtained by calculating the UV-divergences of a topological sufficiently complicated Feynman graph characterize the knot which one obtains when considering the link diagram, associated to the graph according to the rules of section three. The following observation which is the subject of this section justifies the identification of knots with Feynman diagrams: topologically simple rainbow or ladder graphs are free of transcendentals. This sets the stage for identifying knots with Feynman graphs. We will report on the successes of such an identification in the next section, where we will investigate the triangle *Knot Theory - Field Theory - Number Theory* more closely.

We now have to investigate all Feynman graphs which correspond to simple topologies. We define a topology as simple when it corresponds to a braid group expression of at most second degree in all braid generators. These braids, after applying the skein relation n-times, will generate an unknot with writhe number n, amongst even simpler (splitted) terms. This property of being free of knots should reflect itself in the Z-factors as we want to have a chance to identify Z-factors with knots. We claim that there is a one-to-one correspondence between the transcendental numbers in the divergent part of a diagram and the knot in its link diagram, so we better prove that such transcendentals do not appear in simple topologies.

To give the reader an idea what sort of cancellations are necessary we give in the appendix a result for a seven loop ladder topology. The graph itself has transcendentals in abundance in its divergent part, but when we add its counterterm expressions they all disappear.

We proceed in the following way. We first investigate how this cancellation of transcendentals appears for some special choice (ladder topology in a massless Yukawa theory, see appendix for Feynman rules) of the Δ function. In fact, we show that for an arbitrary loop order n the highest possible transcendental $\zeta(n-1)$ will not arise. The proof for the other transcendentals is similar.

We indicate how the proof has to be generalized for the arbitrary tensor case. Then we discuss this cancellation of transcendentals from a broader viewpoint and give a general inductive proof. Recently, Bob Delbourgo et.al.[26] have given an independent proof for the statement. They transferred the Schwinger Dyson Equation for bare ladder diagrams to a differential equation, which they solved for general D, where D refers to the generalized dimension of dimensional regularization. Upon expanding their non-perturbative solution in the coupling constant one confirms the results of this section.

The result here is the following statement: Any Feynman graph in a renormalizable theory which corresponds to a simple topology in its link diagram gives rise to only rational divergences when calculated together with its counterterm graphs.

Here rational divergences means that only rational numbers appear as coefficients of the proper Laurent part in the DR expansion parameter ϵ.

7.1 A combinatorical proof

Let us start considering the following function, which exhibits all typical properties of the observed cancellations:

$$_j\Delta : \qquad \int d^D k \frac{(k^2)^{-\varepsilon j}}{k^2(k+q)^2} =: (q^2)^{-\varepsilon(j+1)}{}_j\Delta,$$

$$\Rightarrow {}_j\Delta = \frac{\Gamma(1+(j+1)\varepsilon)\Gamma(1-\varepsilon)\Gamma(1-(j+1)\varepsilon)}{(j+1)\varepsilon(1-(j+2)\varepsilon)\Gamma(1+j\varepsilon)\Gamma(1-(j+2)\varepsilon)}.$$

Define

$$P_n := \prod_{i=0}^{n-1} {}_i\Delta,$$

$$\Rightarrow P_n = \frac{(\Gamma(1-\varepsilon))^{n+1}\Gamma(1+n\varepsilon)}{n!\varepsilon^n(1-2\varepsilon)\dots(1-(n+1)\varepsilon)\Gamma(1-(n+1)\varepsilon)}.$$

Now use

$$\Gamma(1-z) = \exp(\gamma z)\exp(\sum_{j=2}^{\infty} \frac{\zeta(j)}{j}z^j). \qquad (118)$$

It follows

$$P_n = \frac{1}{n!\epsilon^n(1-2\epsilon)\dots(1-(n+1)\epsilon)}\exp(-n\gamma\epsilon) \times$$

$$\exp(\sum_{j=2}^{\infty}\frac{\zeta(j)}{j}\epsilon^j[n+1+(-n)^j-(n+1)^j]).$$

We conclude immediately that $\zeta(2)$ can not appear in a Z-factor contribution as its coefficient is $(n+1+n^2-(n+1)^2) = -n$, so it can be absorbed in a redefined coupling constant in the same way as γ:

$$g\mu^{-\epsilon} \to g\tilde{\mu}^{-\epsilon}, \ \tilde{\mu} = \mu\exp((\gamma+\epsilon\zeta(2)/2)/2).$$

As any contribution at the n-loop level factors α^n, where $\alpha := g^2/4\pi$, we see that this modification deletes any $\zeta(2)$ dependence, an argument which is familiar from $\overline{MS}$ schemes.[18]

More subtle is the cancellation of higher transcendental ζ's. As an example let us consider $\zeta(n-1)$, the highest possible transcendental appearing in a n-loop calculation. Only the highest pole $\frac{1}{\epsilon^n}$ can generate it, so we have to consider

$$\frac{1}{n!}\frac{1}{\epsilon^n}\frac{\zeta(n-1)}{n-1}\epsilon^{n-1}[n+1+(-n)^{n-1}-(n+1)^{n-1}],$$

---

[18] We remind the reader that the μ-dependence comes in as we demand a dimensionless coupling constant in dimensional regularization. In $\overline{MS}$ schemes one uses this μ-dependence to absorb Eulers constant γ. The demand that physical quantities are independent of μ results in the so-called renormalization group equations.

which is the contribution of P_n to $\zeta(n-1)$.

Also the counterterm expressions have to provide their highest pole. Let us study a 4-loop example:

$$
\begin{aligned}
Z_1^{(4)} \;=\;\; & <P_4- <P_1> P_3- <P_2- <P_1> P_1> P_2 \\
& - <P_3- <P_1> P_2- <P_2- <P_1> P_1> P_1> P_1> . \quad (119)
\end{aligned}
$$

It follows for the coefficient of $\zeta(3)$:

$$
\begin{aligned}
S_4(3) \;:=\;\; & \frac{1}{\epsilon}\frac{1}{4!0!}\frac{1}{3}[5+(-4)^3-5^3] \\
& -\frac{1}{\epsilon}\frac{1}{3!1!}\frac{1}{3}[4+(-3)^3-4^3] \\
& -\frac{1}{\epsilon}\frac{1}{2!2!}\frac{1}{3}[3+(-2)^3-3^3] \\
& -\frac{1}{\epsilon}\frac{1}{1!1!2!}\frac{1}{3}[3+(-2)^3-3^3] \\
& -\frac{1}{\epsilon}\frac{1}{3!1!}\frac{1}{3}[2+(-1)^3-2^3], \\
& \cdots
\end{aligned}
$$

where ... refers to the last three terms in Eq.(119) which add to zero. We have for the coefficient of $\zeta(3)$

$$
S_4(3) = \frac{1}{\epsilon}\sum_{i=1}^{4}(-1)^i\frac{1}{i!(4-i)!}\frac{1}{3}[i+1+(-i)^3-(i+1)^3] = 0.
$$

It is easy to see that in general the coefficient of $\zeta(n-1)$ is given by

$$
S_n(n-1) := \frac{1}{\epsilon}\frac{1}{n-1}\sum_{i=1}^{n}(-1)^i\frac{1}{i!(n-i)!}[i+1+(-i)^{n-1}-(i+1)^{n-1}].
$$

So we have to show $S_n(n-1)=0$. Let us use

$$
(1-a)^n = \sum_{i=0}^{n}\frac{(-1)^i a^i n!}{i!(n-i)!} = \sum_{i=0}^{\infty}\frac{(-1)^i a^i \Gamma(n+1)}{\Gamma(i+1)\Gamma(n-i+1)},
$$

from which we conclude

$$
\delta_{n,0} = \sum_{i=0}^{\infty}\frac{(-1)^i}{\Gamma(i+1)\Gamma(n-i+1)}.
$$

Consider

$$
T_n(r) := \sum_{i=0}^{\infty}\frac{(-1)^i i^r}{\Gamma(i+1)\Gamma(n-i+1)}, \quad r > 0.
$$

which appears in $S_n(n-1)$. It is possible to express i^r as a linear combination of terms

$$
i(i-1)\ldots(i-r+1)+i(i-1)\ldots(i-r+2)+\ldots+i,
$$

so that

$$i^r = \sum_{j=1}^{r} c_{rj} \frac{\Gamma(i+1)}{\Gamma(i-j+1)},$$

and we obtain

$$
\begin{aligned}
T_n(r) &= \sum_{i,j=1}^{r} (-1)^i \frac{c_{rj}}{\Gamma(i-j+1)\Gamma(n-i)} \\
&= \sum_{i,j}^{r} (-1)^{i+j} \frac{c_{rj}}{\Gamma(i+1)\Gamma(n-i-j)} \\
&= \sum_{j=1}^{r} (-1)^j c_{rj} \delta_{n-j,0} \\
&= (-1)^n c_{rn}.
\end{aligned}
$$

We have

$$c_{rn} = 0, \ r < n,$$
$$c_{rn} = 1, \ r = n,$$

and finally

$$T_n(r) = 0 \ \text{ for } 0 < r < n,$$
$$T_n(n) = (-1)^n.$$

By a similar argument we can show that

$$
\begin{aligned}
U_n(r) &:= \sum_{i=0}^{\infty} \frac{(-1)^i (i+1)^r}{i!(n-i)!} = 0 \ \text{ for } 0 < r < n, \\
U_n(n) &= (-1)^n.
\end{aligned}
$$

Combining everything we find

$$S_n(r) = 0, \ r \leq n,$$

which includes the desired result for $S_n(n-1)$. This proof was first obtained in collaboration with Bob Delbourgo.

Some comments might be appropriate. We investigated the above case for $D = 4-2\epsilon$ dimensions, where the function $_j\Delta$ corresponds for example to a Green function in Yukawa theory. Nevertheless it is the generic example for all possible cases in a renormalizable theory. In the case of tensor integrals or dimensions other than four our function would only be modified by a polynomial of ϵ which multiplies it. This leaves the basic structure of the sums above unaffected and the reasoning remains unchanged. We could now proceed to show the absence of the other transcendentals $S_n(r)$ along similar lines. In fact, by inspection one sees that the cases for $\zeta(n-i), i > 1$ follow the same pattern.

Rather we prefer to give a more general argument establishing rational contributions for Z factors from simple topologies for all renormalizable theories.

7.2 A global argument

We argue for the case of a vertex function, the propagator follows similarly.

Let a generalized one-loop function $_j\Delta$ be given. Assume we can render it finite with the help of another function $_j\bar\Delta$

$$< \,_j\Delta - \,_j\bar\Delta >= 0. \qquad (120)$$

According to the Schwinger Dyson equation, we would get the Z factor as

$$Z = < G_R \circ \,_j\Delta > = < G_R \circ \,_j\bar\Delta >, \qquad (121)$$

where we solved the Schwinger Dyson equation Eq.(54) for Z and discarded the finite term containing the full renormalized vertex. It is crucial that in the Schwinger Dyson equation only finite renormalized Green functions appear.

The following examples explain the meaning of our concatenation $\circ$ in Eq.(121):

2 loops: $\quad G_R^{(1)} = \,_0\Delta - < \,_0\Delta > \;\Rightarrow Z^{(2)} = < \,_0\Delta_1\Delta - < \,_0\Delta > \,_0\Delta >,$

3 loops: $\quad G_R^{(2)} = \,_0\Delta_1\Delta - < \,_0\Delta > \,_0\Delta - < \,_0\Delta_1\Delta - < \,_0\Delta > \,_0\Delta > \;\Rightarrow$

$\quad Z^{(3)} = < \,_0\Delta_1\Delta_2\Delta - < \,_0\Delta > \,_0\Delta_1\Delta - < \,_0\Delta_1\Delta - < \,_0\Delta > \,_0\Delta > \,_0\Delta > .$

Now assume that $_j\bar\Delta$ enjoys the following property:

$$< (\prod_{i=0}^{j-1} \,_i\Delta)_j\bar\Delta >\in \mathbf{Q}. \qquad (122)$$

It removes all transcendentals from lower level products of Δ functions.

Then we would easily achieve our aim by induction: $Z^{(n+1)}$ is rational if and only if $Z^{(n)}$ is rational. By the very definition of $Z^{(n+1)}$ it is given as a sum of products of lower level Z factors with concatenated Δ-functions, where we replace the last one by the barred form, as in the above examples. Eq.(121) would give the Z factor immediately as a product of rational functions, if Eq.(122) holds.

So the rationality of the Z factor is proven if we can establish the existence of a family of functions $_j\bar\Delta$ such that

- $_j\Delta - \,_j\bar\Delta$ is finite by power-counting

- Eq.(122) holds.

The structure of the generalized one-loop functions allows us to write

$$_m\Delta =: f_m(D-4) \, \exp g_m(D-4) \Rightarrow \prod_{i=0}^{j-1} \,_i\Delta =: p_j(D-4) \, \exp\left[q_j(D-4)\right], \quad (123)$$

which defines f_m, g_m, p_j, q_j. Here f_j, p_j are rational functions of $(D-4)$. We set

$$_j\bar\Delta := f_j(D-4) \exp\left(-q_{j-1}(D-4)\right). \qquad (124)$$

64

We immediately conclude that Eq.(122) holds:

$$< (\prod_{i=0}^{j-1} {}_i\Delta)_j\bar{\Delta} >= p_j(D-4)f_j(D-4). \tag{125}$$

The demand that ${}_j\bar{\Delta}$ removes the overall divergence by powercounting is easy to achieve. We give an explicit construction in appendix E. We only have to guarantee that the function has the correct asymptotic behaviour. It follows that

$$< G_R \circ ({}_j\Delta - {}_j\bar{\Delta}) >= 0, \tag{126}$$

which completes our proof. Again we explored the fact that a function which is overall finite as $\sim ({}_j\Delta - {}_j\bar{\Delta})$ is finite when all its subdivergences are subtracted.

For the propagator we can argue in a similar way. We only have to take care of the modification in the Schwinger Dyson equations for this case.

We further observe that the difference

$$\left[\prod_{i=0}^{j-1} {}_i\Delta\right] {}_j\bar{\Delta} - \prod_{i=0}^{j} {}_i\Delta , \tag{127}$$

is of order ϵ. So we can allow for one further dressing to be present at some other line or vertex. The difference would be finite for this case. This is still sufficient to replace the ultimate ${}_j\Delta$ by ${}_j\bar{\Delta}$, and thus the proof still goes through. On the other hand any further dressing spoils our argument. This is precisely the behaviour observed in previous sections. Ladder and rainbow topologies considered there were free of transcendentals. We can compare it also with the results in [18], which were already briefly mentioned in section five. There, the examples in Table(1) confirm these findings. We expect transcendentals of the type $\zeta(n), n \geq 3$ to appear as soon as we have three or more dressings. This is indeed the case, and their appearance matches all ways we can assign link diagrams to the Feynman graph. But the real confirmation of a connection between knots and numbers via Feynman graphs will be given in the next section, where we report on recent results exploring this idea by calculating diagrams mostly free of subdivergences, but of complicated topology.

In this section we have learned that the the very special sort of topological simple Feynman diagrams will only generate rational contributions to MS Z-factors.

8   Knots and Transcendentals

In this section we describe results which were obtained recently [13, 14, 15, 16, 17, 18].[19] In these six publications a fascinating connection between field theory, number theory, and knot theory emerges. The starting point of this connection is the result of the previous section connecting topologically simple graphs with the absence of knots in their link diagram, and with the corresponding absence of transcendentals in their counterterms.

So the previous section suggests that the transcendental coefficients of the divergences are related to the topology of the diagram. This relation should be via knot theory. As we will see, field theory initiated the invention of a knot-to-number dictionary, which in turn spurred new findings in number theory and opened a new route for calculations in field theory.

In the following, we will first give elementary examples how to obtain $(2, q)$ torus knots in topologically non-simple diagrams, and compare with the transcendentals $\zeta(q)$ in their counterterms.

Then we will comment in detail on all the six publications mentioned above. Each of them gives new insights and support to the connection between renormalization, knot theory and number theory:

([13]) Here it was shown that at the six loop level for the first time a $(3, 4)$ torus knot was obtained. This matches the appearance of the transcendental $\zeta(3, 5)$ in the counterterm.

([14]) The identification of knots with numbers is used to calculate the scheme independent part of the β-function in ϕ^4 theory to the seven loop level. Knots obtained from the diagrams match and thus predict the transcendentals apparent in the counterterms.

([15]) The existence of a skein relation together with the Ward identities explains the cancellations of transcendentals long known for the quenched β-function in QED.

([16]) Bubble insertions in a basic two-loop topology deliver Euler double sums. The restricted class of knots obtained from these diagrams governs the number of independent double sums, and informs number theory.

([17]) All this led Broadhurst to conjecture a formula for the number of independent Euler sums, and thus solving a major number-theoretic problem. The findings are supported by striking numerical evidence, and agree with field/knot-theoretic expectations whenever a comparison is possible.

([18]) Generalized one-loop functions behave under renormalization in accordance with the demands of link theory. This confirms the identification of knots and numbers in [16] and predicts the entanglement for more general cases.

---

[19]Note added in proof: While this paper was written, further results along the same lines were obtained in [39, 18, 40].

8.1 The $(2, q)$ torus knots and $\zeta(q)$

The most prominent transcendentals stem from the Riemann ζ function evaluated at odd integer argument. They arise from the expansion of the Γ function near unit argument (cf. Eq.(118)) [23].

The first non-trivial candidate would be $\zeta(3)$. Let us consider some three-loop graphs as shown in Fig.(46). It is well known that all the above graphs, even after
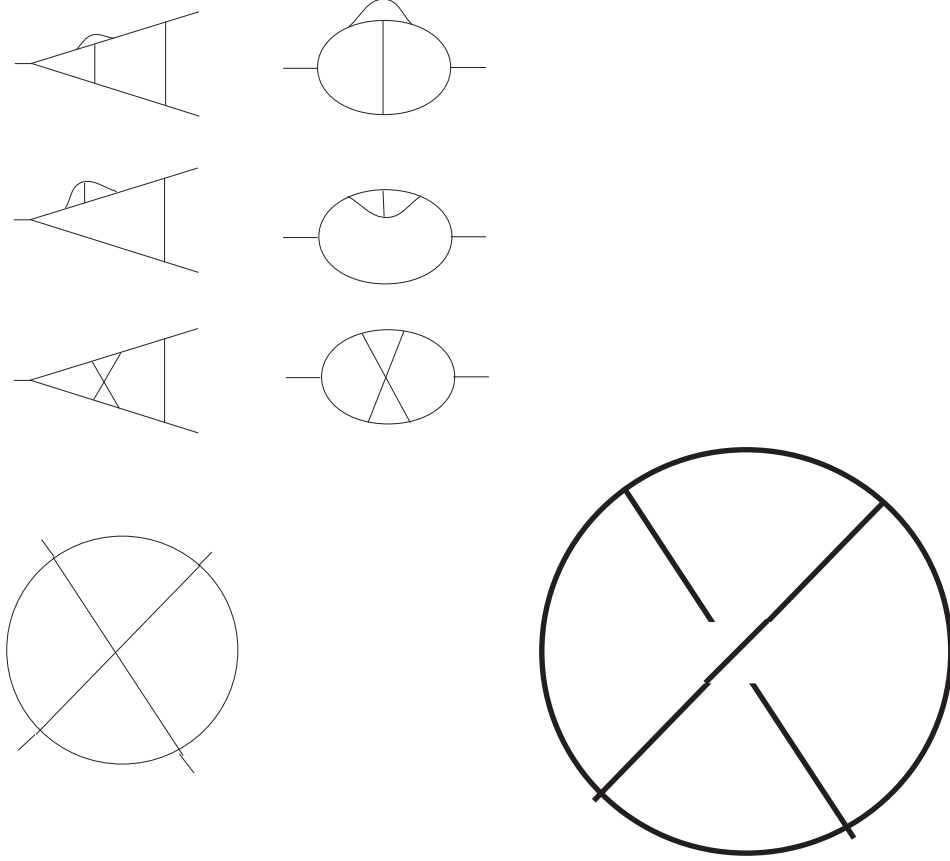

Figure 46: These three-loop graphs involve $\zeta(3)$ in their divergent part. They are all derived from the general topology on the rhs, by coupling two, three or four external particles at different places. The last graph on the lhs below is a ϕ^4 graph and free of subdivergences.

adding their counterterms, give us a non-vanishing coefficient for $\zeta(3)$. For example the overlapping massless two-point function, a prominent example for generating a transcendental series in ε [21], appears as a subgraph in all of the above graphs. Its finite value is $6\zeta(3)$ (for a scalar theory, with the coefficient 6 changing to other rational values for other theories). The counterterm subtracts only the divergent part of the subgraph, and thus there remains the term proportional to $\zeta(3)$ which is then multiplied by the divergence from the final loop integration. The coefficient

of $\zeta(3)$ naturally depends on the actual theory under consideration; we restrict ourselves to scalar theories at the moment for convenience. In appendix D the reader will find an explicit calculation of the counterterm for the ϕ^4 diagram in Fig.(46), deriving the result $6\zeta(3)/\epsilon$ for it. In all cases the corresponding link diagrams have a topology which for the first time involves a mutual entanglement of three links, see Fig.(47). We see that the trefoil knot appears when we apply the
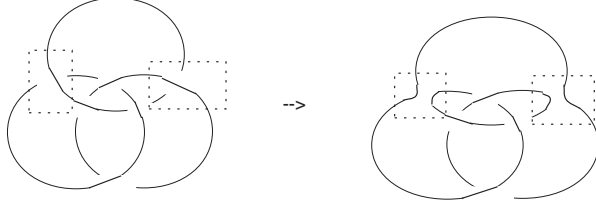

Figure 47: The corresponding link diagrams. The dashed rectangles indicates where the Y part of the skein relation has been applied twice.

Y part of the skein relation twice. This topology gives us the braid expression

$$\sigma_1\sigma_2\sigma_1^2\sigma_2\sigma_1. \tag{128}$$

For the first time we encounter a more complicated word in braid group generators. Applying a skein relation, it splits into various terms. Terms which separate into disjoint components should correspond to counterterm graphs, according to our previous experience. If there are no subdivergences, all the subgraphs are finite, and thus nullified by the projection onto their divergence. To see the pure knot content, consider for example the ϕ^4 graph in Fig.(46). It is free of subdivergences. So the only remaining term in the skein relation comes from considering the application of the Y part. Our aim is to apply it twice in a way which delivers a one-component knot. No matter how we do this, the result is always of the form $\sigma_1\sigma_2\sigma_1^2$. This is the trefoil knot, with an extra curl in it.

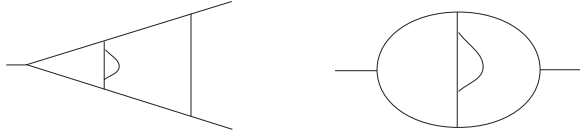Let us comment on the following two graphs of Fig.(48).

Figure 48: Two examples which do not produce $\zeta(3)$, nor the trefoil knot.

In Fig.(49) we compare the generation of the link diagram for them with the generation of link diagrams for the examples in Fig.(46).

Note that in Fig.(46) the example for ϕ^4 theory is unique in the respect that it is a pure skeleton graph itself, without any subdivergences. Summarizing, *we are now prepared to assign $\zeta(3)$ to the trefoil topology.*
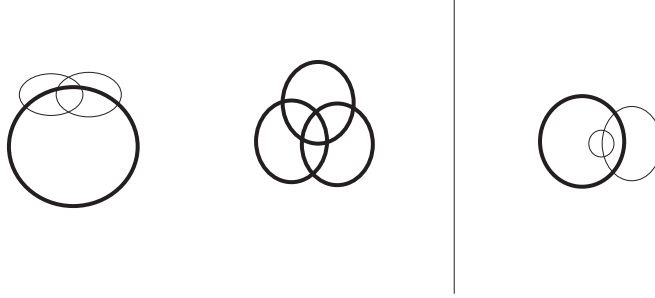
Figure 49: We get the trefoil via these link diagrams. The second one on the lhs is the one for the ϕ^4 diagram (the whole diagram is a skeleton graph), while all the other ones in Fig.(46) provide a one-loop skeleton (thick line), dressed with two-loop subdivergences. On the rhs we give the link diagram for the graphs of Fig.(48).

We note that we can assign loop momenta always in a way that they all encircle a given point • inside the diagram counterclockwise. This point corresponds to an axis in a closed braid diagram where all strands are oriented to encircle it in this manner. Having defined such an axis in the Feynman graph we replace the momentum flow by strands according to our rules of section three and read off the braid group expression from the link diagram. Now, as we have more complicated topologies, over/undercrossings in our link diagram must either correspond to a vertex in the Feynman diagram or to a crossing of propagators in the Feynman diagram, cf. Fig.(46). For the trefoil example we find Fig.(50). The trefoil knot is
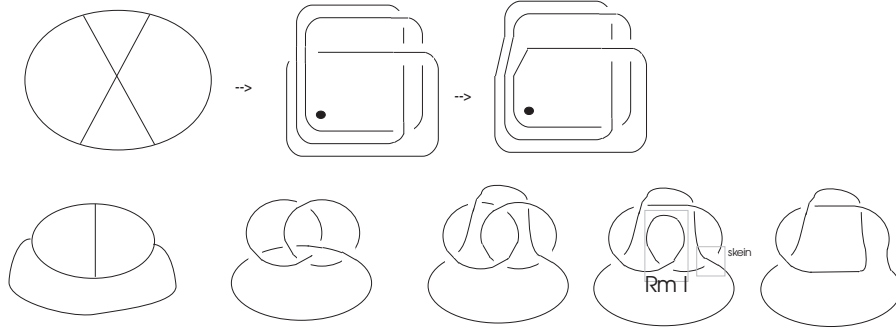

Figure 50: An economic way from a Feynman diagram to a link diagram to a knot. We omit to indicate exterior momenta. So the Feynman graph on the left is generic to all the graphs of Fig.(46). Note that the topological non-simple structure of the graph, the crossing of its internal propagators, directly reflects itself in the braid group expression Eq.(128), by having the generator σ_1 in fourth power. We give two equivalent link diagrams, resulting from different momentum flows.

the $(2,3)$ torus knot [12]. We can readily generalize this example to the n-loop case, demonstrated in Fig.(51).

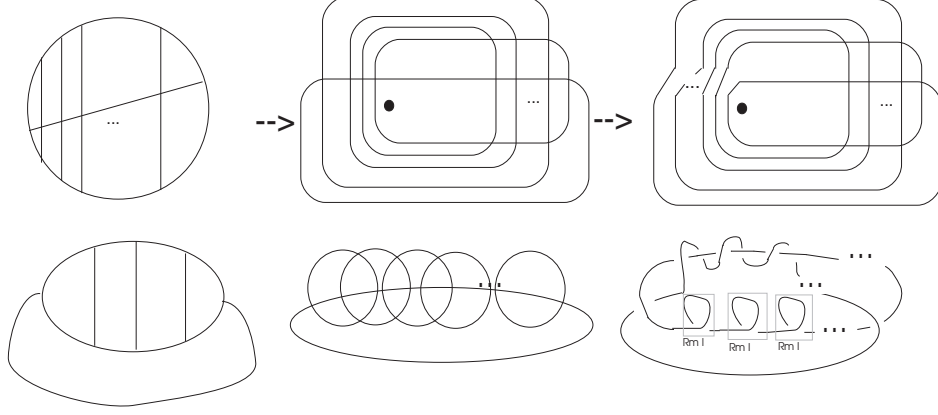It is a well known fact that the Feynman graphs with a slashed ladder topology

69

Figure 51: The same for the n-loop case. The topology of the Feynman diagram is a slashed ladder. External particles may couple at arbitrary places. We observe that $n-1$ loops realize the ladder topology, and one loop goes through the middle of this $n-1$ cable. We omitted over/undercrossings in the above picture, as they are clear from the orientation of the loop momenta. We give two equivalent link diagrams. They produce the same $(2, 2n-3)$ torus knot at the end.

are proportional to $\zeta(2n-3)$ at the n loop level [27]. The corresponding link diagram generates the knot σ^{2n-3}, which is the $(2, 2n-3)$ torus knot. To see this we read off from Fig.(51) the braid group expression:

$$\sigma_{n-1}\ldots\sigma_1\sigma_2\ldots\sigma_{n-1}\sigma_1\ldots\sigma_{n-2} = \sigma_{n-2}^{2n-3},$$

after applying Markov- and Reidemeister-moves. For example, chosing $n = 4$, we calculate

$$\sigma_3\sigma_2\sigma_1\sigma_2\sigma_3\sigma_1\sigma_2 = \sigma_2\sigma_1\sigma_2\sigma_1\sigma_3\sigma_2\sigma_3 =$$
$$\sigma_2\sigma_1\sigma_2\sigma_1\sigma_2\sigma_3\sigma_2 = \sigma_2\sigma_2\sigma_1\sigma_2\sigma_1\sigma_2\sigma_3 =$$
$$\sigma_2\sigma_2\sigma_1\sigma_2\sigma_1\sigma_2 = \sigma_2\sigma_2\sigma_2\sigma_1\sigma_2\sigma_2 =$$
$$\sigma_2^5\sigma_1 = \sigma_2^5,$$

and one easily proves the result for arbitrary n by utilizing $\sigma_i\sigma_{i+1}\sigma_i = \sigma_{i+1}\sigma_i\sigma_{i+1}$. For the second representation given in Fig.(51) the appearance of the $(2, 2n-3)$ torus knot is verified immediately.

So we have the beautiful correspondence $\zeta(2n-3)$ *in the Feynman graphs* $\leftrightarrow$ $(2, 2n-3)$ *torus knot in the link diagram*. Fig.(52) lists some Feynman diagrams, link diagrams, braid words for the knots in them, and numbers obtained from explicit calculation. We stress that we have transcendentals which are single sums, and braid words which rely on a single generator. The power of the generator matches the exponent in the sums. This is the first class of Feynman diagrams whose transcendentals are described by a simple knot class. The counterterms of Feynman diagrams which have the topology of a crossed ladder -Fig.(51)- deliver countertems
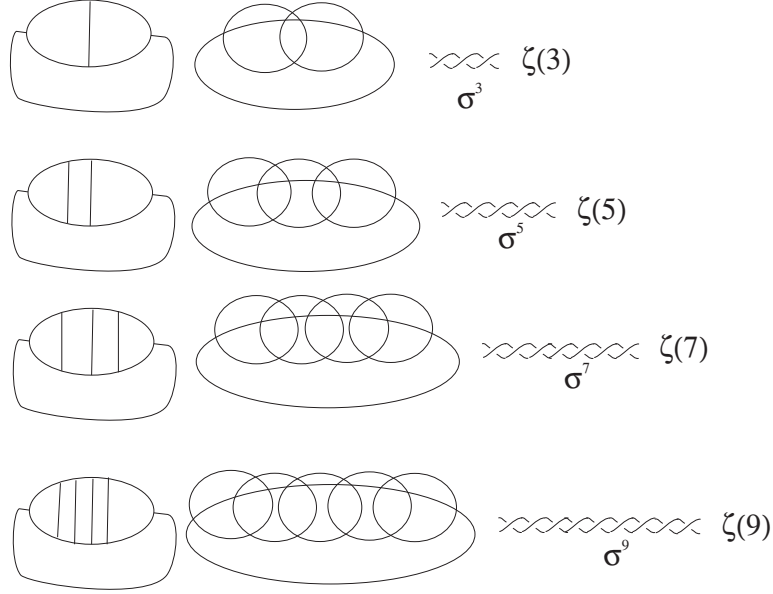
Figure 52: A beautiful coincidence between $(2, q)$ torus knots and transcendental counterterms $\zeta(q) = \sum_{n=1}^{\infty} \frac{1}{n^q} \sim \sigma^q$. We note that the powers of braid generators match the powers in the infinite sum representation of the transcendental $\zeta(2n - 3)$.

which have the form $\sim \zeta(2n - 1)/\epsilon$, and deliver the $(2, q)$ torus knots from the link diagrams. The coefficients of the transcendental depend on the particles realizing the topology. This opens an interesting problem in representation theory: how do the rational coefficients of $\zeta(2n-3)$ change with the particle content of the diagram? This is under investigation at the moment.

8.2 The $(3,4)$ torus knot and the first Euler double sum

We have classified ladder (no knots) and crossed-ladder topologies ($(2,q)$ torus knots). In the next step we generalize this to more complicated topologies. We will see that at the six-loop level for the first time a new knot appears, and that at this level for the first time a new transcendental is obtained. It has the form of an Euler double sum, and thus is a generalized ζ-function of two integer arguments. We identify the new knot with the new transcendental. From now on we denote such transcendentals as knot-numbers, with $\zeta(q)$ being the knot-numbers of the $(2,q)$ torus knots.

An important observation is that all the subdivergence-free diagrams considered here and in the following allow for a Hamiltonian circuit representation. This means that we can find a closed non-singular curve (no self-intersections) in the diagram which traverses all internal vertices. In general, not every three-valent graph allows for a Hamiltonian circuit, but the failure appears at loop orders and topologies which are not relevant for our purposes [29]. In fact, this statement is only true for graphs without subdivergences. For graphs with subdivergences it is very easy to construct examples which do not allow a Hamiltonian circuit.

Having identified such a Hamiltonian circuit it was used in [13] to simplify the search for corresponding link diagrams and knots: assume we draw all propagators in the interior of the Hamiltonian circle. Now let us remove as many propagators as necessary to make the diagram planar (it reduces to a ladder topology). Using our standard momentum routing for this reduced diagram, let us begin to attach the non-planar propagators again, this time always using Reidemeister III moves to avoid crossings with the inner propagators of the Hamiltonian circuit. These inner propagator constitute a ladder topology, which is then disturbed by any further propagator which makes it into a non-trivial topology. Assume we have r such inner propagators. Skeining the r components of the ladder, it is clear that we get $r-1$ Reidemeister I moves for free, removing $r-1$ crossings in the link diagram. There remains a link diagram with $n-r$ components, which still has to be skeined. In Fig.(53) we demonstrate the method, which was also used in the second link diagram in Fig.(51).

We conclude that as far as the knot content of the link diagram is concerned the planar rungs are irrelevant. By chosing the orientations of the components in an appropriate manner we will only obtain positive knots with this method. Topologically non-trivial propagators are drawn in the exterior of the Hamiltonian circuit. They are connected to vertices in the most economic way, avoiding as many crossings as possible.

But in multi-loop calculations one finds occasionally new transcendentals, independent from $\zeta(i)$. A first and prominent example is the transcendental found by David Broadhurst in a six-loop calculation at transcendentality level 8 [28]. According to our experience with ζ-transcendentals, we would expect a knot with 8 crossings to appear in the corresponding Feynman graph, which is confirmed in Figs.(55,56). The corresponding ϕ^4 graph was mapped to a graph with three-point couplings by using a Lagrange multiplier field. From the three ways how to map a four-point coupling to a three-point coupling only those possibilities were considered which did not change the topology of the graph. The first graph which gave
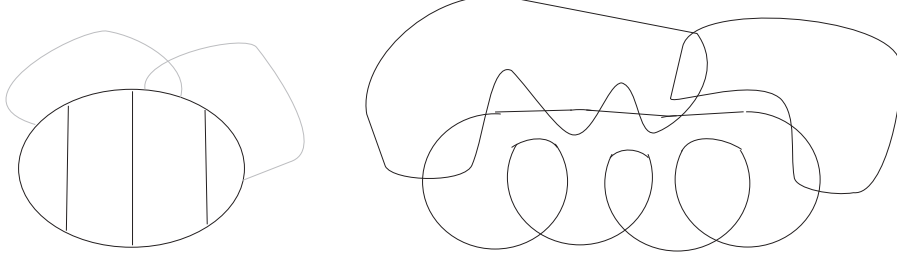
Figure 53: A systematic method to obtain link diagrams. This method proved successful in the investigation of subdivergence-free diagrams. For this example, we would get three *RMI* moves on the rhs for free.
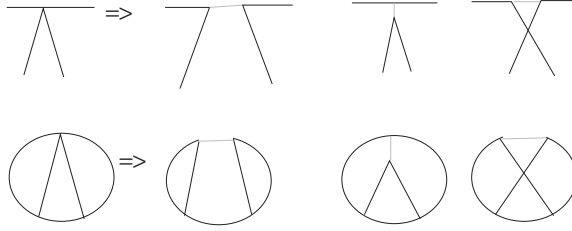

Figure 54: There are three ways to map a four point coupling to two three-point couplings. Some change the topology of the corresponding link diagram. The results exclude the choices which generate extra crossings. In the example, only the first one gives the correct answer, the other two generate extra crossings in the link diagram.

a non-ζ transcendental is the six-loop graph in Fig.(55). Let us map this graph to a link diagram as in Fig.(56) to identify the $(3,4)$ torus knot. The identification of the $(3,4)$ torus knot is achieved by reading off the braid word

$$\sigma_1\sigma_2^3\sigma_1\sigma_2^3 = (\sigma_1\sigma_2)^4$$

in Fig.(56). In general, the (p,q) torus knot has braid word [30]

$$(\sigma_1 \ldots \sigma_{p-1})^q.$$

We expect only positive braid words to appear. Positive braid words have only positive powers of braid generators. The positive braid words up to nine crossings are the $(2,q), q \in \{3,5,7,9\}$ torus knots plus the $(3,4)$ torus knot. Crossing number nine is the transcendentality level nine which is exhausted by graphs up to six loops [28]. An investigation of the results in [28] confirmed this pattern. All six-loop graphs considered deliver knots which faithfully describe the transcendentals in their counterterms.

Further, as the $(3,4)$ torus knot is the only non-ζ-ish transcendental at level 8, we conclude that our knot theoretic approach predicts a relation between the value of the transcendental M which Broadhurst reported in [28] and the level 8 transcendental $U_{6,2}$ which was found in the expansion of the master function [21]. Such a relation was meanwhile established and is given in [14].
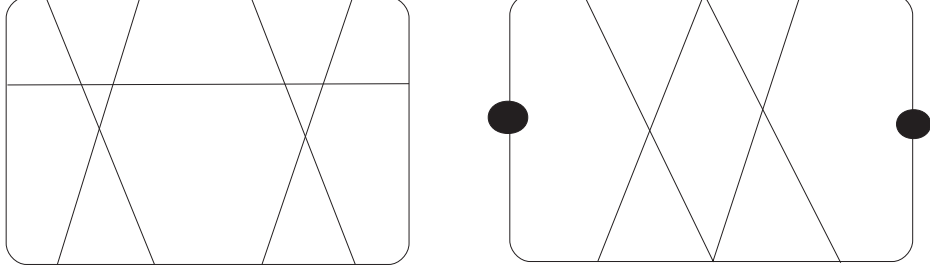
Figure 55: We like to investigate this six-loop Feynman graph. We also give a ϕ^4 graph which is topologically equivalent, and which was investigated by Broadhurst. The two dots in this graph have to be identified. It can be obtained from the graph on the lhs by shrinking three propagators.

Meanwhile, number theorists proved that the new knot number is an independent transcendental indeed [17]. Again there is a striking match between the structure of the possible braid word and the structure of the transcendental. The transcendental comes as a double sum, where the two exponents match the powers of the two braid generators:

$$\text{braid word } \sigma_1\sigma_2^3\sigma_1\sigma_2^3 \Leftrightarrow \sum_{i_1<i_2}^{\infty} \frac{1}{i_1^2 i_2^6}. \tag{129}$$

Other representations of this knot have other 8-crossing braid words, but then other level 8 double sums are equivalent to the one given. This is so as one can prove that there is only one independent level 8 double sum.
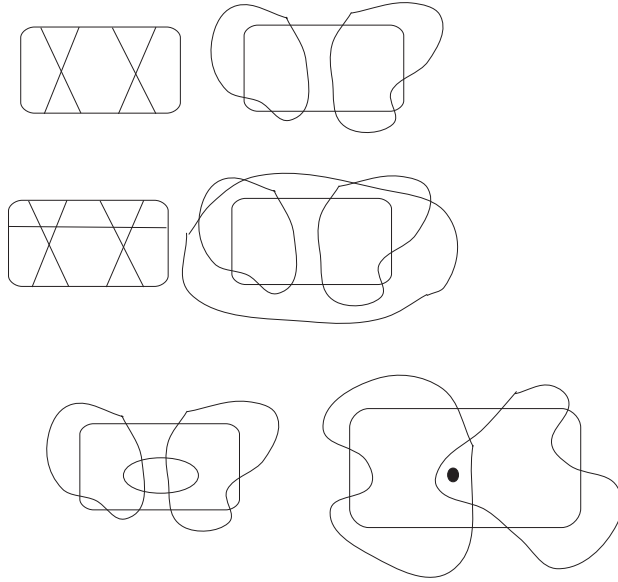
Figure 56: The generation of the $(3,4)$ torus knot. In the first line we have removed one propagator to generate the $\zeta(3)\zeta(3)$ factor knot. Then we attach the last propagator in the most economic way, giving us the link diagram on the bottom rhs. We used Reidemeister II and III moves to get from the second to the third line. We end up with the braid word $\sigma_1^4\sigma_2\sigma_1^4\sigma_2$. (All components encircle the dot in the middle counterclockwise, so that we can read off the braid word.) After skeining the two kidneys we find a knot. It can be identified as the 8_{19} knot in the standard tables [12], which is the $(3,4)$ torus knot.

8.3 ϕ^4 theory: more knots and numbers

This section reports on a major work, which initiated most of the subsequent activities in the field. To test the ideas developed so far a calculation of the β-function in ϕ^4 theory was undertaken. For us it is sufficient to mention that the β-function is a function which is determined by the divergences of the Feynman graphs. In fact, in the MS renormalization scheme, it solely relies on the divergences of the graph. It determines the dependence of the coupling constant on the mass scale.[20] Being calculable in terms of divergences, the β-function is a quantity well-suited to test our ideas.

Having satisfyingly matched all six-loop graphs with the correct knot-numbers, the process was inverted to obtain a method to calculate diagrams analytically, when they were only available numerically. By mapping Feynman diagrams to knots, and by matching knots to knot-numbers, we obtain a conjecture for the transcendentality content of a graph.

Let us say we suspect that a graph G should have the form $G = a_1\zeta_1 + a_2\zeta_2$, for knot-numbers ζ_1, ζ_2 and rational numbers a_1, a_2. The transcendentals ζ_1, ζ_2 are delivered by the link diagram associated with the graph, and a_1, a_2 are yet to be determined. Then, by having a numerical value for the graph G_{num}, we can try to determine the rational numbers a_1, a_2 by solving $G_{num} = a_1\zeta_1 + a_2\zeta_2$, such that a_1, a_2 are simple rational numbers, and then check if the solutions remain unchanged if we increase the accuracy of G_{num}. Numerical as well as number theoretic methods give a precise answer and error estimate for the validity of this approach.

Exploring this method, the authors of [14] calculated all the primitive divergences contributing to the 7–loop β–function of ϕ^4 theory, i.e. all 59 diagrams that are free of subdivergences and hence give scheme–independent contributions. The method delivered analytic results for 56 out of 59 diagrams. Three diagrams, associated with the knots 10_{124}, 10_{139}, and 10_{152}, were only obtained numerically to 10 significant figures. The accuracy was not sufficient to apply the method in a unique manner.[21] Only one hyperbolic knot with 11 crossings was encountered and the transcendental number associated with it was found. It is the only positive knot with 11 crossings other than the torus knot $(2, 11)$.

In addition, the series of 'zig–zag' counterterms, $\{6\zeta(3), 20\zeta(5), \frac{441}{8}\zeta(7), 168\zeta(9), \ldots\}$, was obtained. This series is the equivalent of the crossed ladder topology in the ϕ^4 theory and thus should produce $(2, 2n-3)$ torus knots, corresponding to $\zeta(2n-3)$. And indeed, it was found that the n–loop zig–zag term is $4C_{n-1}\sum_{p>0}\frac{(-1)^{pn-n}}{p^{2n-3}}$, where $C_n = \frac{1}{n+1}\binom{2n}{n}$ are the Catalan numbers, familiar in knot theory.

At seven loops, transcendentals of degree ≤ 11 can occur, and thus we expect knots with up to eleven crossings. With the exceptions of the hyperbolic knots 10_{139}, 10_{152}, and 11_{353}, all positive knots with up to 11 crossings are torus knots.[22] Apart from the $(2, q)$ $q \in \{3, 5, 7, 9, 11\}$ torus knots there are two more torus knots encountered at up to 7 loops: $8_{19} = (4, 3)$ and $10_{124} = (5, 3)$. We know already

---

[20]In DR regularized quantities depend on a scale parameter μ of mass dimension, see the remarks in the appendix.

[21] For the 56 graphs for which the method was successful numerical accuracy was such that the chance of an error is $< 10^{-30}$.

[22]In [14] these three hyperbolic knots were erroneously denoted as satellite knots.

that 8_{19} corresponds to a double sum whose structure matches the structure of the braid word, and for $(3, 5)$ a similar result was obtained.

Also it was found that the triple–sum $N_{3,5,3} \equiv \sum_{l>m>n>0} l^{-3}m^{-5}n^{-3}$ is associated with the knot 11_{353}. Again the corresponding knot had a braid word which matches: $11_{353} \sim \sigma_1\sigma_2^2\sigma_1^2\sigma_3^2\sigma_2^3\sigma_3$. This knot has a braid word in three different generators, with the total powers of the generators matching the exponents in the sum.

Fig.(57) gives an example for the appearance of this knot. We give a Feynman graph which was obtained from a ϕ^4 graph by replacing four-point couplings by three-point couplings, as in Fig.(54). Fig.(58) gives further examples for simple factor knots at the seven loop level.
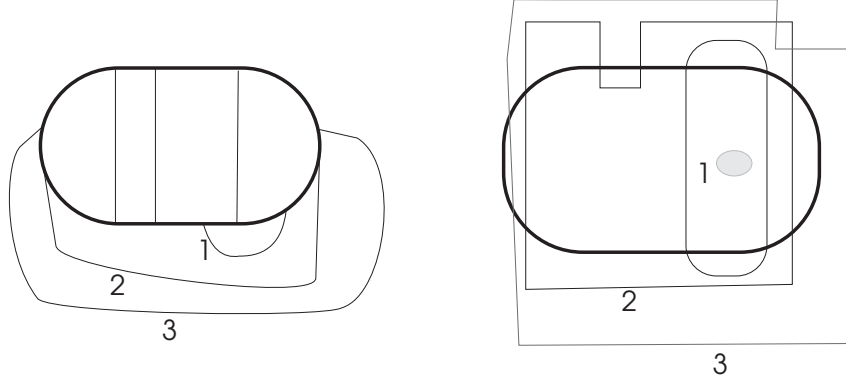

Figure 57: The identification of the knot 11_{353}. There are also $\zeta(3)^2\zeta(5) \sim (2,3)^2(2,5)$ factor knots as well as the $\zeta(11) = (2, 11)$ torus knot in this diagram. We only give one possible link diagram which delivers 11_{353}. The analytic result for this diagram contains $N_{3,5,3}$ as well as $\zeta(11)$ and $\zeta(3)^2\zeta(5)$. It can be found in [14], where this diagram belongs to class $C7$.

The knot $10_{124} = (5, 3)$ was also obtained in [14] and identified with the transcendental double sum $U_{7,3} \equiv N_{7,3}$ [17]. The reader will find a list of all results in [14], and further details and generalizations will figure in [31].
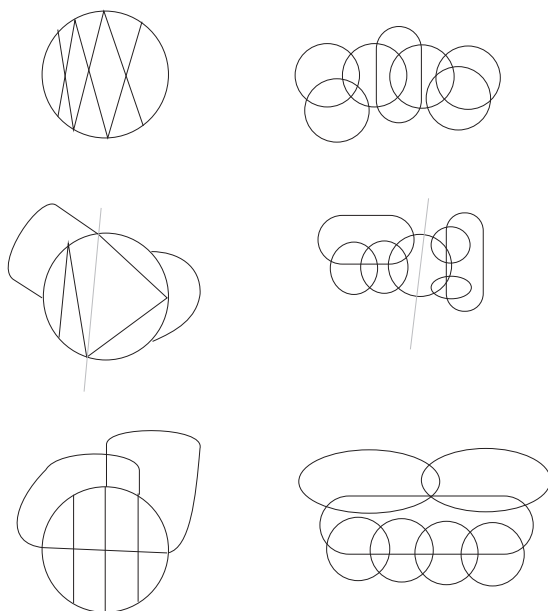
Figure 58: These are easy factor knots. From top to bottom, they deliver $(2,3)^3 \sim \zeta(3)^3$, $(2,5)^2 \sim \zeta(5)^2$, $(2,3) \times (2,7) \sim \zeta(3)\zeta(7)$.

8.4 Rationality and the β-function of quenched QED

In this paper, again a β-function was considered. This time it is the β-function of QED. In fact, the restricted class of diagrams to be considered were diagrams containing only a single fermion loop, which constitute the so-called quenched β-function. The aim was to give a knot-theoretic explanation for the rationality of the quenched QED β function. The following paragraphs are more or less a direct quote from [15], where the reader can find details of the calculation, as well as a confirmation of the mechanism proposed here for usual QED in scalar QED, which is the theory of a photon coupling to scalar particles.

In QED one has a gauge symmetry. On the quantized level this is a powerful tool which establishes relations between various Feynman diagrams. Here we only need to know that the divergences of the fermion propagator match the divergences of the vertex-function, which is expressed as $Z_1 = Z_2$, where Z_1 and Z_2 are the Z-factors of the QED Lagrangian, cf. Eq.(138). We refer to the identity $Z_1 = Z_2$ as the Ward identity.[23] At the link level, the Ward identity entails cancellation of subdivergences generated by one term of the skein relation, which in turn implies cancellation of knots generated by the other term.

Rationality of the three- [32] and four-loop [33] quenched (i.e. single-electron-loop) terms in the QED beta function comes as a surprise. Feynman diagrams with non-trivial knots contribute to it, so that the vanishing of transcendentals demands an explanation. For example the crossed-photon graphs of Figs.(59f,g,h) all realize the link diagram whose skeining contains the trefoil knot. With the experience of the previous subsections in mind we expect to find $\zeta(3)/\epsilon$ in their divergent parts. To explain the cancellation of transcendentals, we must study the interplay between knot-theoretic arguments and the gauge structure of QED.

We propose to associate the cancellation of transcendentals with the cancellation of subdivergences in the quenched beta function of QED, which is an immediate consequence of the Ward identity, $Z_1 = Z_2$.

To see the key role of the Ward identity, consider Fig.(59g). There is an internal vertex correction, which is rendered local by adding the appropriate counterterm graph. Due to the Ward identity, this counterterm graph is the same as that which compensates for the self-energy correction in Fig.(59e). We know that the latter counterterm could be interpreted as the A part of the skein operation on the link diagram of Fig.(59e), associated with the Feynman graph. We assume that this is a generic feature of the relationship between skeining and renormalization and associate the corresponding counterterm for Feynman graph Fig.(59g) with the term obtained from applying A twice to its link diagram, which requires two skeinings to generate the same counterterm, along with the trefoil knot from the B term. The Ward identity thus becomes a relation between crossed and uncrossed diagrams, after skeining:

$$A(A(L(\mathrm{g}))) = A(L(\mathrm{e})) \quad \Rightarrow \quad A(L(\mathrm{g})) = L(\mathrm{e}), \tag{130}$$

where $L(e), L(g)$ refer to the appropriate link diagrams in Fig.(59).

---

[23]The original Ward identity relates the fermion propagator and the vertex function as $S^{-1}(p_1) - S^{-1}(p_2) = (p_1^\mu - p_2^\mu)\Gamma_\mu(p_1, p_2)$, which implies $Z_1 = Z_2$.

The trefoil knot results then from $B(B(L(g)))$, which generates, in general, a $\zeta(3)/\epsilon$ term from Fig.(59g), even after the subtraction of subdivergences. We now use the Ward identity Eq.(130) at the link level to obtain

$$B(B(L(g))) = B(B(A^{-1}(L(e)))), \tag{131}$$

from which we see that it relates the transcendental counterterm from a torus-knot topology, in Fig.(59g), to a knot-free ladder topology, in Fig.(59e). From section seven we know that ladder topologies are free of transcendentals when the appropriate counterterms are added: after subtraction of subdivergences, ladder graphs, such as in Figs.(59a,e), give rational terms in the Laurent expansion in powers of $1/\epsilon$.

We conclude that $\zeta(3)/\epsilon$ should be absent from the bare diagram of Fig.(59g) when it is calculated in the gauge where the bare diagram of Fig.(59e) is free of $\zeta(3)/\epsilon$, i.e. in the Landau gauge, where the latter is free of subdivergences.[24] In Fig.(59) we summarize this argument. By a similar argument, we also conclude that the other graphs with the trefoil topology, namely Figs.(59f,h), should be free of $\zeta(3)/\epsilon$ in the Landau gauge. Which was indeed confirmed by explicit calculation in [15].

---

[24]In gauge theories, the local gauge symmetry allows such welcome accidents: that certain graphs may be free of divergences in a special gauge.
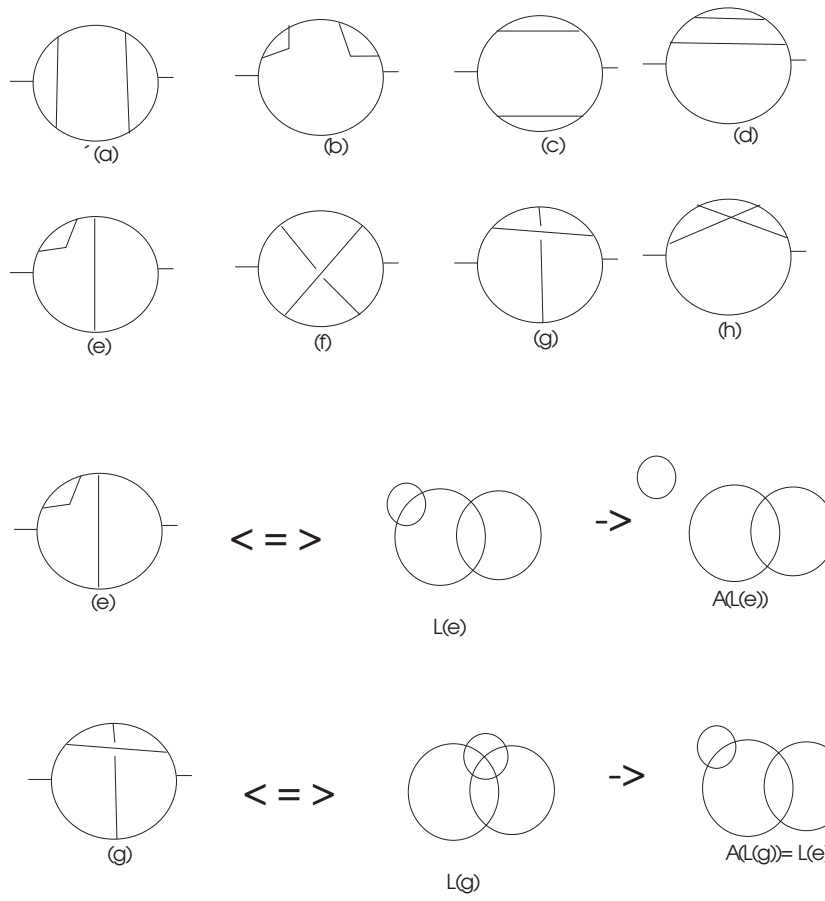
Figure 59: This figure summarizes the argument in [15] which explains the absence of transcendentals in the quenched QED β-function.

8.5 Euler double sums and the expansion in the two-loop master function

Here the investigation of knots and numbers was pushed further to level 12. The diagrams considered are the dressed master function, which incorporates one-loop bubbles in the basic trefoil topology of Fig.(60). The results are in agreement with the results of section five, and with the upcoming results in [18].

At first sight the analysis in [16] seemed to be in conflict with the number theory in [34]. In Fig.(61) we demonstrate the appearance of twelve crossing knots in the diagrams considered in [16].
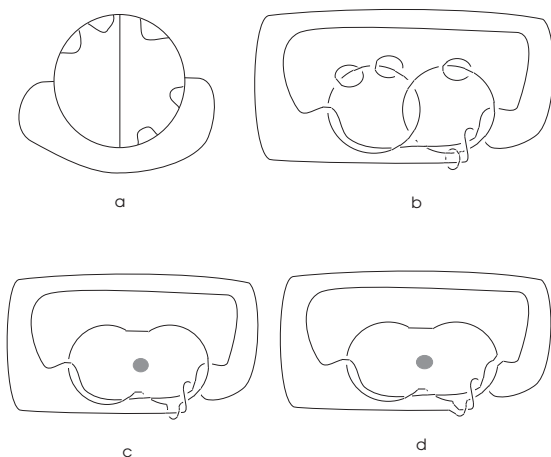

Figure 60: These graphs which come from dressing the basic trefoil topology generate double sums and correspond to three-braids on the other hand. The treatment of the bubbles coincide with the experience of section five and the results in [18].

The 'rule of 3' discovered in [34], for non-alternating sums $\zeta(a,b) = \sum_{n>m} 1/n^a m^b$ of level $l = a + b$, demands, at even level $l = 2p + 2$, as much as $\lfloor p/3 \rfloor$ irreducibles.[25] On the other hand the number of positive three-braid knots generated from topologies as in Fig.(60) grows by a rule of two, giving $\lfloor p/2 \rfloor$ knots at $l = 2p + 4$ crossings. So there are two 12-crossing knots, while [34] only have one level 12 irreducible.

This problem initiated a major finding in number theory by David Broadhurst [17], which we will comment in the next section. For now, we directly quote from there: "Faced with a 12-crossing knot in search of a number, we saw two ways to turn: to study 4-fold non-alternating sums, or 2-fold sums with alternating signs. The first route is numerically intensive: it soon emerges that well over 100 significant figures are needed to find integer relations between 4-fold sums at level 12. The second route is analytically challenging; it soon emerges that at all even levels $l \geq 6$ there are relations between alternating double sums that cannot be derived from any of the identities given in [34].

Remarkably, these two routes lead, eventually, to the *same* answer. The extra 12-crossing knot is indeed associated with the existence of a 4-fold non-alternating sum,

---

[25]$\lfloor x \rfloor$ is the nearest integer $\leq x$.

$\zeta(4, 4, 2, 2) = \sum_{n>m>p>q} 1/n^4 m^4 p^2 q^2$, which *cannot* be reduced to non-alternating sums of lower levels. It is, equivalently, associated with the existence of an irreducible *alternating* double sum, $U_{9,3} = \sum_{n>m} [(-1)^n/n^9][(-1)^m/m^3]$. The equivalence stems from the unsuspected circumstance that the combination $\zeta(4, 4, 2, 2) - (8/3)^3 U_{9,3}$, and only this combination, is reducible to non-alternating double sums. Moreover, $l = 12$ is the lowest level at which the reduction of non-alternating 4-fold sums necessarily entails an alternating double sum. The 'problem pair' of knots are a problem no more. Their entries in the knot-to-number dictionary [31] record that they led to a new discovery in number theory: *the reduction of non-alternating sums necessarily entails alternating sums.*"

The family of positive knots [16] that gave rise to this investigation has braid words

$$\{\sigma_1 \sigma_2^{2a+1} \sigma_1 \sigma_2^{2b+1} \mid a \geq b \geq 1\}, \tag{132}$$

whose enumeration matches that of the irreducible $\{U_{2a+3,2b+1} \mid a \geq b \geq 0\}$.[26] Fig.(61) gives an example for the level 12 members of this family. The observation that more bubbles will only generate the knot family given in Eq.(132), together with the reduction of the quantity $I(\mu)$ to a double sum in [16], initiated the findings in [17].
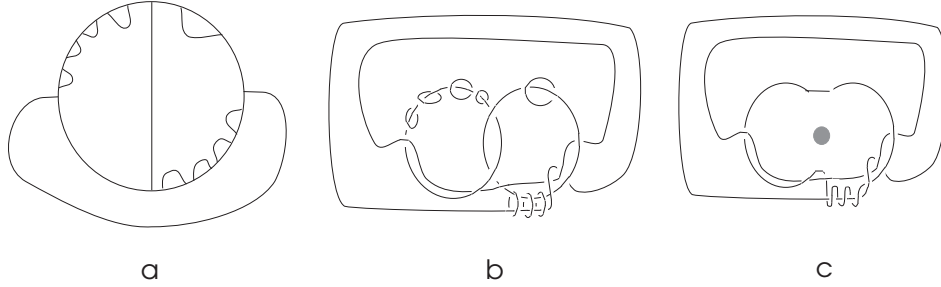

Figure 61: An example for the characteristic knot class for double sums.

---

[26] Conventions as in [17]. These irreducibles furnish all the transcendentals associated with the family of three-braids in Eq.(132) which was confirmed up to level $a + b \leq 20$ in [17].

8.6 General Euler sums

We mentioned already Broadhursts investigation of the number of irreducible Euler sums [17]. Guided by knot theory, he finds [17] "a generating function for the number, $E(l,k)$, of irreducible k-fold Euler sums, with all possible alternations of sign, and exponents summing to l. Its form is remarkably simple: $\sum_n E(k+2n,k)\,x^n = \sum_{d|k}\mu(d)\,(1-x^d)^{-k/d}/k$, where μ is the Möbius function. Equivalently, the size of the search space in which k-fold Euler sums of level l are reducible to rational linear combinations of irreducible basis terms is $S(l,k) = \sum_{n<k}\binom{\lfloor(l+n-1)/2\rfloor}{n}$."

Irreducible Euler sums are found to occur in explicit analytical results, for counterterms with up to 13 loops, yielding transcendental knot-numbers, up to 23 crossings. In [17] we can find a dramatic account how these results were obtained, supported by and support the connection between knot theory and field theory as proposed here.

8.7 Identities demanded by knot theory

In this work we consider results from one and two-loop bubble insertions in various Feynman diagrams which were iterated from the first term in the skeleton expansion. We obtain identities reflecting the demands of link theory and show that the diagrams fulfil these identities. Some basic results are already given in section five, and are extended in [18] to higher loop orders. The findings confirm the analysis of [16].

8.8 Field Theory, Knot Theory, Number Theory

From the results of [13, 14, 16, 17] it is clear that for the case of field-theory counterterms up to L loops, the irreducible Euler sums

$$\{\zeta(2a+1) \mid L-2 \geq a > 0\}, \tag{133}$$

$$\{U_{2a+1,2b+1} \mid a > b > 0,\ L-3 \geq a+b\}, \tag{134}$$

$$\{\zeta(2a+1,2b+1,2c+1) \mid a \geq b \geq c > 0,\ a > c,\ L-3 \geq a+b+c\}, \tag{135}$$

appear [17].[27]

It is not yet known whether Euler sums exhaust the transcendentals in counterterms at $L \geq 7$ loops. In addition to $10_{124} \simeq U_{7,3}$, there are two further positive knots with 10 crossings, namely [30] 10_{139} and 10_{152}, which 7-loop analysis [14] suggests are *not* associated with Euler sums of depth $k < 4$. All those, and *only* those, subdivergence-free 7-loop ϕ^4 diagrams whose link diagrams skein to 10_{139} and 10_{152} appear, on the basis of numerical evidence, to give counterterms that cannot be reduced to Euler sums with depth $k \leq 3$. Hence it is an open (and fascinating) question whether they belong to the class of Euler sums at all or provide different transcendentals. Table(3) gives a summary of the achievements so far. It summarizes the work of Broadhurst and Kreimer and is taken from [17].

Let us collect the successes of the empirical association of knots and numbers, initiated by the calculation of counterterms in renormalizable field theories. The

---

[27]$\zeta(2a+1,2b+1,2c+1) := \sum_{n>m>r}\frac{1}{n^{2a+1}m^{2b+1}r^{2c+1}} \equiv N_{2a+1,2b+1,2c+1}$.

Table 3: Positive prime knots related to Euler sums, via field-theory counterterms.

crossings	knots	numbers
$2a+1$	$(2, 2a+1) = \sigma_1^{2a+1}$	$\zeta(2a+1)$
8	$(3, 4) = 8_{19} = \sigma_2\sigma_1^3\sigma_2\sigma_1^3$	$N_{5,3}$
9	none	none
10	$10_{124} = (3, 5) = \sigma_2\sigma_1^3\sigma_2\sigma_1^5$	$N_{7,3}$
	$10_{139} = \sigma_2\sigma_1^3\sigma_2^3\sigma_1^3$	?
	$10_{152} = \sigma_2^2\sigma_1^2\sigma_2^3\sigma_1^3$	?
11	$\sigma_1^2\sigma_2^2\sigma_1\sigma_3\sigma_2^3\sigma_3^2$	$N_{3,5,3}$
12	$\sigma_2\sigma_1^7\sigma_2\sigma_1^3$	$N_{9,3}$
	$\sigma_2\sigma_1^5\sigma_2\sigma_1^5$	$N_{7,5} - \frac{\pi^{12}}{2^5.10!}$
	$\sigma_2\sigma_1^3\sigma_2^5\sigma_1^3$	?
	$\sigma_2\sigma_1^3\sigma_2^3\sigma_1^5$	?
	$\sigma_2^2\sigma_1^2\sigma_2^3\sigma_1^5$	?
	$\sigma_2^2\sigma_1^3\sigma_2^3\sigma_1^4$	?
	$\sigma_2^3\sigma_1^3\sigma_2^3\sigma_1^3$	?
13	$\sigma_1\sigma_2^3\sigma_1^2\sigma_3\sigma_2^4\sigma_3^2$	$N_{3,7,3}$
	$\sigma_1^2\sigma_2\sigma_1^3\sigma_3^2\sigma_2^2\sigma_3^3$	$N_{5,3,5}$
	$\sigma_1\sigma_2^3\sigma_1\sigma_3\sigma_2^5\sigma_3^2$	?
	$\sigma_1^2\sigma_2\sigma_1^3\sigma_3^3\sigma_2\sigma_3^3$	?
	$\sigma_1\sigma_2^3\sigma_1\sigma_3^2\sigma_2^3\sigma_3^3$	?
	$\sigma_1^2\sigma_2^2\sigma_1(\sigma_3\sigma_2^3)^2$	?
	$(\sigma_2\sigma_1\sigma_3\sigma_2)^3\sigma_1$	?
	$(\sigma_2\sigma_1\sigma_3\sigma_2)^3\sigma_2$	?

Euler sum $\zeta(2L - 3)$, corresponding to the 2-braid torus knot $(2L - 3, 2)$, first appears in anomalous dimensions or β-functions at L loops [14]. Only further symmetries like gauge symmetries might guarantee its absence [16]. This is the only transcendental which results from subdivergence-free diagrams with less than 6 loops, because no other positive knot has less than 8 crossings. On the other hand at 6 loops 3-braids start to appear [13]. The first of these is $8_{19} \simeq N_{5,3}$. The irreducibility of its knot-number was confirmed in [34]. Further at 7 loops 4-braids start to appear with the knot 11_{353}. The irreducibility of its knot-number was confirmed in [35], following communication of its appearance in field theory [14]. From there on, the findings in [16] and [17], supported by [18], inform number theory. The reader will find further comments and results in the quoted papers as well as in [31].

9 Conclusions

In this paper we established a useful algebra to facilitate calculations for topological simple Feynman graphs. Remarkably, this algebraic structure could be established whenever the topology was of ladder type, so that we could use the same one-loop algebra for nested as well as overlapping divergences. Starting from this algebra, we proved in section seven a striking connection between topological simplicity and a number theoretic property. In section eight we reported results which strongly suggest a yet to be explored connection between field theory, knot theory and number theory. When musing about the results achieved a few obvios things come to mind. The Euler sums which so pertinently appear in the counterterms of renormalizable field theories have relations to quantum groups and recent results in topology. For example in [36] we can find them in relation to the Drinfeld associator and Kontsevichs work. This opens fascinating questions to be explored in the future. Also, our use of the Hamiltonian circuit brings to mind chord diagrams. Any three-valent graph which allows for a Hamiltonian circuit can be directly related to chord diagrams.[28] This indicates that one should explore four-term relations for their usefulness in classifying and simplifying the divergences of a pQFT. This is under investigation at the moment. We hope that in the future it might be possible not only to identify the transcendentals in the Z-factor by considering the associated link diagram, but also hope to be able to predict the actual coefficients of these transcendentals, when the theory under investigation is specified. This would enable us to calculate Z-factors to arbitrary loop order just from a knowledge of the topology of the graph and knowledge of its particle content.

Acknowledgements

---

[28] In [37] the authors tried to explore this idea to map Feynman diagrams to knots using singular knot projections. Unfortunately, they fail. Their "connectivity rules" where strictly designed to get the correct results up to the three loop level, where they reproduce $\zeta(3) \sim$ trefoil. But their rules give wrong results even for the four loop example. Contrary to the hope the authors express in their paper, the incorporation of the resolution of singular points in terms of over- and undercrossings *a la Vassiliev* [38] cannot cure their results, which one sadly but easily confirms by explicit calculation.

References

[1] S. Schweber, *QED and the men who made it: Dyson, Feynman, Schwinger, Tomonaga* Princeton Univ. Press (1994), and references there.

[2] G.'t Hooft, Nucl.Phys.B33 (1971) 173; Nucl.Phys.B35 (1971) 167.

[3] B.W. Lee, in *Methods in Field Theory*, ed. R. Balian, J. Zinn-Justin (1976) North-Holland.

[4] F.J. Dyson, Phys.Rev.75 (1949) 486, 1736.

[5] A. Salam, Phys.Rev.82 (1951) 217, 84, 426.

[6] S. Weinberg, Phys.Rev.118 (1960) 838.

[7] N.N. Bogoliubov, D.V.Shirkov, *Introduction to the theory of quantized fields*, Wiley (1980).

[8] W. Zimmermann, Comm.Math.Phys.15 (1969) 208.

[9] D. Kreimer, *Renormalization and Knot Theory*, Univ. of Tasmania preprint UTAS-PHYS-94-25 (1994). This preprint contains most of the material of sections 3,4,6,7 here. Following a suggestion of Lou Kauffman, we added section 2. Section 5 is new. Section 8 reviews recent results and contains a few new results as well.

[10] M.Kaku, *QFT*, Oxford UP 1993.

[11] J.Collins, *Renormalization*, Cambridge UP 1984.

[12] C.C. Adams, *The Knot Book*, Freeman (1994).
D. Rolfsen, *Knots and Links*, Publish or Perish (1976).
L.H. Kauffman, *Knots and Physics*, World Scientific (1991).

[13] D. Kreimer, Phys.Lett.B354 (1995) 117.

[14] D.J. Broadhurst, D. Kreimer, Int.J.Mod.Phys.C6 (1995) 519.

[15] D.J. Broadhurst, R. Delbourgo, D. Kreimer, Phys.Lett.B366 (1996) 421.

[16] D.J. Broadhurst, J. Gracey, D. Kreimer, Z.Phys.**C**75 (1997) 559;
see also D.J. Broadhurst, A.V. Kotikov, *Compact analytical form for non-zeta terms in critical exponents at order* $1/N^3$, hep-th/9612013.

[17] D.J. Broadhurst, *On the enumeration of irreducible k-fold Euler sums and their roles in knot theory and field theory*, to appear in J.Math.Phys., OUT-4102-62 (hep-th/9604128).

[18] D. Kreimer, *On Knots in subdivergent Diagrams*, to appear in Z.Phys.**C**, MZ-TH/96-31 (hep-th/9610128).

[19] H. Lehmann, K. Symanzik, W. Zimmermann, Nuovo Cim.1, (1955) 1425.

[20] R.Haag, *Local Quantum Physics*, Springer 1992.

[21] D.J. Broadhurst, Z.Phys.C32 (1986) 249;
D.T. Barfoot, D.J. Broadhurst, Z.Phys.C41 (1988) 81.

[22] D. Kreimer, Mod.Phys.Lett.A9 (1994) 1105.

[23] V.A. Smirnov, *Renormalization and Asymptotic Expansions*, Birkhäuser (1991).

[24] K.G. Chetyrkin, A.L. Kataev, F.V. Tkachov, Nucl.Phys.B174 (1980) 345, see also [23] and references there.

[25] C. Itzykson, J.-B. Zuber, *Quantum Field Theory*, McGraw-Hill (1980).

[26] R. Delbourgo, A. Kalloniatis, G. Thompson, Phys.Rev.**D54** (1996) 5373;
R. Delbourgo, D. Elliott, D.S. McAnally, Phys.Rev.**D55** (1997) 5230.

[27] V.V. Belokurov, N.I. Ussyukina, J.Phys.A16 (1983) 2811.
A.I. Davydychev, N.I. Ussyukina, Phys.Lett.B298 (1993) 363; Phys.Lett.B305 (1993) 136.
D.J. Broadhurst, Phys.Lett.B164 (1985) 356; Phys.Lett.B307 (1993) 132.

[28] D.J. Broadhurst, *Massless Scalar Feynman Diagrams: Five Loops and Beyond*, (1985) Open Univ. preprint OUT-4102-18.

[29] D.Barnette, *Map Coloring, Polyhedra, and the Four-Color Problem*, The Dolcani Mathematical Expositions (1983).

[30] V. Jones, Annals of Math.126 (1987) 335.

[31] D. Kreimer, *Knots and Feynman diagrams*, Cambridge UP, in preparation.

[32] J.L. Rosner, Phys.Rev.Lett.17, (1966) 1190; Ann.Phys.44 (1967) 11.

[33] S.G. Gorishny, A.L. Kataev, S.A. Larin, L.R. Surguladze, Phys.Lett.B256 (1991) 81.

[34] D. Borwein, J.M. Borwein, R. Girgensohn, Proc.Edin.Math.Soc.38 (1995) 273.

[35] J.M. Borwein, R. Girgensohn, CECM research report 95-053 (1995), Electronic J. Combinatorics **3** (1996) R23, with an appendix by D.J. Broadhurst.

[36] C. Kassel, *Quantum Groups*, Springer 1995.

[37] I. Tsohantjis, A.C. Kalloniatis, P.D. Jarvis, *Chord diagrams and BPHZ subtractions* UTAS-PHYS-96-03, (hep-th/9604191).

[38] Dror Bar-Natan, Topology 34,2 (1995) 423.

[39] D.J. Broadhurst, D. Kreimer, Phys.Lett.**B393** (1997) 403;
D.J. Broadhurst, *Conjectured Enumeration of irreducible Multiple Zeta Values, from Knots and Feynman Diagrams*, hep-th/9612012.

[40] D. Kreimer, *Weight Systems from Feynman Diagrams*, to appear in JKTR, MZ-TH/96-36, (hep-th/9612010);
D.J. Broadhurst, D. Kreimer, *Feynman Diagrams as a Weight System: Four-Loop Test of a Four-Term Relation*, MZ-TH/9612011, (hep-th/9612011), subm. to PLB.

A   Conventions

In explicit results given in this paper we usually omit trivial factors of $2^D \pi^{D/2}$, typically generated by Eqs.(43,44), with the only exception being the results for ϕ_6^3 given in section two, where we obey the conventions of [11].

We also omit to give explicitly the dependence on the renormalization scale μ. Such a scale results from the demand to have a coupling constant which has no dimension in DR, so that one redefines the coupling $g^2 \to g^2(\mu^2)^\epsilon$, where μ has the dimension of a mass. Renormalized quantities are independent of μ.

B   Feynman Rules

We gave the Feynman rules for ϕ^4 in four dimensions in section two. Here we give the Feynman rules for some other theories.

B.1 ϕ_6^3

There is a modification in the symmetry factor. The Lagrangian comes now with a coupling $g/3!$. The vertex $-ig$ connects to three propagators. The loop integration is with respect to a measure

$$\int \frac{d^6 k}{(2\pi)^6} \tag{136}$$

which becomes in DR $\int \frac{d^D k}{(2\pi)^D}$, with $D = 6 - 2\epsilon$. One has three Z-factors as in ϕ^4, one for each monomial in the Lagrangian. This theory is renormalizable in six dimensions. All other theories considered in this paper are renormalizable in four dimensions.

B.2   QED

In QED one finds the following set of rules:

- For each internal electron line, associate a propagator given by:

  $iS_F(p) = \frac{i}{\not{p}-m+i\eta} = \frac{i(\not{p}+m)}{p^2-m^2+i\eta}$

- For each internal photon line (in the Feynman gauge), associate a propagator:

  $iD_F(p)_{\mu\nu} = -\frac{ig_{\mu\nu}}{p^2+i\eta}$

- At each vertex place a factor of:

  $-ie\gamma_\mu$

- For each internal loop, integrate over:

  $\int \frac{d^4q}{(2\pi)^4}$

- Incoming electrons have momenta entering the diagram, while incoming positrons have momenta leaving the diagram. Internal fermion lines appear with arrows in both clockwise and counterclockwise direction. However, topologically equivalent diagrams are counted only once.

We see that one can almost read off these Feynman rules from the Lagrangian of QED:

$$\mathcal{L} = \bar{\psi}(i\gamma^\mu(\partial_\mu + ieA_\mu) - m)\psi - \frac{1}{4}F_{\mu\nu}F^{\mu\nu} - \frac{1}{2}(\partial_\mu A^\mu)^2 \tag{137}$$

and the propagators above appear as the inverse of the equation of motion for the noninteractiong electron and photon fields. The Z-factors are as follows.

$$\mathcal{L} = \bar{\psi}(i\gamma^\mu(Z_2\partial_\mu + iZ_1 eA_\mu) - Z_m m)\psi - \frac{1}{4}Z_3 F_{\mu\nu}F^{\mu\nu} - \frac{1}{2}Z_a(\partial_\mu A^\mu)^2 \tag{138}$$

B.3   Scalar QED

This is the theory of an abelian gauge theory coupling to charged scalar particles. We only give the modifications compared to QED.

- At each scalar-scalar-vector vertex place a factor of:
  $-ie(p + p')_\mu$, where p and p' are the momenta for the scalar line.

- Insert a factor of $2ie^2 g_{\mu\nu}$ for each four-point vector-vector-scalar-scalar vertex.

The Lagrangian is

$$\mathcal{L} = (\partial_\mu - ieA_\mu)\phi^\dagger(\partial_\mu - ieA_\mu)\phi - m^2\phi\phi^\dagger. \tag{139}$$

B.4   Yukawa theory

This is the coupling of fermions with scalar particles. We have an interaction term $g\phi\bar{\psi}\psi$ and a Z-factor Z_g for it with vertex $-ig$, as well as the usual free Lagrangians of scalar and fermionic particles. Yukawa theory provides convenient examples. For example the three-point one-loop vertex function becomes (zero-mass limit, zero momentum transfer)

$$\int d^D k \frac{1}{\not{k}\not{k}(q+k)^2} = \int d^D k \frac{1}{k^2(k+q)^2}, \tag{140}$$

and thus provides a very simple example for a one-loop function Δ.

C   Form Factors

C.1   A QED example

The situation is most easily explained by studying a example. Consider the case of a one-loop vertex correction in massless QED at zero momentum transfer:

$$\int d^D l \, \frac{1}{(l+k)^2} \gamma_\rho \frac{1}{\slashed{l}} \gamma_\mu \frac{1}{\slashed{l}} \gamma_\rho =$$
$$(\Delta_{11}\gamma_\mu + \Delta_{21}\slashed{k}k_\mu)(k^2)^{-\varepsilon},$$

which allows for two form factors Δ_{11} and Δ_{21}. Only Δ_{11} is UV divergent.

Iterating this in nested topologies both form factors may replace the tree level vertex γ_μ. So we also have to consider functions where the vertex structure is $\slashed{k}k_\mu$ for some momentum k, and this gives us two more Δ functions:

$$\int d^D l \, \frac{(l^2)^{-\varepsilon i}}{(l+k)^2} \gamma_\rho \frac{1}{\slashed{l}} \gamma_\mu \frac{1}{\slashed{l}} \gamma_\rho =$$
$$(k^2)^{-\varepsilon(i+1)}[{}_i\Delta_{11}\gamma_\mu + {}_i\Delta_{21}\frac{\slashed{k}k_\mu}{k^2}],$$
$$\int d^D l \, \frac{(l^2)^{-\varepsilon i}}{(l+k)^2} \gamma_\rho \frac{1}{\slashed{l}} \frac{\slashed{l}l_\mu}{l^2} \frac{1}{\slashed{l}} =$$
$$(k^2)^{-\varepsilon(i+1)}[{}_i\Delta_{12}\gamma_\mu + {}_i\Delta_{22}\frac{\slashed{k}k_\mu}{k^2}].$$

At the one-loop level we have

$$Z_1^{(1)} = <\Delta_{11}\gamma_\mu + \Delta_{21}\frac{\slashed{k}k_\mu}{k^2}> = <\Delta_{11}> \gamma_\mu,$$

by definition. At the next order we find

$$Z_1^{(2)} = <(\Delta_{11} \, {}_1\Delta_{11} + \Delta_{21} \, {}_1\Delta_{12})\gamma_\mu$$
$$+(\Delta_{11} \, {}_1\Delta_{21} + \Delta_{21} \, {}_1\Delta_{22})\frac{\slashed{p}p_\mu}{p^2}>$$
$$- <<\Delta_{11}> (\Delta_{11}\gamma_\mu + \Delta_{21}\frac{\slashed{p}p_\mu}{p^2})>$$
$$= <(\Delta_{11} \, {}_1\Delta_{11} + \Delta_{21} \, {}_1\Delta_{12})\gamma_\mu> - <<\Delta_{11}> \Delta_{11}\gamma_\mu>$$

as $<\Delta_{21}\Delta_{22}> = 0$. We used

$$<\Delta_{11} \, {}_1\Delta_{21}> - <<\Delta_{11}> \Delta_{21}> = 0,$$

by Weinberg's theorem (we subtracted out the subdivergence from an overall convergent form factor $\sim \slashed{p}p_\mu$). UV-divergences only appear in the form factor $\sim \gamma_\mu$, as it should be. But we see that, at higher order, contributions of the other form factor mix into the result. Nevertheless, the concatenation works when we take this mixing iteratively into account. The above considerations are easily generalized to

more complicated cases involving other form factors, r say. We would obtain an $r \times r$ matrix of Δ functions Δ_{ij}, which concatenates in the way outlined above.

The same considerations apply to the two-point case, and the results of the example in the text concerning the two-loop fermion self-energy were obtained along these lines.

C.2 Quadratic divergences

Occasionally one has to confront quadratic divergences. The gauge boson propagator in a gauge theory provides such an example. We describe how to handle these quadratic divergences. It is sufficient to consider the case of a massless theory. As an example we take Fig.(39) for this case, and we assume that this topology is realized as a correction to the photon propagator in QED. The quadratic divergent term is of the form

$$\frac{Tr(\slashed{l}\gamma_\mu\slashed{l}\gamma_\rho\slashed{k}\gamma_\nu\slashed{k}\gamma^\rho)}{l^2(l+q)^2(l-k)^2k^2(k-q)^2},$$

(141)

Using Eq.(45) we subtract zero

$$\frac{Tr(\slashed{l}\gamma_\mu\slashed{l}\gamma_\rho\slashed{k}\gamma_\nu\slashed{k}\gamma^\rho)}{l^2(l+q)^2(l-k)^2k^2(k-q)^2}$$
$$-\frac{Tr(\slashed{l}\gamma_\mu\slashed{l}\gamma_\rho\slashed{k}\gamma_\nu\slashed{k}\gamma^\rho)}{l^2(l)^2(l-k)^2k^2(k)^2}$$
$$=\frac{Tr(\slashed{l}\gamma_\mu\slashed{l}\gamma_\rho\slashed{k}\gamma_\nu\slashed{k}\gamma^\rho)(l^2k^2-(l+q)^2(k-q)^2)}{l^4(l+q)^2(l-k)^2k^4(k-q)^2}$$
$$=\frac{Tr(\slashed{l}\gamma_\mu\slashed{l}\gamma_\rho\slashed{k}\gamma_\nu\slashed{k}\gamma^\rho)(l^2(q^2-2k.q)+2l.q(k^2-2k.q+q^2)+q^2(k^2-2k.q+q^2))}{l^4(l+q)^2(l-k)^2k^4(k-q)^2},$$

and no term is worse than linear divergent by powercounting, and thus amenable to the usual treatment.

D Generation of $\zeta(3)$

We want to calculate the divergent part of the three-loop ϕ^4 graph in Fig.(46). We use a variant of the Gegenbauer polynomial x-space technique [23, 24]. We use Gegenbauer polynomials in four dimensions, Chebyshev polynomials that is.

The analytic expression for the graph is

$$I := \int d^D k d^D l d^D r \frac{1}{r^2 l^2 k^2} \frac{1}{(l-k)^2(r-l)^2(k-r)^2}.$$

(142)

We use an expansion of a propagator in Gegenbauer polynomials $C_n^1(x)$.

$$\frac{1}{(p-q)^2} = \sum_{n=0}^{\infty} \frac{1}{\max(p,q)^2} \min(\frac{p}{q}, \frac{q}{p})^n C_n^1(\hat{p}.\hat{q}).$$

(143)

The $C_n^1(x)$ fulfil

$$C_n^1(1) = n+1, \quad \int d\hat{q} C_{n_1}^1(\hat{x}.\hat{q}) C_{n_2}^1(\hat{y}.\hat{q}) = \frac{1}{n_1+1}\delta_{n_1,n_2} C_{n_1}^1(\hat{x}.\hat{y}),$$

$$C_0^1(x) = 1, \quad \int d\hat{q} = 1, \tag{144}$$

where $p := \sqrt{p^2}$, $\hat{p}_\mu := p_\mu/p$, $\hat{p}_\mu \hat{p}^\mu = 1$.

The integral is totally symmetric in l, r, k. Therefore we consider only one sector, $l < r < k$, say. We have six such sectors, and the total result is just six times the result for one such sector. We are only interested in the divergent part of I, which appears when all three loop momenta become large. So in our chosen sector we can take as integration measure

$$I = C \int_1^\infty dk^2\, dl^2\, dr^2\, (l^2)^{-\epsilon}(r^2)^{-\epsilon}(k^2)^{-\epsilon} \int d\hat{k} d\hat{l} d\hat{r} \sum_{n_1,n_2,n_3} \frac{1}{k^2 l^2 r^2}$$

$$\frac{1}{\max(l,r)^2}\min(\frac{l}{r},\frac{r}{l})^{n_1} C_{n_1}^1(\hat{l}.\hat{r})$$

$$\frac{1}{\max(l,k)^2}\min(\frac{l}{k},\frac{k}{l})^{n_2} C_{n_2}^1(\hat{l}.\hat{k})$$

$$\frac{1}{\max(k,r)^2}\min(\frac{k}{r},\frac{r}{k})^{n_3} C_{n_3}^1(\hat{k}.\hat{r}).$$

C incorporates trivial factors as the volume of the four-dimensional unit-sphere. Using Eqs.(144) we can do the angular integrations easily. Then we evaluate the radial integrations in our specified sector

$$I = C \int_1^\infty dk^2\, dl^2\, dr^2\, (l^2)^{-\epsilon}(r^2)^{-\epsilon}(k^2)^{-\epsilon} \frac{1}{r^2}\frac{1}{k^4}\sum_{n=0}^\infty \frac{1}{n+1}\left[\frac{l^2}{k^2}\right]^n \tag{145}$$

$$\sim \sum_{n=0}^\infty \frac{1}{(n+1)^3} \sim \zeta(3), \tag{146}$$

in DR. Here we used that we can do the angular integrations in four dimensions. One easily verifies that the result in D dimensions only modifies the finite part. We also used that in DR all radial integrations vanish at infinity. Inserting all factors one confirms the well-known result $6\zeta(3)$.

E   A Regulator Function

We want to define a function $_j\bar{\Delta}$ which fulfils Eq.(122) and renders $_j\Delta$ finite by power-counting. This is easily achieved by constructing a function which has the same behaviour for large loop momentum. Let $F(k)$ be the integrand of the generalized one-loop function $_j\Delta$. Then $\Theta(k^2-1)F(k)$ provides an integrand which has the same asymptotic behaviour for large k. We then can always define a function $G(k)$ so that

$$_j\bar{\Delta} := \int d^D k [\Theta(k^2-1)F(k) + \Theta(1-k^2)G(k)], \tag{147}$$

94

has the desired properties.

F Cancellations of Transcendentals

We give an example for the concatenated product $B^6(\Delta)$, which corresponds to a seven loop calculation, compared with $(-A+B)^6(\Delta)$, for the example

$$\Delta = \int d^D k \, \frac{1}{k^2(k+q)^2} \mid_{q^2=1} .$$

We also give the lower order terms, as it is quite interesting to see the conspiracy of rationals appearing. So in the following $G(r)$ is a $r+1$ loop Green function, and $Z(r)$ the corresponding counterterm expression. 'ge' is the Euler γ and 'zet(i)' means $\zeta(i)$ and $x := D - 4$. We do not use a renormalization which would absorb the γ and $\zeta(2)$, and also do not use that $\zeta(2)^3$, $\zeta(4)\zeta(2)$ and $\zeta(6)$ are all dependent $(\sim \pi^6)$, as we want to exhibit the generated rationals in their purest form.

```
         1    -1    1    -2
Z(1):=----*x    -  ---*x
         2          2


       -1                5     1    -2
G(1):=x    *( - ge + ---)  + ---*x
                        2      2


         2    -1    1    -2    1    -3
Z(2):=----*x    -  ---*x    + ---*x
         3          2          6


       -1        1                3     2    9          55
G(2):=x    *( - ---*zet(2)  + ---*ge   - ---*ge  + ----)
                 4                4        2          6


         -2        1         3     1    -3
     + x    *( - ---*ge + ---)  + ---*x
                   2         2      6


         5    -1    19   -2    1    -3    1     -4
Z(3):=----*x    - ----*x    + ---*x    - ----*x
         4         24          4         24


       -1        23                1                7              4    3
G(3):=x    *( - ----*zet(3)  + ---*zet(2)*ge  - ---*zet(2)  - ---*ge
                  6                1                7              3
```

95

```
                9                 3               6               9


              14    2     125         455
            + ----*ge  - -----*ge + -----)
              3           6          12



        -2       1                1   2     7         125
      + x   *( - ----*zet(2) + ---*ge  - ---*ge + -----)
                 12             3         3         24



         -3       1        7        1   -4
       + x   *( - ---*ge + ----) + ----*x
                  6        12       24



        14   -1    19   -2    11   -3    1    -4    1    -5
   Z(4):=----*x   - ----*x   + ----*x   - ----*x   + -----*x
         5          12         24         12          120



        -1       133                335                335
   G(4):=x   *( - -----*zet(4) + -----*zet(3)*ge - -----*zet(3)
                  96             72                 18



            5        2    25          2    25
          + -----*zet(2)  - ----*zet(2)*ge  + ----*zet(2)*ge
            192             96                 12



            245              125    4    125    3    1225    2
          - -----*zet(2) + -----*ge  - -----*ge  + ------*ge
            48               576        36           48



            595         6727        -2      67
          - -----*ge + ------) + x   *( - ----*zet(3)
            6            40                72



           5               5              25    3    25    2
         + ----*zet(2)*ge - ----*zet(2) - -----*ge  + ----*ge
           48               12            144          12



           245         119
         - -----*ge + -----)
           24          6
```

$$
+ x^{-3} *(\ -\ \frac{1}{48}*zet(2)\ +\ \frac{5}{48}*ge^2\ -\ \frac{5}{6}*ge\ +\ \frac{49}{24})
$$

$$
+ x^{-4} *(\ -\ \frac{1}{24}*ge\ +\ \frac{1}{6})\ +\ \frac{1}{120}*x^{-5}
$$

$$
Z(5):=7*x^{-1}\ -\ \frac{1313}{360}*x^{-2}\ +\ \frac{47}{48}*x^{-3}\ -\ \frac{25}{144}*x^{-4}\ +\ \frac{1}{48}*x^{-5}
$$

$$
-\ \frac{1}{720}*x^{-6}
$$

$$
G(5):=x^{-1} *(\ -\ \frac{512}{75}*zet(5)\ +\ \frac{183}{80}*zet(4)*ge\ -\ \frac{1647}{160}*zet(4)
$$

$$
+\ \frac{23}{30}*zet(3)*zet(2)\ -\ \frac{23}{5}*zet(3)*ge^2\ +\ \frac{207}{5}*zet(3)*ge
$$

$$
-\ \frac{4991}{45}*zet(3)\ -\ \frac{3}{80}*zet(2)^2*ge\ +\ \frac{27}{160}*zet(2)^2
$$

$$
+\ \frac{3}{20}*zet(2)*ge^3\ -\ \frac{81}{40}*zet(2)*ge^2\ +\ \frac{217}{20}*zet(2)*ge
$$

$$
-\ \frac{903}{40}*zet(2)\ -\ \frac{9}{100}*ge^5\ +\ \frac{81}{40}*ge^4\ -\ \frac{217}{10}*ge^3
$$

$$
+\ \frac{2709}{20}*ge^2\ -\ \frac{19369}{40}*ge\ +\ \frac{62601}{80})\ +\ x^{-2}*(
$$

$$- \frac{61}{160} \cdot zet(4) + \frac{23}{15} \cdot zet(3) \cdot ge - \frac{69}{10} \cdot zet(3)$$

$$+ \frac{1}{160} \cdot zet(2)^2 - \frac{3}{40} \cdot zet(2) \cdot ge^2 + \frac{27}{40} \cdot zet(2) \cdot ge$$

$$- \frac{217}{120} \cdot zet(2) + \frac{3}{40} \cdot ge^4 - \frac{27}{20} \cdot ge^3 + \frac{217}{20} \cdot ge^2 - \frac{903}{20} \cdot ge$$

$$+ \frac{19369}{240}) + x^{-3} \cdot (- \frac{23}{90} \cdot zet(3) + \frac{1}{40} \cdot zet(2) \cdot ge$$

$$- \frac{9}{80} \cdot zet(2) - \frac{1}{20} \cdot ge^3 + \frac{27}{40} \cdot ge^2 - \frac{217}{60} \cdot ge + \frac{301}{40})$$

$$+ x^{-4} \cdot (- \frac{1}{240} \cdot zet(2) + \frac{1}{40} \cdot ge^2 - \frac{9}{40} \cdot ge + \frac{217}{360})$$

$$+ x^{-5} \cdot (- \frac{1}{120} \cdot ge + \frac{3}{80}) + \frac{1}{720} \cdot x^{-6}$$

$$Z(6) := \frac{132}{7} \cdot x^{-1} - \frac{277}{30} \cdot x^{-2} + \frac{839}{360} \cdot x^{-3} - \frac{19}{48} \cdot x^{-4} + \frac{7}{144} \cdot x^{-5}$$

$$- \frac{1}{240} \cdot x^{-6} + \frac{1}{5040} \cdot x^{-7}$$

$$G(6) := x^{-1} \cdot (- \frac{20641}{4320} \cdot zet(6) + \frac{49567}{3600} \cdot zet(5) \cdot ge - \frac{49567}{720} \cdot zet(5)$$

98

```
     1687                 11809              2
+ ------*zet(4)*zet(2) - -------*zet(4)*ge
   5760                   5760


     11809              28679            102487         2
+ -------*zet(4)*ge - -------*zet(4) + --------*zet(3)
    576                 480              12960


    5929                      5929
- ------*zet(3)*zet(2)*ge + ------*zet(3)*zet(2)
   4320                      864


    41503           3    41503            2
+ -------*zet(3)*ge   - -------*zet(3)*ge
   12960                 864


    100793           44891            49           3
+ --------*zet(3)*ge - -------*zet(3) - -------*zet(2)
    360                72             34560


     343         2   2    343         2        833        2
+ -------*zet(2) *ge   - ------*zet(2) *ge + -----*zet(2)
   11520                  1152                 960


    2401            4    2401            3
- -------*zet(2)*ge   + ------*zet(2)*ge
   34560                1728


    5831          2   2597              49049
- ------*zet(2)*ge   + ------*zet(2)*ge - -------*zet(2)
   480               48                    480


    16807      6   16807     5   40817     4    18179     3
+ --------*ge   - -------*ge  + -------*ge   - -------*ge
   518400          17280         2880            144


    343343    2   116039          4753177        -2
+ --------*ge   - --------*ge + --------) + x   *(
    480             48            1260


   7081             1687                 1687
```

```
      1             1                 1
  - ------*zet(5) + ------*zet(4)*ge - ------*zet(4)
    3600            2880              576


      847                 5929            2
  + ------*zet(3)*zet(2) - ------*zet(3)*ge
    4320                    4320


      5929             14399            49        2
  + ------*zet(3)*ge - -------*zet(3) - ------*zet(2) *ge
    432                 360             5760


      49        2    343             3    343           2
  + ------*zet(2)  + ------*zet(2)*ge  - -----*zet(2)*ge
    1152            8640                 576


      833             371            2401     5    2401     4
  + -----*zet(2)*ge - -----*zet(2) - -------*ge  + ------*ge
    240               48             86400         3456


      5831    3    2597    2    49049          16577     -3
  - ------*ge  + ------*ge  - -------*ge + -------) + x  *(
    720          48           240             48


      241             847             847
  - ------*zet(4) + ------*zet(3)*ge - -----*zet(3)
    2880            2160              432


      7        2    49             2    49
  + ------*zet(2)  - ------*zet(2)*ge  + -----*zet(2)*ge
    5760           2880                 288


      119             343     4    343    3    833    2
  - -----*zet(2) + -------*ge  - -----*ge  + -----*ge
    240             17280        864         240


      371         7007     -4       121
  - -----*ge + ------) + x  *( - ------*zet(3)
    24          240                2160


      7                  7             49    3    49    2
  + ------*zet(2)*ge - -----*zet(2) - ------*ge  + -----*ge
```

```
         1440                288              4320              288


           119         53
       -  -----*ge + ----)
          120          24



         -5        1                  7      2      7          17
     + x   *( - ------*zet(2) + ------*ge   - -----*ge + -----)
                 1440              1440         144        120



         -6        1        1        1     -7
     + x   *( - -----*ge + -----) + ------*x
                 720        144       5040
```

List of Figures

List of Tables